UNIVERSITÉ DU QUÉBEC

SENSITIVITY OF THE SNOW COVER AND THE ACTIVE LAYER TO LANDSCAPE SPATIAL HETEROGENEITY AND CLIMATE CHANGE OVER A CANADIAN HIGH ARCTIC TUNDRA ENVIRONMENT

SENSIBILITÉ DE LA COUVERTURE DE NEIGE ET DE LA COUCHE ACTIVE À L'HÉTÉROGÉNÉITÉ SPATIALE DU PAYSAGE ET AUX CHANGEMENTS CLIMATIQUES SUR UN ENVIRONNEMENT CANADIEN DE TOUNDRA DANS LE HAUT ARCTIQUE

THÈSE PRÉSENTÉE
COMME EXIGENCE PARTIELLE DU

DOCTORAT EN SCIENCES DE L'ENVIRONNEMENT
OFFERT PAR L'UNIVERSITÉ DU QUÉBEC À MONTRÉAL
EN ASSOCIATION AVEC
L'UNIVERSITÉ DU QUÉBEC À TROIS-RIVIÈRES

PAR
HADI MOHAMMADZADEH KHANI

Janvier 2024

UNIVERSITÉ DU QUÉBEC À TROIS-RIVIÈRES

DOCTORAT EN SCIENCES DE L'ENVIRONNEMENT (Ph. D.)

Programme offert par l'Université du Québec à Montréal (UQAM)

en association avec

l'Université du Québec à Chicoutimi (UQAC)

l'Université du Québec à Rimouski (UQAR)

l'Université du Québec en Abitibi-Témiscamingue (UQAT)

et l'Université du Québec à Trois-Rivières (UQTR)

Cette thèse a été dirigée par:

Christophe Kinnard, Ph. D.	Université du Québec à Trois-Rivières
Directeur de recherche, grade	Rattachement institutionnel
Esther Lévesque, Ph. D.	Université du Québec à Trois-Rivières
Codirectrice de recherche, grade	Rattachement institutionnel

Jury d'évaluation de la thèse :

Christophe Kinnard, Ph. D.	Université du Québec à Trois-Rivières
Directeur de recherche, grade	Rattachement institutionnel
Esther Lévesque, Ph. D.	Université du Québec à Trois-Rivières
Codirectrice de recherche, grade	Rattachement institutionnel
Kathy L. Young, Ph. D.	York University
Prénom et nom, grade	Rattachement institutionnel
Alexandre Langlois, Ph. D.	Université de Sherbrooke
Prénom et nom, grade	Rattachement institutionnel
Alexandre Roy, Ph. D.	Université du Québec à Trois-Rivières
Prénom et nom, grade	Rattachement institutionnel

Thèse soutenue le 15 Décembre 2023

ACKNOWLEDGEMENTS

First and foremost, I am extremely grateful to my supervisors, Prof. Christophe Kinnard and Prof. Esther Lévesque for their invaluable advice, continuous support, and patience during my PhD study. Their immense knowledge and plentiful experience have encouraged me in all the time of my academic research and daily life.

I appreciate the jury members' time in reviewing my dissertation: Prof. Kathy L. Young, Prof. Alexandre Langlois, and Prof. Alexandre Roy.

My appreciation also goes out to Catarina Leote F. Pio for her exceptional problem-solving skills and technical support.

I would like to thank my friends, lab mates, colleagues and research team from GlacioLab for their technical support and a cherished time spent together in the lab, and in social settings. Saida Nemri, Ghada Bzeouich, Vasana Dharmadasa, Okan Aygun, Matthieu Loyer, Shahabedin Taghiporjavi, Arthur de Grandpré, Olivier Larouche, Hafsa Bouamri, and Lisane Arsenault-Boucher. Arash Khalatbari and Elizabeth Grater thank you for being awesome friends.

Finally, I want to thank my wife and my family for their endless support and love. Thank you for trying to understand what I do and why I do it.

This research was funded by the Natural Sciences and Engineering Council of Canada, grant numbers RGPIN-2015-03844 (C. Kinnard) and RGPIN-2015-05319 (E. Lévesque), the Canada Research Chair program, grant number 231380 (C. Kinnard) and the Centre de Recherche sur les interactions Bassins Versants Écosystèmes Aquatiques (RIVE) (H. Mohammadzadeh Khani). Logistical support was provided by the Polar Continental Shelf Program (Natural Resources Canada). Support from the Community of Pond Inlet, Parks Canada and the Centre d'Études Nordiques (CEN) is acknowledged. We thank Prof. Gilles Gauthier for his logistical management of the research camp, and Maria Peter, Matthieu Loyer, Denis Sarrazin and Audrey Roy for their participation in fieldwork.

TABLE OF CONTENTS

LIST OF FIGURES

LIST OF TABLES

ABSTRACT

The High Arctic (HA) is a remote and extremely cold environment underlined by permafrost. Significant connections between biological, hydrological, and climatological elements influence the permafrost in HA ecosystems. The permafrost has been demonstrated to be particularly sensitive to changes in atmospheric moisture and increasing air temperatures. Also, climate change (both present and future) may have a profound effect on the regional hydrological cycle with transformative impact on associated environments. Yet, surface conditions may moderate the effects of global warming on permafrost. While there has been extensive researches on the impact of surface conditions on the temperature regime of permafrost at the hillslope scale, microscale variability has received far less attention. This necessitates a deeper comprehension of the environmental factors, particularly in varied tundra landscapes, that regulate the thermal regime and the depth of the permafrost active layer. This thesis seeks to address the influence of spatial heterogeneity and climate change on the sensitivity of snow cover and permafrost active layer to landscape spatial heterogeneity and climate change over a High Arctic tundra environment in Bylot Island, Nunavut, Canada. First, the impact of multi-environmental variables on the thermal regime of permafrost and the spatial variability of the active layer was examined at a very fine scale (< 1 m). In this case, one-year ground surface temperature and thaw depth measurements across a network of 100 micro loggers were used to analyze the spatial relationships between thaw depths and ground surface temperature (GST) with environment controls at micro and hillslope scales. Second, a physically based model (GEOtop) was used to simulate the spatial variability of snow cover, a crucial factor affecting the spatial variability of the permafrost active layer, at a fine spatial scale (>= 10 m). Eventually, the model was used to assess the effect of blowing snow

processes on the sensitivity of snow cover to anticipated changes in precipitation and temperature.

The field measurement data and statistical results showed that microscale (within-landform) variability in ground surface temperature and thaw depth was quite large, especially in summer, and sometimes surpassed the variability at the hillslope scale. Due to the highly heterogeneous snow cover produced by blowing snow, late-winter snowpack thickness was found to be the primary influence on the spatial variability in winter soil temperatures, and this thermal effect persisted into summer. However, microtopography, altitude, and moss thickness were the main contributors to the spatial heterogeneity of summer ground surface temperature. On the other hand, moss thickness had the strongest impact on the spatial heterogeneity of thaw depths. Thus, active layer growth was controlled by summer microclimate conditions, while a thicker snowpack favored soil cooling in the following summer, due to the later disappearance of snow cover.

The performance of the GEOtop 3.0 model was evaluated through statistical and graphical analyses of simulated metrics related to snow cover, including snow water equivalent, snow depth, and snow cover fluxes. The results indicated that the model closely replicates observed patterns of snow depth distribution and interannual variability at both individual point and spatial levels, with Nash-Sutcliffe Efficiency (NSE) values of 0.81 and 0.68, respectively. The inclusion of blowing snow processes in snow cover simulation increased the coefficient of variation of snow depth from 0.07 to 0.38, approaching the observed coefficient of variation (0.58). The results emphasized the significance of appropriately parameterizing the model during different phases of snow accumulation and ablation. Additionally, it revealed that blowing snow processes and landscape topography play crucial roles in governing the local distribution and overall accumulation of snow water equivalent throughout winter.

The study findings also demonstrated that the inclusion of blowing snow processes had a notable impact on the response of snow cover to climate change. The results showed that the effect of blowing snow on the climate sensitivity of the snow metrics was greater under colder and drier scenarios, and smaller in warmer and wetter scenarios. While it is observed that the response of max snow water equivalent (SWE) timing to the projected climate scenario will be significantly influenced by disabling blowing snow processes, peak SWE demonstrated the lowest sensitivity to the disabling BS. Among the snow cover metrics, snow cover heterogeneity was observed to be the most sensitive snow metric when disabling BS. Furthermore, temperature warming was projected to reduce blowing snow transport in the study area, with estimates ranging between 5 and 10% compared to present-day.

These findings have implications for similar tundra regions that share similar hydroclimatic characteristics to Bylot Island, as they may also experience significant changes in hydrological processes resulting from climate change. Furthermore, the documented alteration of snow cover characteristics and spatial heterogeneity in response to climate change is expected to significantly impact the thermal regime of the permafrost active layer, and calls for a better representation of the fine-scale landscape heterogeneity within land surface models.

Keywords: Bylot Island, climate change, permafrost, snow spatial variability, blowing snow.

RÉSUMÉ

Le Haut-Arctique (HA) est un environnement éloigné et extrêmement froid souligné par le pergélisol. Des liens importants entre les éléments biologiques, hydrologiques et climatologiques influencent le pergélisol dans les écosystèmes du HA. Il a été démontré que le pergélisol est particulièrement sensible aux changements d'humidité atmosphérique et à l'augmentation de la température de l'air. En outre, le changement climatique (actuel et futur) peut avoir un effet profond sur le cycle hydrologique régional avec un impact transformateur sur les environnements associés. Pourtant, les conditions de surface pourraient atténuer les effets du réchauffement climatique sur le pergélisol. Bien que des recherches approfondies aient été menées sur l'impact des conditions de surface sur le régime de température du pergélisol à l'échelle des pentes, la variabilité à micro-échelle a reçu beaucoup moins d'attention. Cela nécessite une compréhension plus approfondie des facteurs environnementaux, en particulier dans les paysages variés de toundra, qui régulent le régime thermique et la profondeur de la couche active du pergélisol. Cette thèse aborde l'influence de l'hétérogénéité spatiale et du changement climatique sur la sensibilité de la couverture neigeuse et de la couche active du pergélisol dans un environnement de toundra du Haut-Arctique sur l'île Bylot, Nunavut, Canada. Dans un premier temps, l'impact des variables multi-environnementales sur le régime thermique du pergélisol et la variabilité spatiale de la couche active a été examiné à une échelle très fine (< 1 m). Dans ce cas, des mesures sur un an de la température de surface du sol et de la profondeur de dégel sur un réseau de 100 micro-enregistreurs ont été utilisées pour analyser les relations spatiales entre les profondeurs de dégel et la température de surface du sol (GST) avec des contrôles environnementaux à l'échelle micro et des pentes de colline. Deuxièmement, un modèle physique (GEOtop) a été utilisé pour simuler la variabilité spatiale de la couverture neigeuse, un facteur crucial affectant la variabilité spatiale de la couche active du

pergélisol, à une échelle spatiale fine (>= 10 m). Finalement, le modèle a été utilisé pour évaluer l'effet des processus de poudrerie sur la sensibilité de la couverture neigeuse aux changements anticipés de précipitations et de température.

Les données de mesure sur le terrain et les résultats statistiques ont montré que la variabilité à micro-échelle (au sein du relief) de la température de la surface du sol et de la profondeur du dégel était assez importante, surtout en été, et dépassait parfois la variabilité à l'échelle de la pente. En raison de la couverture neigeuse très hétérogène produite par la poudrerie, l'épaisseur du manteau neigeux à la fin de l'hiver s'est avérée être la principale influence sur la variabilité spatiale des températures du sol en hiver, et cet effet thermique a persisté jusqu'en été. Cependant, la microtopographie, l'altitude et l'épaisseur de la mousse sont les principaux contributeurs à l'hétérogénéité spatiale de la température estivale de la surface du sol. En revanche, l'épaisseur de la mousse a le plus fort impact sur l'hétérogénéité spatiale des profondeurs de dégel. Ainsi, la croissance de la couche active était contrôlée par les conditions microclimatiques estivales, tandis qu'un manteau neigeux plus épais favorisait le refroidissement du sol l'été suivant, en raison de la disparition tardive de la couverture neigeuse.

Les performances du modèle GEOtop 3.0 ont été évaluées au moyen d'analyses statistiques et graphiques de métriques simulées liées à la couverture neigeuse. Les résultats ont indiqué que le modèle reproduit fidèlement les modèles observés de distribution de l'épaisseur de neige et de variabilité interannuelle aux niveaux individuel et spatial, avec des valeurs d'efficacité de Nash-Sutcliffe (NSE) de 0,81 et 0,68, respectivement. L'inclusion des processus de poudrerie dans la simulation de la couverture neigeuse a augmenté le coefficient de variation de l'épaisseur de la neige de 0,07 à 0,38, se rapprochant du coefficient de variation observé (0,58). Les résultats ont souligné l'importance de paramétrer correctement le modèle pendant les différentes phases d'accumulation et d'ablation de la neige. En outre, l'étude a révélé que les processus de poudrerie et la topographie du paysage jouent un rôle crucial dans la

répartition locale et l'accumulation globale de l'équivalent en eau de neige tout au long de l'hiver.

Les résultats de l'étude ont également démontré que l'inclusion des processus de poudrerie avait un impact notable sur la réponse de la couverture neigeuse au changement climatique. Les résultats ont montré que l'effet de la poudrerie sur la sensibilité climatique des mesures de neige était plus important dans les scénarios plus froids et plus secs, et plus faible dans les scénarios plus chauds et plus humides. Bien qu'il soit observé que le moment du maximum de l'équivalent en eau de la neige (SWE) du scénario climatique projeté était considérablement influencé par les processus de poudrerie, le pic du SWE a très peu varié en absence de poudrerie. Parmi les mesures de la couverture neigeuse, l'hétérogénéité de la couverture neigeuse s'est avérée être la mesure la plus sensible lors de la désactivation de BS. De plus, le réchauffement de la température devrait réduire considérablement le transport de la poudrerie dans la zone d'étude, avec des estimations allant de 5 à 10 % par rapport à aujourd'hui.

Ces résultats ont des implications pour des régions similaires partageant des caractéristiques hydroclimatiques similaires à celles de l'île Bylot, car elles pourraient également connaître des changements importants dans les processus hydrologiques résultant du changement climatique. De plus, l'altération des caractéristiques du couvert neigeux et de l'hétérogénéité spatiale en réponse au changement climatique démontré dans cette recherche, pourrait impacter le régime thermal de la couche active du pergélisol, requérant une meilleure représentation de l'hétérogénéité spatiale du paysage dans les modèles de surface terrestre.

Mots-clés: île Bylot, changements climatiques, pergélisol, variabilité spatiale de la neige, poudrerie.

INTRODUCTION

Motivation and relevance

The Arctic is a remote and extremely cold biome that has recently received the attention of policy makers, engineers, and scientists (Saito *et al.,* 2013). The Arctic is characterized by ecosystems that lack trees (Williams and Smith, 1989). These northern treeless ecosystems of Arctic includes a broad diversity in ecosystem structure that corresponds with a latitudinal gradient extending from the forest treeline to the polar desert regions. In the High Arctic (HA) region (the northernmost part of the Arctic), the ground cover consists mainly of lichens, mosses, sedges, and grasses (Campbell *et al.*, 2012) and their biological activity is restricted by low temperature and sudden spring and fall climatic oscillations to 3-4 months per year (Bliss e*t al.,* 1973). The HA land surface is underlined by permafrost, which is a ground frozen for a minimum of two consecutive years (Williams and Smith, 1989; Woo, 2012). Permafrost is a thermal process that is sensitive to air temperature warming. Several studies reported that the air temperature in the Arctic is rising at a rate that is two to three times faster than the average rate globally (AMAP, 2017; Stuecker *et al.,* 2018; Rantanen *et al.,* 2022). Climatic changes over the previous 50 years led to an increase in permafrost temperature, and a deepening of the active layer (the top layer of soil thawing in summer and refreezing in winter (Ballantyne *et al.*, 1990) in multiple locations across the HA (Slater and Lawrence, 2013). For example, a study carried out in the Canadian High Arctic exhibited that abnormally warm summers between 2003 and 2016 resulted in mean thawing indices being 150-240% higher than the 1979-2000 baseline (Farquharson *et al.,* 2019). As a result, a ground subsidence of up to 90 cm occurred over the 12-year observational span. Active layer deepening caused by permafrost thawing has significant effects on surface and subsurface hydrology. The aquatic and terrestrial ecosystems as well as associated northern traditional livelihoods will be

impacted by altered hydrology (Smith *et al.,* 2005). For example, when permafrost thaws, the soil organic matter and minerals within it become available for remobilization, introduction into aquatic systems and eventually release to the atmosphere. In terms of hydrology, permafrost thawing leads to increasing groundwater flow, hydraulic conductivity and flow path lengths (Walvoord *et al.,* 2015). In addition, through the release of accumulated soil organic carbon into the atmosphere, active layer deepening has the potential to accelerate global climate change (Biskaborn *et al.,* 2019).

Although climate change has a significant impact on the thermal state of permafrost, the formation of an active layer during certain seasons is recognized as a process that is both spatially diverse and subject to temporal variability (Belshe *et al.,* 2012; Yi *et al.,* 2018). Also, the complex interactions between the different hydrological processes and environment variables at play makes it difficult to predict future hydrological conditions, and their potential impacts on permafrost and active layer condition under climate change scenarios. As a result, although climatic warming plays a significant role in causing permafrost to thaw and increase in active-layer thickness (ALT), the primary local drivers of the permafrost seasonal response to climatic changes are surface factors (vegetation, snow, and soil) (Chapin *et al.,* 2005; Jing-Yi, 2018; Lara *et al.,* 2018). Thus, in order to predict future changes in permafrost a comprehensive understanding of the interaction between variables, which affect the spatiotemporal variability of permafrost active layer is essential. Several methods have been used to investigate the changes in permafrost thermal regime under ongoing climate change conditions. Yet, permafrost models and remote-sensing-driven monitoring approaches are still limited in their representation of small-scale spatial variability of snow and vegetation (Grünberg *et al.,* 2020).

In the High Arctic region, where snow covers the land for most of the year and is frequently redistributed by wind, it is crucial to study the evolution of snow in response

to ongoing climate changes. This is particularly important because snow serves as an insulating layer for the permafrost active layer for a significant portion of the year (Williams and Smith, 1989; Woo, 2012) and also has a significant effect on Arctic wildlife (Gauthier *et al.,* 2013). In order to study the complex interactions between subsurface and surface mass and energy fluxes in cold regions, robust hydrological models are needed (Engel *et al.*, 2017; Krogh *et al.*, 2017; Bui *et al.*, 2020a). The use of hydrological models can help compensate for the inability to observe the hydrological cycle in ungauged basins and the decline in the coverage of Arctic monitoring networks (Krogh and Pomeroy, 2018). The GEOtop model is an example of a spatially distributed and physically based model developed to simulate snow cover heterogeneity and hydrological processes in cold regions and can be used to assess the climate sensitivity of snow cover. The GEOtop model has been widely used in various regions and contexts, including permafrost regions. GEOtop can simulate the thermal regime of the soil, allowing for the representation of permafrost dynamics. This is crucial in permafrost regions where the presence of permanently frozen ground affects water movement, energy exchanges, and ecosystem dynamics. GEOtop is capable of simulating snow processes, including snowpack accumulation and melting, which are important factors influencing the hydrological regime in cold environments. GEOtop considers both surface water and groundwater interactions. In permafrost regions, where the water table and permafrost conditions can impact the movement of water between surface and subsurface, this capability is essential for understanding the overall hydrological dynamics.

The main objective of this thesis is to perform a sensitivity analysis of the snow cover and the active layer to landscape spatial heterogeneity and climate change over a Canadian High Arctic tundra environment. The primary objective is subdivided into three specific objectives: 1) first to identify the most important environmental controls that seasonally affect the spatial variability of active layer thickness and its thermal regime; 2) to test the ability of a fine-scale (< 10 m) blowing snow-enabled model

(GEOtop 3.0) to simulate the snow cover heterogeneity in the open terrain of the High Arctic; 3) to assess how blowing snow processes affect the response of snow cover conditions to climate change scenarios, using a sensitivity-based approach.

The fundamental hydrological processes that occur in the cold climate of the High Arctic are reviewed in the section that follows using existing hydrological models and documented impacts of projected climate change on snow cover of High Arctic regions.

Theoretical background

High Arctic hydrology

Most of the Arctic land surface (23 percent of the exposed land surface area of the northern hemisphere, Zhang *et al.,* 2008) is underlined by permafrost. The permafrost region is made up of a wide variety of settings, and the terrain, soil, and vegetation of these areas (Figure 1), together with the region's freezing climate, result in different combinations of permafrost hydrological processes (Woo *et al.,* 2008). The High Arctic is the most northern habitat, and it has the shortest growing season (Bliss *et al.,* 1973; Woo, 2012). Lichens and mosses are more common than vascular plants in many areas. Vascular plants are often smaller than their Low Arctic counterparts, and herbaceous species predominate over woody ones (Bliss *et al.,* 1973). Except in polar oases, covered in part by continuous tundra because of milder conditions, the majority of surfaces in the High Arctic are covered by sparse vegetation.

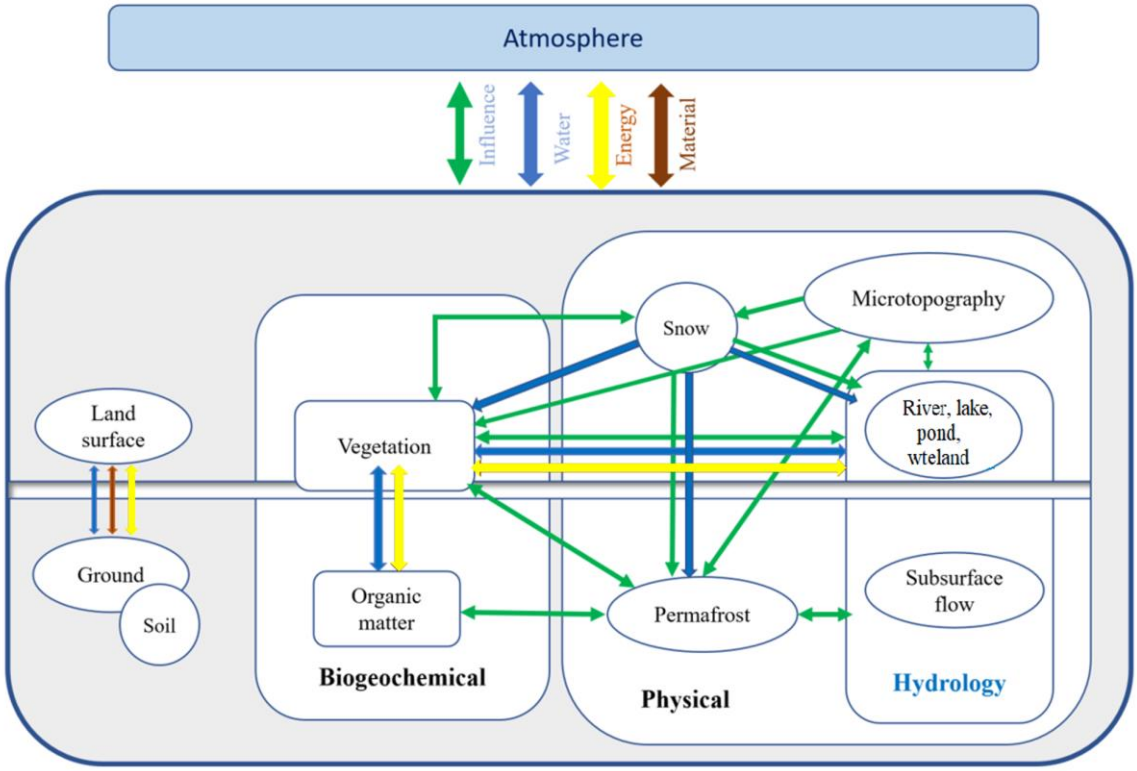

Figure 1 Schematic illustration outlining the linkages between components of the dynamic terrestrial Arctic system (modified from Saito *et al.,* 2013). The green arrows demonstrate overall relationships between components. The blue arrows indicate one-way flow of water; the yellow arrows highlight the energy, and dark brown arrows show material exchanges between components.

While mean air temperatures in July normally do not rise above 10 °C, the average January temperature in the HA typically stays below -15 °C and in some extreme locations, below -30 °C (Yang *et al.,* 1999; Pavelsky and Smith, 2006; Woo, 2012). Snow is the dominant form of precipitation (normally below 200 mm/year) which depends on the ambient temperature (Williams and Smith, 1989; Woo, 2012; Woo and Young, 2014). Seasonal snowfall accumulates during the course of the long winters, or it does so permanently in the form of snowbanks or glaciers. Throughout the spring

and summer, rainfall and snowmelt water saturate the active layer, and any overflow that cannot percolate into the ground rushes off to feed rivers, marshes, and lakes, which may keep this surface water for a variety of timeframes (Woo, 2012; Godin *et al.*, 2016).

Variations in active-layer thickness (ALT) are determined primarily by changes in air and ground temperature, especially during summer (Sazonova *et al.*, 2004; Francis *et al.*, 2009). These variations also depend on vegetation, snow depth, the composition and water content of the earth materials, as well as heat flow condition in the ground (Zhang, 2005) (Figure 1). Since the vast majority of the ecosystem and hydrological processes in permafrost terrains occur within the active layer, including carbon fluxes, monitoring changes in ALT is essential (Phoenix and Bjerke, 2016; Goetz *et al.,* 2018).

The dynamic of the active layer in continuous permafrost environments such as the Arctic tundra has a significant influence on the hydrology and ecology of these regions. Its extent and thickness over a region play a key role in the surface-subsurface interactions such as surface runoff, infiltration, and subsurface flow at large and local scales (Woo *et al.,* 2008; Zorigt *et al.*, 2016). Unlike the large-scale impact of climate change, local-scale impacts are more difficult to predict due to local feedback and interactions. The multiple interactions and feedbacks which characterize the Arctic terrestrial system (Figure 1) are acting simultaneously and synergistically (or antagonistically) within the system and, thus, may work as positive or negative feedback (Lizarralde *et al.,* 2004; Saito *et al.,* 2013; Van Der Kolk *et al.,* 2016). Predicting future changes in permafrost conditions, such as its temperature and the depth of the active layer is difficult because of the large microclimate variability, where seasonal interactions between the soil, snow, and vegetation can strongly buffer large-scale climate change (Yokohata *et al.,* 2020). Understanding the nature of these interactions is paramount for better projecting the future state of the Arctic ecosystem, permafrost feedback on climate (carbon release), as well as the hazards related to

permafrost degradation. Thawing of ice-rich permafrost can cause ground subsidence with negative implications for infrastructure, ecosystems, and human lives and livelihoods (Suter *et al.,* 2019; Gibson *et al.,* 2021).One key point is that the influence of each of the factors (snow depth, vegetation, and organic layer thickness) on the thermal regime is relatively well-known and can be deduced from physical principles, but the influence of their interactions on the thermal regime in response to large scale warming remains difficult to predict (Loranty *et al.,* 2018). These natural systems are complex and characterized by many non-linear processes that operate and interact over different scales. The interactions among the different hydrological processes at play (snow accumulation, redistribution, and ablation, interception of precipitation by plants, evapotranspiration, infiltration, and surface and subsurface runoff) make it difficult to predict future hydrological conditions, and their potential impacts on the ground thermal regime and vegetation under climate change scenarios. For these reasons, recent studies have resorted to physical models to try to disentangle the respective influences of climate and ecosystem factors and their interactions on the thermal regime (Atchley *et al.,* 2016).

Hydrological modeling in cold regions

Hydrological simulation and prediction in cold regions encounter substantial obstacles attributable to the dearth of adequate basin-scale information and hydrological models able to represent cold region processes (Zhou *et al.*, 2014; Bui *et al.*, 2020a; Pomeroy *et al.*, 2022a). Thus, the need arises to use a more reasonable hydrological framework that caters to the demands of cold regions. Hydrological models are streamlined depictions of a catchment hydrological behavior (e.g., surface water, soil water, wetland, groundwater, estuary) that aid in understanding, predicting, and managing water resources (Sorooshian *et al.*, 2020). There is a large diversity of models available to simulate hydrological processes and their response to climate change in cold regions with the occurrence of perennially frozen ground together with seasonally changing

active layer thickness (ALT). They can be divided into two categories: conceptual and physically based models according to how much physical theory was used (Devia *et al.*, 2015). The physical processes in a catchment are often represented by a number of connected reservoirs in conceptual models, and the parameters of the model are derived through both field observation and calibration. Compared to physically based models, conceptual models are more straightforward to apply. These models have been extensively utilized to anticipate streamflow volumes and floods in a water management setting and are particularly useful for modeling rainfall/snowmelt-runoff correlations. However, conceptual models heavily rely on calibration, frequently on streamflow alone, which is vulnerable to the quality of measured data (Devia *et al.*, 2015). Contrarily, physically-based hydrological models provide a detailed, and maybe more accurate, description of the hydrological processes in the watershed. In physically based hydrologic modeling the hydrological processes of water movement are modeled either by the finite difference approximation of the partial differential equation representing the mass, momentum and energy balance or by empirical equations (Loranty *et al.*, 2018). Physically based hydrological models can be either completely distributed, in which case a river basin is discretized as a rectangular grid mesh, or semi-distributed, in which case the basin is divided into a small number of sub-basins based on the topography, land cover and drainage network. In physically based hydrologic modeling, the resolution of the horizontal discretization may be a significant factor to derive model parameters from the terrain properties. Although conceptual models can be used to quickly analyze the effects of various climate change scenarios, physical-based models are better able to simulate the effects of both climate change and land use change (Aygün *et al.,* 2020).

Numerous physically-based hydrological models have been formulated and tailored for regions characterized by cold climates such as GEOtop (Zanotti *et al.,* 2004; Endrizzi *et al.,* 2014), CRHM (Pomeroy *et al.* 2007), Alpine 3D (Michlmayr *et al.*, 2008), and Raven (Craig *et al.* 2020). Most of these hydrological models consider the large variety

of hydrological processes happening in cold regions, however, not all of them consider snow processes at very fine scales. For example, CHRM model, which has been widely used to diagnose cold region hydrological processes, including redistribution of blowing snow (Krogh *et al.,* 2017; Aygün *et al.,* 2020), requires a careful delineation of the hydrological representative units (HRUs). In contrast, GEOtop is a fully distribute hydrological grid-based model built on digital elevation models (DEMs) (Zanotti *et al.,* 2004) where the energy and mass balances are concurrently solved, and the effects of topography on the interplay between radiation physics, the energy balance, and the hydrological cycle are accurately addressed. GEOtop is particularly well suited to calculate hydrological processes for a variety of scales, especially for those that happen at very small scales.

Projected effects of climate change on snow cover of High Arctic regions

Snow is the principal form of precipitation and a primary cryospheric characteristic in the High Arctic (HA), where it predominately covers its land, sea, lake, and river ice surfaces for a considerable period of the year (Ballantyne *et al.*, 1990; Woo, 2012). Notably, the snow cover within the HA region has far-reaching implications for hydrology and ecology in the coldest biome in the Northern Hemisphere (Morgner *et al.,* 2010; Callaghan *et al.,* 2011). Additionally, it is a contributing component of the climatic feedback, a significant factor that affects the global climate system (Cohen and Rind, 1990). The long-term stability of the snow cover in the HA is threatened due to the current global warming trend and accompanying polar amplification (Woo and Young, 2014). Previous research examining ground-based and satellite measurements has shown that the Arctic's regional snow cover depth and extension has decreased in response to warming temperatures and rising winter precipitation during the past 40 to 50 years (Brown and Robinson, 2011; Callaghan *et al.,* 2011; Brown *et al.,* 2017).

The hydrological cycle in the Arctic is becoming more intense as the Arctic region warms two to three times faster than the world mean leading to significant changes in snowfall and snow cover conditions, especially in the High Arctic region (Hansen *et al.,* 2014). The majority of global climate models (GCMs) forecasted that the amount of winter precipitation (and snowfall, specifically) at the high latitudes of the Arctic will increase dramatically (Meehl *et al.,* 2007). The reason for the increase in precipitation seems to be mostly connected to the greater moisture holding capacity of the warmer air rather than to large-scale circulation changes (Cassano *et al.,* 2007). As a result, future snow cover trends are expected to continue changing throughout the 21st century and are impacted by snowfall rates, atmospheric circulation, surface air temperature, and radiative forcing (Lawrence and Slater, 2010; Mohammadzadeh Khani *et al.*, 2022). Several studies have projected future changes in snow cover condition for the current century over the Arctic region. For example, Shi and Wang (2015) projected global mean annual and seasonal snow water equivalent (SWE) for three different time periods including 2015–2035, 2046–2065, and 2080–2099. Their objective was to assess how SWE will respond to different representative concentration pathway (RCPs) scenarios in the 21st century in terms of the magnitude, timing and seasonality across the Northern Hemisphere. They projected that SWE will increase across the Canadian HA and the West Siberian HA, while they found an decrease in SWE across the North European HA (Mohammadzadeh Khani *et al.*, 2022). According to a study by Brown *et al.* (2017) both RCP4.5 and RCP8.5 emission scenarios for the time span 2006–2090 predict a decrease in annual snow cover duration (SCD) across the HA. Thackeray *et al.* (2016) analyzed the spring snow cover extension (SCE) projected by the CMIP5 ensemble models for the near term 2011–2040 period. Their results showed that by the mid-century, there will be significant losses of snow cover extent, particularly in northern Europe compared to 2010 (10%). They also predicted that, under the RCP8.5 scenario, the June snow cover could entirely disappear by the second half of the twenty-first century as a result of the rising global average temperature. Despite the fact that there have been many studies that projected future

changes in snow cover conditions, these investigations still do not take snow heterogeneity into account in their modeling. In particular, these models either fail to account for or do not adequately account for blowing snow sublimation, transport, and erosion primary potentially important sources of uncertainty (Agosta *et al.,* 2013), especially in the tundra and High Arctic regions where these snow processes are crucial (Scarchilli *et al.* 2010; Lenaerts and van den Broeke 2012). These models are therefore unable to predict how snow processes will be altered in response to climate change or how these changes would impact the spatial variability of the snow.

Research objectives, scope, and importance

Investigating the interactions between climate, surface conditions, and the ground thermal regime and thaw depth can be difficult based on field measurements alone, given the numerous interactions among these elements (Gubler *et al.,* 2013). While controlled laboratory experiments allow to better isolate specific variables of the system, they are difficult to use to test simultaneously a large number of interactive variables typical of environmental systems. Modeling offers another way to explore the sensitivity of key variables (snow cover, active-layer depth and moisture) to climate, and to pinpoint interactions (feedback effects) between these variables. The overall objective of this PhD project is to explore the sensitivity of the snow cover and the active layer to landscape spatial heterogeneity and climate change over a Canadian High Arctic tundra environment. The study will be carried out at a long-term monitoring site in a high-Arctic tundra ecosystem on Bylot Island, Nunavut, Canada.

The following research objectives motivate the proposed research and will be specifically addressed within the three chapters of this thesis.

Objective 1: Measure and investigate the spatial heterogeneity of surface temperature and thaw depth and their relationship with snow depth, the type and height of

vegetation, soil type, soil moisture and topography. This objective aims to answer the following question:

Q1: How does seasonal surface temperature vary spatially in response to topography, vegetation, soil moisture and snow conditions at both the meso and micro scales?

In this research, we hypothesize that the heterogeneity of the land surface in the study area will cause significant spatial variability in ground surface temperature (GST) that will be assessed for summer (T_S) and winter (T_W), mainly driven by the microtopography, snow depth, vegetation (presence and absence, type), soil moisture and the interaction among these variables. The snow depth and vegetation (presence and type) are the main drivers of spatial variability in T_S yet may act differently depending on the season. Our assumption is that during winter the microrelief amplitude represents a substantial fraction of the total snow depth, which has a strong effect on the thermal regime and thus on TS. Spatial differences in TS due to snow depth variations induced by the microrelief will, however, be more significant when the snow depth is thin.

Objective 2: Test the ability of a physically-based and spatially-distributed snow model to simulate the fine-scale (<10 m) snow cover heterogeneity at the study site. This objective aims to answer the following question:

Q2: Can the snow cover be well simulated using the physically-based, snowdrift permitting GEOtop model in a High-Arctic tundra environment?

It is anticipated that the physically-based model GEOtop 3.0, recently enriched with a blowing snow module, is able to properly simulate the spatiotemporal variability of the snow cover at the studied site at a fine (<10m) spatial scale. It is expected that the

addition of blowing snow processes will greatly improve the representation of snow heterogeneity in open terrain of the High Arctic tundra.

Objective 3: Explore the impact of blowing snow processes on the sensitivity of snow cover to projected changes in precipitation and temperature for the case study area. This objective aims to answer the following questions:

Q3: Does considering or ignoring blowing snow processes impact the simulated climate sensitivity of snow cover conditions (peak accumulation and timing, snow cover duration)?

The current cold season temperature regime of our study area is changing in response to global warming. In response to increased snowfall during winter, snow depth (SD) and SWE will increase. However, local factors such as topographic variability and blowing snow transport will complicate the snow cover climate response and their impact can only be evaluated through modeling. We hypothesize that increasing air temperature will result in a decrease in blowing snow transport, thus resulting in a lesser spatial variability of snow cover.

Thesis outline

There are three primary chapters in this dissertation, one for each of the objectives listed above in the "Research Goals, Scope and Significance" section.

Chapter I intends to accomplish the dissertation's first objective by quantifying the influence and importance of the spatiotemporal relationships between ground surface temperature (GST) and active layer thaw depth (or frost table depth) with environmental conditions at two spatial scales (micro and hillslope scales) in a High Arctic tundra landscape.

Chapter II is related to the 2nd objective of the dissertation and the purpose is first to test the sensitivity of the snow depth for a range of parameters, to determine how these impact model outputs for snow deposition. Then to evaluate the capability of the snow model of GEOtop 3.0 to simulate the snow cover evolution at the point and spatial scale over a 15-years period for a High Arctic catchment. And finally, to examine the variability of snow cover (accumulation and distribution) due to wind redistribution and blowing snow (BS).

Chapter III addresses the third objective of the dissertation to quantify and evaluate the effect of blowing snow on the climate sensitivity of the snow cover condition at Bylot Island (Nunavut) in response to predicted variations in temperature and precipitation. The snow cover condition at point and spatial scale was simulated in the western coast of Bylot Island for the historical 2005-2019 period, including (BS-enabled) or excluding (BS-disabled) the blowing snow routine. Then, the snow model was disturbed using climate change projections and used to assess the influence of blowing snow on the climate sensitivity of the snow cover metrics under RCP 8.5 scenarios (low percentile, median and high percentiles).

CHAPTER I

FINE SCALE ENVIRONMENT CONTROL ON GROUND SURFACE TEMPERATURE AND THAW DEPTH IN A HIGH ARCTIC TUNDRA LANDSCAPE.

Hadi Mohammadzadeh Khani[1-2*], Christophe Kinnard[1-2], Simon Gascoin[3], Esther Lévesque[1-2]

[1] Research Centre for Watershed-Aquatic Ecosystem Interactions (RIVE), University of Québec at Trois-Rivières, Québec, Canada.

[2] Centre for Northern Studies (CEN), Québec City, Québec, Canada

[3] Centre d'Études Spatiales de la Biosphère (CESBIO), Université de Toulouse.

[*]Corresponding author: Hadi.Mohammadzadeh.Khani@uqtr.ca

This article is published in Permafrost and Periglacial Processes journal (DOI: **https://doi.org/10.1002/ppp.2203**).

Abstract

Surface conditions are known to mediate the impacts of climate warming on permafrost. This calls for a better understanding of the environmental conditions that control the thermal regime and the depth of the active layer, especially within heterogeneous tundra landscapes. This study analyzed the spatial relationships between thaw depths, ground surface temperature (GST), and environmental conditions in a High Arctic tundra environment at Bylot Island, Nunavut, Canada. Measurements were distributed within the two dominant landforms, namely earth hummocks and low-center polygons, and across a topographic gradient. Our results revealed that GST and thaw depth were highly heterogeneous, varying by up to 3.7°C and by more than 20 cm over short distances (<1 m) within periglacial landforms. This microscale variability sometimes surpassed the variability at the hillslope scale, especially in summer. Late-winter snowpack thickness was found to be the prime control on the spatial variability in winter soil temperatures due to the highly heterogeneous snow cover induced by blowing snow, and this thermal effect carried over into summer. However, microtopography was the predominant driver of the spatial variability in summer GST, followed by altitude and moss thickness. In contrast, the spatial variability in thaw depth was influenced predominantly by variations in moss thickness. Hence, summer microclimate conditions dominated active layer development, but a thicker snowpack favored soil cooling in the following summer, due to the later disappearance of snow cover. These results enhance our understanding of High Arctic tundra environments and highlight the complexity of considering surface feedback effects in future projections of permafrost states within heterogeneous tundra landscapes

Keywords: ground surface temperature, High Arctic, landscape heterogeneity, permafrost active layer, snow cover, thaw depth.

1.1 Introduction

The High Arctic (HA) has experienced unprecedented changes over the last three decades (Smith *et al.*, 2010; Lara *et al.*, 2018; Mohammadzadeh Khani *et al.*, 2022). Recent studies and observations have shown that permafrost (soil or rock at or below 0°C for at least two consecutive years (Williams and Smith, 1989) is warming and thinning over Arctic regions, including the High Arctic (Nelson *et al.*, 2002; International Permafrost Association, 2008; Smith, 2011; Biskaborn *et al.*, 2019). Climatic changes over the previous 50 years led to a reduction in permafrost extent, an increase in permafrost temperature, and an increasing of the active layer thickness (the top layer of soil thawing in summer and refreezing in winter) in multiple locations across the High Arctic (Slater and Lawrence, 2013). Permafrost thawing leads to a deeper active layer, which modifies surface and subsurface hydrology, and impacts aquatic and terrestrial ecosystems and northern traditional lifestyles (Smith *et al.*, 2005). Permafrost thaw creates new freshwater ecosystems, while at the same time modifying the existing lakes, streams, and rivers that are impacted by thaw (Vonk *et al.*, 2015). Active layer deepening also can amplify climate change at a global scale, due to the release of stored soil organic carbon to the atmosphere (Biskaborn *et al.,* 2019).

Although climatic warming is important in driving permafrost thawing and increasing of active-layer thickness (ALT), surface (vegetation and snow) and subsurface conditions (soil) are the main local drivers of the seasonal response of permafrost to climate (Chapin *et al.*, 2005; Jing-Yi, 2018; Lara *et al.*, 2018). In order to accurately project the effects of climate change on permafrost and related ecosystem functions, a good understanding of surface feedback processes and their spatial scales of occurrence is needed, so that these processes may be better represented within models (Aalto *et al.,* 2018; Smith *et al.,* 2022).

The development of a seasonal active layer is a temporally dynamic and spatially heterogeneous process, due to the variation in topography, vegetation and soil conditions (Belshe *et al.,* 2012; Yi *et al.,* 2018). Vegetation in the High Arctic is often dominated by heterogeneous moss and lichen covers, which form an insulating layer overlying the mineral soil (Woo, 2012). During summer, the ground surface is buffered from air temperatures by the vegetation cover that shades and cools the underlying soil. Vegetation also increases the surface roughness (refers to variations in height and irregularities on the surface of the ground), which increases evapotranspiration and further cools the soil (Sturm *et al.,* 2005; Barrere *et al.,* 2017; Van Huissteden, 2020).

While summer climate and surface conditions are key drivers of active layer development, winter preconditioning effects can also be important. Snow cover insulates the ground from cold winter temperatures, which delays cooling of the underlying soil in winter, while in the spring a longer-lasting snow cover delays ground warming and thawing (Goodrich, 1982; Zhang, 2005; Riseborough *et al.*, 2008). In High Arctic tundra landscapes devoid of erect vegetation, the snow cover is thin and continuously redistributed by the wind into topographic depressions, resulting in pronounced snow cover heterogeneity. As such, the micro-relief often represents a substantial fraction of the total snow depth variability (Sturm *et al*., 2005). Microtopography has also been shown to impact the structure and thermal characteristics of the snow and underlying ground (Gisnås *et al.,* 2014).

While the impact of surface conditions (snow, vegetation and soil) on the thaw depth and ground surface temperature (GST) have been well studied at the hillslope scale, (e.g. M. Sturm and Holmgren, 1994; Zhang *et al.*, 2005; Apaloo *et al.,* 2012) the microscale variability has been comparatively less studied although it controls the response of permafrost to climate change at larger scales (Smith and Riseborough, 2002a; Gubler *et al.*, 2011; Gisnås *et al.*, 2014; Porada *et al.*, 2016). There is thus a need to better characterize and understand the spatial interactions between active layer

thermal states and its environmental drivers to better constrain land surface feedbacks on climate-driven permafrost thawing and carbon release (Elmendorf *et al.*, 2012). While process-based models are useful to disentangle climate and land cover impacts on the active layer thickness, statistical modeling represents a useful and alternative step for this purpose (Williams and Smith, 1989). The objective of this study is to assess the influence of environmental conditions (topography, snow, vegetation and soil) on the spatial variability of GST and the thaw depth at two spatial scales (microtopographic and hillslope scales) in a High Arctic tundra landscape.

1.2 Data and methods

1.2.1 Study site

The study area is located in a High Arctic tundra environment on the western plain of Bylot Island, off the northern coast of Baffin Island in Nunavut, Canada (Figure 1-1). The specific site is situated on the hillslope ranging in elevation from 20 to 350 m a.s.l. and underlain by an ~400-m-thick continuous permafrost (Maxwell, 1982). The land surface is comprised of mineral-earth hummocks and low center polygons (Figure 1-1). The prostrate vegetation is relatively diverse for this latitude, with more than 166 vascular plant species and a rich bryophyte flora (Duclos *et al.*, 2006). Wetlands occur generally at lower elevation with both high- and low-centered polygons dominated by sedges (*Carex aquatilis, Eriophorum angustifolium, Eriophorum scheuchzeri*), grasses (*Dupontia fisheri, Pleuropogon sabinei*) and fen mosses (*Drepanocladus* spp.) (Ellis *et al.*, 2008; Pouliot *et al.*, 2009; Perreault *et al.*, 2016). Mesic environments, found across a broad range of conditions including low-centered polygon rims, gently sloping terrain and hummocky tundra, support a more diverse group of species including *Salix* spp., *Vaccinium uliginosum, Arctagrostis latifolia, Poa arctica* and *Luzula confusa* with *Aulacomnium* spp. as dominant moss species (Zoltai and McCormick, 1983).

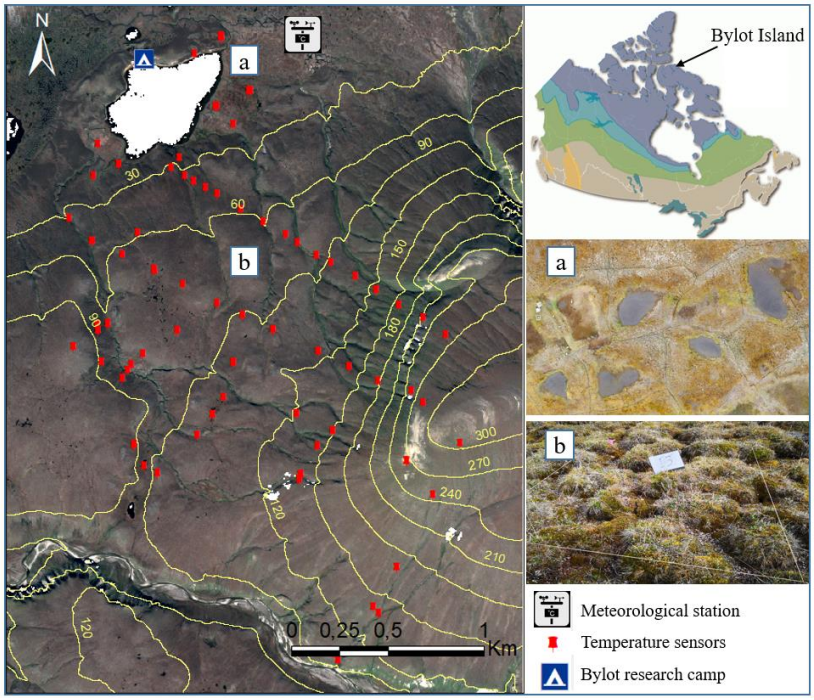

Figure 1-1 Study area and site. Top right: general location of Bylot Island on the Canada permafrost map (Smith, 2010); Left: map of study area showing the location of automatic weather stations and the sites with ground surface temperature sensors. Image source: Pléiades © CNES 2016 Distribution Airbus DS. (a) drone aerial photo of low center polygons; (b) photo of earth hummocks.

The annual mean temperature at the Bylocamp station (Table S1-1), operated by the Center for Northern Studies (CEN), was -15.1°C for the 1981-2010 period, with a noticeable warming trend over the last five decades (CEN, 2021). The annual precipitation over the same period was 191 mm, mostly (76%) falling as snow. The annual average winter snowpack typically reaches 35 to 45 cm and snow accumulation is spatially variable due to topographic heterogeneity and winter snow drifting from predominant easterly winds (Fortier and Allard, 2005; Gagnon *et al.*, 2010).

1.2.2 Air temperature, ground surface temperature and thaw depth measurements

The air temperature was measured at the Bylocamp station during 2016-2018 with an interval of 1 hour and the data was retrieved from Nordicana website (CEN, 2021). GST was measured continuously from 2016-07-01 to 2018-07-01 (730 days) with a network of 100 temperature micro data loggers (Figure 1-1). Loggers were small (< 2 cm) iButtons (DS1922L model) with a 0.5°C accuracy and set at a three hour sampling interval. The loggers were installed at 3 cm below the ground surface (bare soil or moss) to avoid direct insolation during the snow-free season. The moss cover was considered part of the ground rather than part of the vegetation canopy so some of the loggers were recording the temperature inside mosses. The objective of the sampling design was to efficiently distribute the available loggers across the range of elevation and slope aspect and over contrasting morphological features (hummocks, polygons) (Figure 1-1). 18 hummocks and 7 low center ice-wedge polygons were chosen randomly. More loggers were allocated to hummocks as these landforms are predominant at the site. Loggers were deployed at the top and bottom of the hummocks (18 pairs) and on the rims and centers of the polygons (7 pairs). The remaining loggers were distributed over mostly flat terrain (Table S2-2). The position of each logger was recorded with a differential global navigation satellite system (FOIF A30 GNSS) with ± 1 cm accuracy. The loggers were collected on early July 2018 and the ground surface temperature data was retrieved. The second year of data was excluded from the analysis because the loggers were removed in early July 2018, shortening the representation of summer GSTs. Thaw depth (ThawD) were measured twice per season at each logger, in early July and late August using a graduated steel rod. Thaw depths obtained by probing could be affected by the presence of rocks; however extensive soil sampling done in summer 2018 revealed mostly fine-textured soils down to 1 m.

1.2.3 Environmental variables, topoclimatic variables and meteorological data

Environmental variables (including vegetation type and cover, soil moisture and texture, and snow depth) were measured sporadically next to all temperature loggers during summer 2016 and 2017, and snow thickness during late winter 2017 (Table 1-1). The portion of ground covered either by bare soil or vegetation was estimated visually within a 2 m x 2 m plot centred around each logger in summer 2017 using cover classes (0-1, 1-5%, 5-10%, 10-25%, 25-50%, 50-75%, >75%). However just the data from 93 plots were used because 7 loggers were lost and the data around these loggers were no longer useful for any interest analysis in this study. The vegetation cover was measured separately for deciduous shrubs, evergreen shrubs, graminoids, forbs, mosses, lichens and cryptogamic crust. To simplify the statistical analyses, the measured vegetation types were merged into three groups: vascular plants (including deciduous shrubs, evergreen shrubs, graminoids and forbs), mosses, and lichen-cryptogamic crust. The cover per strata was calculated as the sum of the mid class value (Braun-Blanquet, 1932). Vegetation cover can exceed 100 % because some vegetation strata overlap each other inside the plot. The thickness of organic material and moss cover (both dead and live), were measured at each logger location. Near-surface soil moisture (top 10 cm of the soil) was measured twice per season at each logger, in early July and late August using a time-domain reflectometry (TDR) moisture probe (Delta-T HH2, 4% accuracy on volumetric water content). A distinct TDR probe calibration was used for organic and mineral soils, based on a preconfigured probe calibration. Soil texture classes were identified onsite using the manual (‘feel’) method (Rowell, 1994; Burt, 2009). A two-meter resolution digital elevation model (DEM) built from Pleiades stereo images acquired on 28 July 2016 was used to calculate topographic indices across the study site including slope and aspect. The DEM was generated using the Ames Stereo Pipeline (Shean *et al.*, 2016) using the same configuration as a previous study in the Pyrenee mountains in Europe (Marti *et al.*, 2016).

Table 1-1 Environmental variables measured at the logger (j) and site (i) levels.

Variable	Definition	Unit	Range	Measurement method
Alt_j	Altitude	m	20-325	GNSS
Slp_i	Slope	°	0-90	DEM
WE_i	Eastern exposure	-	-1 to +1	sin (aspect)
SN_i	Northern exposure	-	-1 to +1	cos (aspect)
$MicT_j$	Microtopography index: (exposed=1, sheltered=0)	binary	0 or 1	Field interpretation
Rad_i	Mean summer potential solar radiation	WH/m^2	-	ArcGIS
$VegT_j$	Dominant Vegetation type	-	5 types	2x2 meter plot
$VegC_i$	Vegetation cover (moss, vascular plants, lichen and cryptogamic-crust)	%	0 to 100	2x2 meter plot
$MossT_j$	Moss thickness	cm	0 to 5	2x2 meter plot
$SoilMJ_j$	Soil moisture at the beginning of July	%	0 to 100	TDR sensor
$SoilMA_j$	Soil moisture at the end of August	%	0 to 100	TDR sensor
$SoilT_j$	Soil texture	-	6 types	"Feel" method
$ThawD_j$	Thaw depth at the end of August	cm	20 to 150	Steel probe
SD_j	End-of-winter snow depth	cm	20 to 180	Steel probe
SDD_j	Snow disappearance date	day of year	165 to 190	From GST records
SOD_j	Snow onset date	day of year	240 to 255	From GST records
Ta	Air temperature	(°C)	-45 to 22	YSI 44033 sensors (1 hour interval)
$T_{win,\,j}$	Winter ground surface temperature at 3 cm depth	(°C)	-40 to 0	iButtons sensors (3 hours interval)
$T_{sum,\,j}$	Summer ground surface temperature at 3 cm depth	(°C)	0 to 15	iButtons sensors (3 hours interval)

Snow depth was measured continuously at the Bylocamp station (Figure 1-1) by an ultrasonic gauge (Campbell Scientific SR50 with an accuracy of ±1 cm) while GST was measured at 2 cm below the surface by a Campbell Scientific 107 probe. Snow depth was measured by probing at each logger in 2017 close to the approximate time of maximum snow accumulation based on recorded snow depth at Bylocamp station (1-7 May 2017). In addition to end of winter snow depth measurements, the snow disappearance date (SDD) and snow onset date (SOD) were estimated at each micrologger based on the 3-hourly GST records, following the methods from Staub and Delaloye (2016). A full description of snow indices extraction and their calibration and validation is explained in Appendix S1 in supplementary materials. The SOD and SDD were further used to define the summer and winter periods in the statistical analyses. The mean SDD of all the loggers was determined to be the start of the summer season in order to discretize the seasonal ground temperature between summer and winter.

1.2.4 Statistical analyses

1.2.4.1 Microtopographic scale (logger level) analysis

A nonparametric Wilcoxon signed-rank test was applied to test whether significant differences in GST and thaw depth occurred between exposed location (hummock tops and polygon rims) and more sheltered locations (hummock troughs and polygon centers). In addition, a Fisher variance ratio test (F test) was used to compare the within-landform (logger level) versus among landform (site level) spatial variability in GST and thaw depth.

1.2.4.2 Hillslope scale (site-level) analysis

Redundancy analysis (RDA) was used to explore the potential relationships between response variables (summer GST: T_{sum}, winter GST: T_{win} and thaw depth: ThawD) and explanatory environmental variables. RDA finds the multidimensional axes that explain most of the variation in the response variables and that are explained by the independent, spatial environmental variables (Legendre *et al.*, 2012). For sites with paired loggers, GST records from both loggers were averaged in this analysis. Site and variable scores were displayed on triplots using 'type-II scaling', emphasizing the correlative relationships between variables (Ter Braak, 1994). The significance of the overall RDA model and individual RDA axes was assessed with a permutation test (Legendre *et al.*, 2011). Prior to RDA, all numerical variables were transformed to a normal distribution using square root and log transformations and then centred to their means (Legendre *et al.*, 2012).

1.2.4.3 Multilevel analysis

The spatial variables which affect the ground surface temperature and thaw depth were explored using multilevel regression models, or 'mixed models' (Zuur *et al.*, 2010). Multilevel models account for grouping in observations; these grouping variables are known as random effects and can account for correlation in residuals within the groups (Pinheiro and Bates, 2000). In this study, each logger represents an observation which can be grouped within a site, i.e. where pairs of loggers were installed within periglacial landforms. Random-intercept multilevel models were thus developed to predict GST and thaw depth from spatial environmental variables (fixed effects) with the site as grouping variable (or "random effect") using the lme4 package in R (Crawley, 2010). The same data transformations and standardization used for RDA were applied on the predictor variables in order to compare their relative contribution within the models. Because our data include binary variables, the continuous variables were scaled by

twice the standard deviations so that the range of continuous variables is more similar to the range of binary variable (Gelman and Hill, 2018). Multicollinearity was assessed with the variance inflation factor (VIF) and pairwise correlations amongst predictors (Cohen, 1977). Predictors with a VIF larger than 10 or a pairwise correlation greater than 0.7 were flagged as collinear and discarded from the multilevel analysis. A model was developed for each dependent variable, i.e. T_{sum}, T_{win} and the maximum thaw depth, as measured in late August. A full model was first constructed using all fixed and random effects. This global or 'beyond optimal' model was then simplified by sequentially removing non-significant predictors ($p < 0.05$) (Zuur *et al.*, 2010). Conditional and marginal pseudo coefficients of determination (R^2) were used to evaluate model fit. The marginal pseudo-R^2 reflects the proportion of variance explained by the fixed environmental effects only, while the conditional pseudo-R^2 also includes the random (site) effect (Nakagawa, Johnson, *et al.*, 2017). Model residuals were analysed to check model assumptions for normality, homogeneity of variance and independence. Table 1-1 lists all the variables used within the RDA and multilevel analyses.

1.3 Results

1.3.1 Variations of ground surface temperature, thaw depth and environment variables

The mean daily air temperature at the Bylocamp station varied between -45 °C and 1 °C in winter and between -1 °C and 18 °C during summer for hydrological year of 2016-2017 (1st September to 31st August). The mean daily ground temperature varied across the sites from -18°C to -6 °C during winter and from 2.7 °C to 11.8 °C during summer (Figures 1-2 and S1-3). The thaw depth probed in August varied from 20.5 cm to 80 cm across sites. The snowpack typically started to accumulate in early September and melted out by mid-June (Figure 1-2). The total vegetation cover over our 93 plots

throughout the landscape varied from 34 to 145% with 3 to 88% for mosses and 3 to 63% for vascular plants (Figure S1-1).

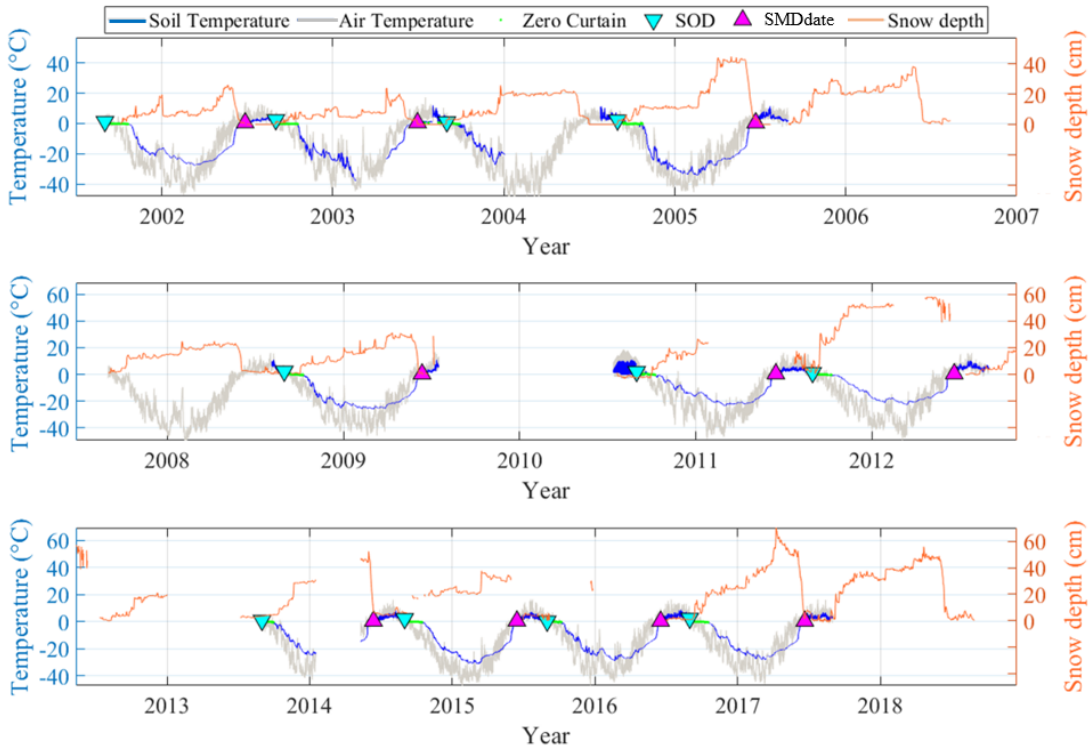

Figure 1-2 Air and ground temperature records at the Bylocamp station. The snow onset dates (SOD) and snow disappearance dates (SDD) were calibrated on the ground temperature records during 2002-2008 period and validated during 2009-2018. The brown line represents daily snow height, the blue line represents ground surface temperatures, and the grey line represents daily air temperature with a three-hour interval. The estimated SOD and SDD are indicated as cyan and purple triangles, respectively, while green dots indicate zero-curtain (ZC) periods.

Moss thickness varied from 1.8 to 4.5 cm. Snow accumulation reached a maximum of 70 cm on May 10th of 2017 at the Bylocamp weather station, while end-of-winter snow depths varied between 17 cm and 156 cm across the logger sites. This strong spatial variability in snow depth reflects the influence of blowing snow redistribution. The

snowmelt period was short, typically lasting two weeks (Figure 1-2). After applying calibrated and validated thresholds (explained at section 1.2.4) on the later Bylocamp record (2009-2018), the spatial variability of the SOD across sites (standard deviation = 13 days) was found to be larger than that of SDD (9 days).

1.3.2 Microscale variability in GST

No significant difference in annual GST was found between exposed and sheltered locations for hummocks (median difference between tops and bottoms = 0.22 °C, p = 0.38) and polygons (median difference between rims and centers = 0.74 °C, p = 0.06) (Table 1-2). However, significant seasonal differences were found for hummocks, with the exposed tops being colder than the sheltered bottoms in winter (median difference = 0.60 °C, p = 0.01), and warmer than the bottoms in summer (median difference = 1.95 °C, $p < 0.001$) leading to significantly deeper thaw depths on hummock tops compared to bottoms (by 13.2 cm, $p < 0.001$) while no difference was found in GST within polygons at the seasonal scale, yet, thaw depth was significantly deeper in the centers compared to the rims (by 13.7 cm, p = 0.01, Table 1-2).

The spatial variability in mean annual GST at hummocks sites was significantly greater among sites than within the hummocks (F = 0.07, $p < 0.001$), while there was no significant difference for polygons (F = 0.68, p = 0.211) (Table 1-2). In winter, the GST for hummocks was found to be more variable among sites than within the hummocks (F = 0.45, $p < 0.001$) but this pattern reversed in summer:

Table 1-2 Annual and seasonal ground surface temperature (GST) and maximum thaw depth (ThawD) within and among dominant microscale landforms. Differences in GST and thawD between exposed (hummock tops and polygon rims) and sheltered (hummocks bottoms and polygon centers) locations were assessed with the Wilcoxon sign rank test. The spatial variability of GST and thawD was partitioned into within and among landform variability and the variance ratio (within/among) tested with the Fisher variance test (F-test).

Wilcoxon test								
Period	Median: hummocks (*n:18*)			Median: polygons (*n:7*)				
	top	bottom	*p* value	rim	center	*p* value		
Annual GST (°C)	-11.4	-11.2	0.38	-11.5	-10.7	0.06		
Winter GST (°C)	-15.4	-14.8	0.01	-15.7	-14.6	0.69		
Summer GST (°C)	5.2	3.3	< 0.001	4.5	6	0.16		
ThawD (cm)	37.6	24.4	< 0.001	23.3	37.0	0.015		
Fisher test								
	Standard deviation: hummocks (*n:18*)				Standard deviation: polygons (*n:7*)			
Period	Within	Among	F	p	Within	Among	F	p
Annual GST (°C)	0.27	1.04	0.07	<0.001	0.67	0.81	0.68	0.211
Winter GST (°C)	0.45	1.24	0.13	<0.001	0.96	0.67	2.05	0.069
Summer GST (°C)	1.02	0.83	1.51	0.2	0.73	1.22	0.36	0.018
ThawD (cm)	8.7	9.8	0.78	0.62	8.2	8.0	1.04	0.96

GST varied slightly more at the microscale (within hummocks) than at the hillslope scale, where the difference between the warmer tops and colder bottoms can be ascribed to micro topographic shading and differences in soil moisture. For polygons, GST varied more among sites in summer (F = 0.36, p = 0.018) but more within polygons in winter (F = 2.05, p = 0.069). The variability in thaw depth was similar at the microscale and hillslope scale for both polygons and hummocks (Table 1-2). These results show that at the seasonal scale, the microscale (within-site) variation can surpass variability at the hillslope scale.

1.3.3 Hillslope scale (site-level) heterogeneity analysis

The RDA results for September 2016 to August 2017 are shown in Table 1-3 (the second year of data was excluded from the analysis because the loggers were removed in early July 2018, shortening the representation of summer GSTs). Results from the RDA showed that 61.1% of the variation in the response variables (Twin, Tsum, and ThawD) at the site level was constrained by the variation of the environmental variables in the first three axes (Table 1-3). However, the permutation tests showed that only the first two RDA axes were significant (p < 0.001), respectively accounting for 37.1% and 16. 9% of the variance of the dependent variables. The first two RDA axes clearly separate the site scores and explanatory variables according to processes associated with the winter (Axis 1) and the summer (Axis 2) seasons (Figure 1-3, Table 1-3 and Table S1-4). However, the variance of the two dominant axes (54%), showed that site-level GST and thaw depth variability is not entirely explained by the existing environmental variables.

Table 0-3 Results from the redundancy analysis (RDA) of the inter-site spatial variability of thaw depth and summer and winter GST**.**

Partitioning of correlations						
	Variance	Proportion				
Total	3	1				
constrained	1.836	0.6118				
Unconstrained	1.164	0.3882				
Eigenvalues, and their contribution to the correlations						
	RDA1	RDA2	RDA3	PC1	PC2	PC3
Eigenvalues	0.278	0127	0.053	0.185	0.065	0.041
Proportion Explained	0.371	0.169	0.071	0.246	0.087	0.055
Cumulative Proportion	0.371	0.54	0.611	0.858	0.945	1
Accumulated constrained eigenvalues						
	RDA1	RDA2	RDA3			
Total	0.278	0127	0.053			
constrained	0.606	0.277	0.116			
Cumulative Proportion	0.606	0.883	1.00			
Response variable scores	RDA1	RDA2	RDA3	PC1	PC2	PC3
Thaw depth	1.297	-0.116	-0.402	0.126	0.346	0.547
T_{win}	-0.559	0.75	-0.438	1.01	0.41	-0.216
T_{sum}	-0.746	0.765	0.369	0.819	0.556	0.18

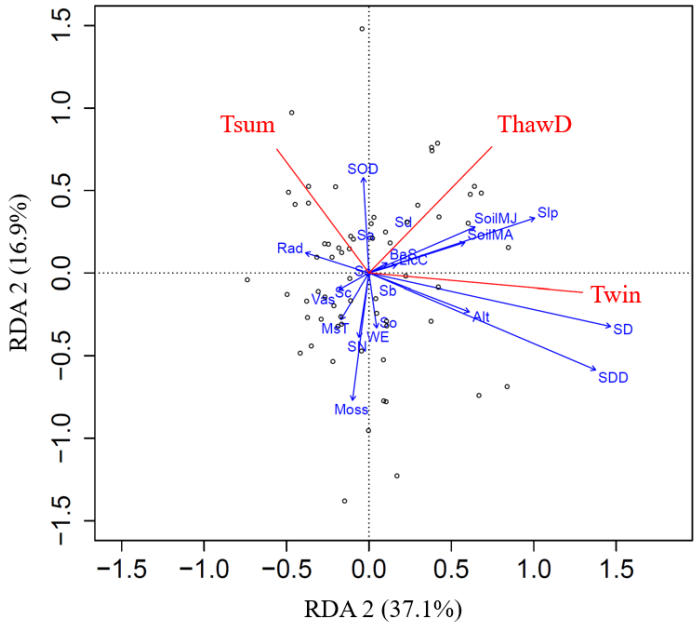

Figure 1-3 Triplot for RDA1 and RDA2 axes. Red arrows: dependant variables (winter ground temperature (T_{win}), summer ground temperature (T_{sum}), Thaw depth (ThawD)); blue arrows: independent variables; dots: site scores. The angles between arrows reflect the linear correlation between variables. Soil type (S) are: Sa: gravely soil, Sb: sandy soil, Sc: sandy loam soil, Sd: loamy soil, Se: clay soil, So: peat soil. Snow cover indices are snow onset date (SOD), snow disappearance date (SDD) and snow depth (SD). Vegetation parameters moss thickness (MsT), moss cover (Moss), vascular plants (Vas). Topographic parameters include solar radiation (Rad), northern exposure (SN), and eastern exposure (WE).

Axis 1 is characterized by positive relationships of T_{win} with snow depth (SD), snow disappearance date (SDD), and slope (Slp), and to a lesser extent July and August soil moisture (SoilMJ and SoilMA) while also showing a weak inverse relationship with solar radiation (Rad) (Table 1-3 and Figure 1-3). The small but positive effect of altitude on T_{win} results in the valley bottom being colder than upslope areas in winter (Figure S1-2). Hence, the spatial heterogeneity of Twin is primarily controlled by the spatial variability of the late-winter snow depth, and by solar radiation.

Axis 2 is mainly defined by negative relationships between summer ground surface temperature (T_{sum}) and moss thickness (MossT), moss cover, and WE and SN aspect (Figure 1-3). Hence, a thicker and more extensive moss layer promoted cooler soils in summer. T_{sum} is also positively correlated, albeit weakly, with solar radiation, and negatively correlated with altitude and snow depth. Hence colder air temperatures promoted cooler soils at higher elevation in summer (Figure S1-2). The negative correlation between Tsum and snow depth shows that sites with thicker snowpacks tended to be cooler in summer.

ThawD is loaded positively both on the 'winter' (RDA1) and 'summer' (RDA2) axes (Figure 1-3), suggesting that both winter processes and summer conditions influenced thaw depths. Thaw depth notably displays a positive correlation with early and late summer surface moisture, with greater thaw depth occurring at wetter sites (Figure 1-3). Sites with greater thaw depths were also associated with increased topographic slope, as well as thinner moss cover and lower vascular and moss vegetation cover (Figure 1-3). Solar radiation was poorly correlated with all three RDA axes, and no clear influence of soil type on GST or thaw depth was found (Table S1-4 and Figure 1-3).

1.3.4 Multiscale environmental control on thaw depth and seasonal GST

The preliminary collinearity test identified three redundant potential predictors, namely SDD (collinear with SD), measured soil moisture in July (SoilMJ: collinear with measured soil moisture in August) and SN (collinear with solar radiation) (Figure S1-4). SN and SoilMJ were dropped, while SDD was dropped for the T_{win} model, but kept for the T_{sum} model since it is more physically linked with summer GST than SD. The model selection procedure described in the method section led to the following final models for each response variable:

$$T_{win,\,j} = \alpha_{i\,[j]} + \beta_1 SD_j + \beta_2 Slp_i + \beta_3 BareSoil_i + \beta_4 site_i + \varepsilon_{ij} \quad (1.1)$$

$$T_{sum,\,j} = \alpha_{i\,[j]} + \beta_1\,Alt_j + \beta_2\,SDD_j + \beta_3\,MsT_j + \beta_4\,MicT_j + \beta_5\,LicCr_i + \beta_6\,BarSoil_i + \varepsilon_{ij} \quad (1.2)$$

$$ThawD_j = \alpha_{i\,[j]} + \beta_1\,SoilMA_j + \beta_2\,Slp_i + \beta_3\,MsT_j + \beta_4\,site_i + \varepsilon_{ij} \quad (1.3)$$

Where α represents the intercept, β the regression slopes of each variable, εij is random errors, and i and j refer to site and logger respectively. Model (1) explained 80.3% of the variance of Twin across all sites (conditional R2), from which 66.6% is explained by fixed effects (marginal R2) and 13.7% by random (site) effects (Table 1-4). The variance of the random effect ($\tau00 = 0.05$) is small, which indicates limited random variation among sites, while the residual variance ($\sigma2 = 0.07$) shows only slightly larger unexplained variation within sites. Consequently, the intra-class correlation (Nakagawa, Paul C D Johnson, *et al.,* 2017) was moderate (ICC = 0.41), reflecting moderate clustering among paired observations within sites. These results show that the microscale (landform scale) heterogeneity in T_{win} is well explained while some of the inter-site (hillslope scale) variability remains unexplained by the environmental variables. Model 1 shows that spatial variations in snow depth exert the strongest influence on the ground surface temperature, with a thicker snowpack leading to warmer soil temperatures in winter (Figure 1-4a and Table 1-4). Increasing topographic slope also resulted in warmer soil temperatures (Figure 1-4b and Table 1-4). Increasing bare soil exposure led to small, but still significant soil cooling in winter (Figure 1-4c and Table 1-4).

Table 1-4 Parameter estimates and statistical significance for the fitted multilevel models of winter (T_{win}) and summer (T_{sum}) ground surface temperature, and thaw depth (ThawD). Only the potential predictors from Table 1 that were found to be statistically significant in at least one model are reported in this table. σ^2 is the residual variance, τ_{00} is the variance of the random effect, ICC is the intra-class correlation and N represent number of sites.

	T_{win}			T_{sum}			ThawD		
Predictors	**Est**	**CI**	**p**	**Est**	**CI**	**p**	**Est**	**CI**	**p**
Intercept	1.93	1.85 – 2.02	<0.001	0.96	0.86–1.06	<0.001	6.12	5.68 – 6.56	<0.001
SD	0.9	0.73 – 1.08	<0.001						
SDD				-0.28	-0.47 to -0.09	0.004			
Bare soil	-0.18	-0.35 – -0.01	0.037	0.24	0.03–0.45	0.025			
Altitude				-0.34	-0.56 to -0.13	0.002			
Slope	0.19	0.0 – 0.38	0.047				0.79	0.35 – 1.22	<0.001
Microtopography				-0.41	-0.63 to -0.18	0.001			
Soil moisture							0.44	0.03 – 0.84	0.0.34
Lichen-cryptogamic crust				-0.24	-0.45 to -0.02	<0.033			
Moss thickness				-0.31	-0.5 to -0.11	0.003	-0.96	-8.5 – -3.6	<0.001
Random Effects									
σ^2 / τ_{00}		0.07/0.05			0.14/0.01			0.64/0.05	
ICC		0.41			0.08			0.08	
N(sites) / Observations		63/81			63/81			63/81	
Marg R^2/ Cond R^2		0.666/0.803			0.417/0.464			0.465/0.505	

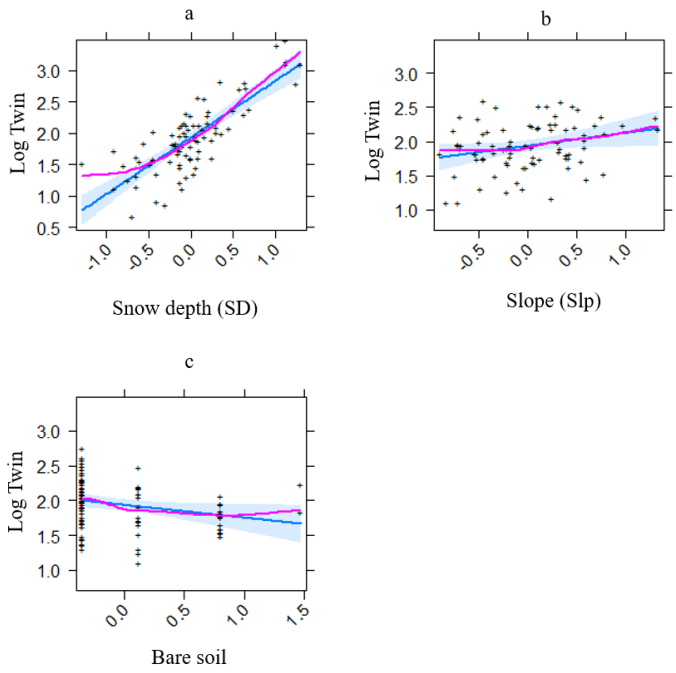

Figure 1-4 Partial residual plots for the main effects of the winter ground temperature (Twin) multilevel model. The x - axis represents the environmental variables (standardized scale) and the y - axis the log-transformed response variable (Twin). Shaded areas delineate the 95% confidence bands. (a) Snow depth (SD); (b) slope angle; (c) bare soil. The blue line shows the expected residuals if the relationship between the predictor and response variable was linear. The pink line shows the actual residuals.

Model 2 explained 46.4% of the variance of T_{sum} (conditional R^2), from which 41.7% was explained by fixed effects (marginal R^2) and 4.7% by random (site) effects (Table 1-5). The inter-site (hillslope scale) variability in T_{sum} was well explained by the environmental variables (τ_{00} = 0.01). Also comparatively large microscale (landform scale) heterogeneity was explained (σ^2 = 0.14, ICC = 0.08). Partial residual plots in Figure 1-5 show that microtopography was the dominant variable that had a negative effect on T_{sum} (Figure 1-5c and Table 1-4) so that exposed locations ($MicT_j$ = 0: hummock tops and polygon rims) tended to be warmer than sheltered locations ($MicT_j$

= 1: hummock bottoms and polygon centers). As expected, increasing altitude favoured cooler T_{sum} (Figure 1-5f, Table 1-4). Moss thickness had a negative influence on T_{sum}, so that a thicker moss cover favoring soil cooling in summer (Figure 1-5a and Table 1-4). An inverse relationship is also observed between the snow disappearance date and T_{sum}, so that longer-lasting snowpacks led to cooler summer ground surface temperature (Figure 1-5b and Table 1-4). While increasing lichen-cryptogamic crust cover led to soil cooling in summer (Figure 1-5e and Table 1-4), increasing bare soil exposure led to warming T_{sum} (Figure 1-5d).

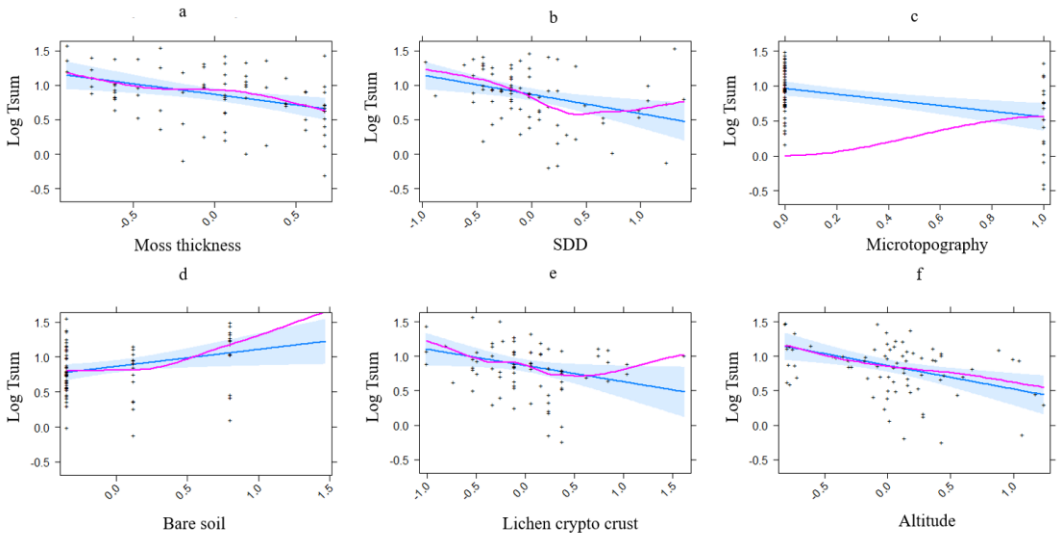

Figure 1-5 Partial residual plots for the main effects of the summer ground temperature (Tsum) mixed model. The x - axis represents the environmental variables (standardized scale) and the y - axis the log-transformed response variable (Tsum). Shaded areas delineate the 95% confidence bands. (a) Moss thickness; (b) SDD; (c) microtopography (d) bare soil; (e) lichen-cryptogamic crust; (f) altitude. The blue line shows the expected residuals if the relationship between the predictor and response variable was linear. The pink line shows the actual residuals.

Model 3 explained 50.5% of the variance of thaw depth (conditional R^2), from which 47.2% was explained by fixed effects (marginal R^2) and 3 % by random (site) effects

(Table 1-5). The inter-site (hillslope scale) variability in thaw depth was adequately explained by the environmental variables (τ_{00} = 0.05, ICC = 0.08) but significant microscale (within landform) heterogeneity remained unexplained (σ^2 = 0.64). Moss thickness was the dominant variable influencing thaw depth, with increasing moss thickness causing shallower thaw depths (Figure 1-6c and Table 1-4). Greater surface moisture in August and increasing topographic slope resulted in deeper thaw depths (Figure 1-6b-a and Table 1-4).

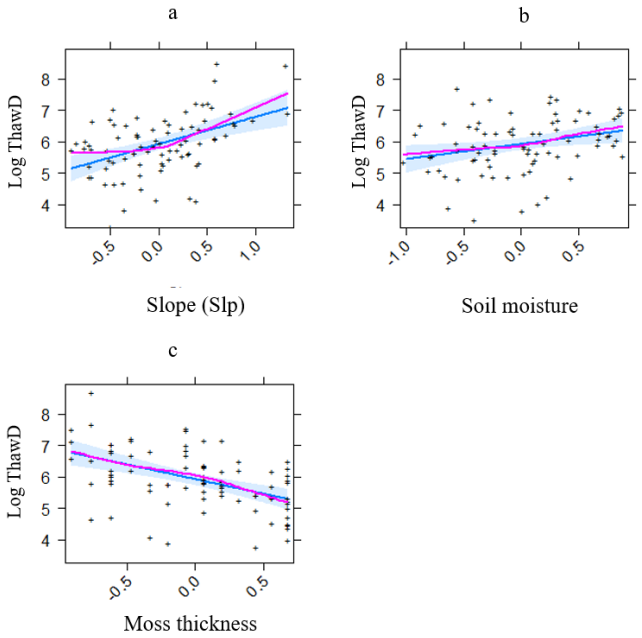

Figure 1-6 The partial residual plot of the main effects for thaw depth mixed model. The x - axis represents the environmental variables and the y - axis the response variable (thaw depth). Colorful areas indicate confidence band (0.95). (a) Moss thickness; (b) soil moisture; (c) slope angle. The blue line shows the expected residuals if the relationship between the predictor and response variable was linear. The pink line shows the actual residuals.

1.4 Discussion

1.4.1 Scale-dependent variability of ground surface temperature and thaw depth

Our results showed that GST and thaw depth can vary over short distances in response to surface morphology and associated biophysical conditions. This is similar with previous findings in alpine environments such as in the eastern Swiss Alps, where mean annual GST differences up to 2.5 °C were reported over distances less than 14 m in homogeneous terrain (Gubler *et al.*, 2011). We found greater differences over even shorter distances (less than 1 m) across hummocks and polygons. Despite the significant heterogeneity of GST within these landforms, differences in mean annual GST were still larger at the hillslope scale (up to 9.2 °C over the elevation range of 320 m), which is also more than previously reported elsewhere for tundra environments, such as in Trail Valley Creek in the northwestern Canadian Arctic (up to 4 °C within a 0.5 km^2 area) (Grünberg *et al.*, 2020), in the Low Arctic Torngat Mountains of Labrador (up to 5 °C over an elevation ranges of 420 meters) (Davis *et al.*, 2021), at Ny-Ålesund, in Svalbard (up to 5.1 °C over an elevation range of 500 m) (Gisnås *et al.*, 2014) and over a High Arctic landscape at Cape Bounty, Nunavut (up to 8 °C over an elevation range of ~150 m in the study area with the lowest elevation located along the coast) (Garibaldi *et al.*, 2021). This hillslope-scale heterogeneity found in this study is also greater than that reported in mid-latitude mountains, such as the Swiss Alps (up to 6 °C within an elevational band of 300 m) (Gubler *et al.*, 2011) and the Chilean Andes (up to 5 °C) (Apaloo *et al.*, 2012). This difference can be due to high snow drifting in the windswept and treeless tundra environment of Bylot Island (Gisnås *et al.*, 2014). The large spatial heterogeneity in GST and thaw depth at the micro- and hillslope scales across our study site implies that it must be carefully considered in field sampling designs as well as in remote sensing and modeling studies of tundra land surfaces.

1.4.2 Environmental controls on GST and thaw depth

Spatial variations in winter GST were more pronounced at the hillslope scale than at the micro (landform) scale, with differences up to 11.6 °C among landforms and up to 3.7 °C within landforms. This is due to the large heterogeneity in snow depth at the hillslope scale resulting from blowing snow over the exposed tundra landscape, whereas microtopographic depressions become quickly filled by snow. This difference (11.6 °C) is greater than those previously reported, e.g. 7.2 °C at Imnavait Creek in Alaska (Matthe Sturm and Holmgren, 1994) and 6.3 °C at Samoylov in the Lena River delta, Siberia (Gouttevin *et al.*, 2018) due to snow cover spatial heterogeneity. A direct preconditioning effect of the snow cover disappearance date on summer GST was also found from both the hillslope (RDA) and multiscale analyses (Figures 1-3 and 1-5, Table 1-4). This finding is important and corroborates recent modeling studies that showed ground surface temperatures to be sensitive to shifts in snow timing (Jan and Painter, 2020; Rixen *et al.*, 2022). Also, Lafrenière and Lamoureux (2013) found a weak but significant inverse correlation between ALT and snow depth on Melville Island, in the Canadian High Arctic. This is due to the contrasting effects of snow cover on ALT, where the warming effect in winter (insulation) can be offset by delayed ground thawing in spring under a thicker snow cover (Park *et al.*, 2015).

While snow cover conditions dominated the spatial variability of winter GST and also impacted summer GST, vegetation conditions were the primary driver of the spatial variability of thaw depth and also showed a significant contribution to the spatial variability of summer GST. Despite its prostrate stature, the tundra vegetation cover had a buffering effect on ground surface temperature, i.e. reducing heat loss in early winter and reducing heat gains in summer over vegetated soils (Heijmans *et al.*, 2022). Moss cover and its thickness had the strongest effect on thaw depth, consistent with the known insulating effect of dry mosses (Turetsky *et al.*, 2012; Voortman *et al.*, 2014; Hrbáček *et al.*, 2020). While the summer cooling effect of mosses was apparent in the

hillslope scale RDA analysis, it was less important than vegetation cover (mostly moss cover and to a lesser extent vascular plant cover) (Figure 1-3). However, moss thickness was the most important predictor of thaw depth and one of main variables that determined the spatial variability of summer GST at the multilevel scale (Table 1-4, Figure 1-5 and 1-6). This highlights the strong spatial heterogeneity of vegetation at the landform scale and its impact on the ground surface temperature and moisture regime. For example, on mesic slopes, the sheltered and shaded hummock troughs had colder ground temperature and shallower thaw depths (Table 1-3). Cooling in hummock troughs promotes moisture accumulation and favorable conditions for moss growth, which further insulate the soil and promote ice-rich and shallower active layers (Figure S1-1). Unlike a previous study conducted in the boreal forest, the vascular plant cover did not emerge as an important predictor (Williams *et al.*, 2020). This is due to the low biomass and lower leaf area index of vegetation in the Arctic environment (Garibaldi *et al.*, 2021). An increased cover of lichen-cryptogamic crusts also led to small soil cooling in summer, similar to previously published results that simulated a cooling effect from lichens in the pan-Arctic region (Porada *et al.*, 2016).

Previous studies in Alaska and Northwest Territories of Canada found that soil moisture modulates the cooling effect of moss thickness on soils (O'Donnell *et al.*, 2009; Fisher *et al.*, 2016). In our case, soil moisture did not emerge as a significant predictor of summer GST both at the site-level (Figure 1-3) and multilevel (Figure 1-4) scales. Even though soil moisture did not emerge as a significant predictor of summer GST, it significantly promoted thaw depth (Table 1-4, Figure 1-6). This is similar to previous findings in the tundra of Trail Valley Creek, where soil moisture was found to promote permafrost thawing (Grünberg *et al.*, 2020). Studies conducted further south in the boreal forest also reported soil moisture to have a strong controlling influence on the soil thermal regime (Fisher *et al.*, 2016; Williams *et al.*, 2020). However, unlike the boreal forest where soil moisture was controlled by the balance between evapotranspiration and precipitation, soil moisture at our tundra site, as at the

Trail Valley Creek site (Grünberg *et al.*, 2020), appeared to be largely controlled by the snow thickness, slope position and microtopography, and not by evapotranspiration losses from vegetation, due to the low biomass (Figure S1-1). A contradictory effect of soil moisture on thaw depth was observed regarding microtopography effect. While in the open surfaces, an increase in soil moisture led to an increase in soil thermal conductivity and depth of thawing in shaded areas (Micro-topographic depressions induced by cryoturbation processes), an increase in soil moisture resulted in increased moss growth and moisture accumulation (Figure S1-5), leading to enhanced insulation provided by the moss structure which decreased the latent heat transfer between the ground surface and air temperature. The contradictory effect of soil moisture on thaw depth is consistent with a previous study in Alaska and Canada which found that while increased soil moisture increases soil thermal conductivity, which leads to deeper active layers, it also increases the latent heat of vaporization for thawing (Clayton *et al.*, 2021).

When considering the microscale variability in the multilevel models, bare ground cover emerged as a significant, albeit weak, positive predictor of GST: in winter, increased exposure of bare soil led to small cooling, while the reverse occurred in summer, i.e., warming over bare soils (Table 1-4, Figures 1-4 and 1-5). This finding is similar to those reported from the McMurdo Dry Valleys of Antarctica (Lacelle *et al.,* 2016) where GSTs were found to be warmer than air temperature in summer due to solar heating of the bare ground surface, while GST were cooler than the air in winter.

The primary topoclimatic variables controlling the surface energy balance in summer (altitude and solar radiation) had a moderate effect on summer GST at hillslope scale while altitude was one of main variables determining the spatial variability of summer GST at microscale. As expected increasing altitude led to cooler ground surface temperature during summer. This is similar study in a valley in the Andes of Santiago (Apaloo *et al.*, 2012) that highlighted the altitude as the main factor determining the

GST spatial variability, however in current study it seems that strong effect of the altitude was moderate by snow depth (during winter) and microtopography and vegetation (during summer). The effect of solar radiation has been shown to be modified significant by mictorotopography and the presence of moss due to their shading and insulation effect on the ground. For example a study conducted in the Quartermain Mountains, Antarctica (Lacelle *et al.*, 2016) suggested that solar heating largely determines summer ground surface temperatures in the bare landscape, unlike the Arctic and boreal forest, where vegetation, surface organic layer, snow cover and/or moist active layers significantly influence the relations between atmospheric and ground thermal conditions through the surface and thermal offsets (Smith and Riseborough, 2002b; Fisher *et al.*, 2016; Way and Lewkowicz, 2017).

1.5 Conclusion

This research provides a multivariable assessment of environmental effects on the ground surface temperature and thaw depth in a typical High Arctic tundra environment at Bylot Island, Nunavut, Canada. Our results revealed that seasonal GST and thaw depth are highly heterogeneous, varying over short distances due to microtopography related to hummocks and ice-wedge polygons. The microscale (within-landform) variability in GST and thaw depth was large and sometimes surpassed the variability at the hillslope scale. Late-winter snowpack thickness was found to be the prime control of winter soil temperatures due to the highly heterogeneous snow cover caused by blowing snow in this open tundra landscape. This thermal effect was found to carry over in summer through the cooling effect from a delayed snowpack disappearance. However, a variety of environment controls determined the spatial variability of summer GST and thaw depth patterns. The microscale biophysical diversity exerted a larger influence on the spatial heterogeneity of summer GST and active layer depth, compared to winter GST. In winter, the hillslope scale variability in snow depth was greater than at the microscale, due to landforms rapidly filling with snow.

Our results highlight the importance of considering surface feedback effects in future projections of active layer thermal conditions within heterogeneous tundra landscapes. Our results also underscore the importance of accurately simulating the snow cover in future climate projections in order to properly capture the impact of snow depth and snow cover duration on permafrost temperature and thawing. Given the formidable spatial heterogeneity of the snow cover in Arctic tundra landscapes, this is still a challenging task for large scale models. On the other hand, future increases in vegetation productivity could counteract warming-induced active layer deepening in summer, but this simple extrapolation hides the significant microtopographic heterogeneity of High Arctic tundra environments and associated plant communities: the affinity of mosses for shaded and wet depressions exerts a dominant influence on soil temperature and thaw depths in summer. The evolution of moss cover under future climates remains a key component of active layer development in High Arctic tundra landscapes.

Acknowledgments

This research was funded by the Natural Sciences and Engineering Council of Canada, grant numbers RGPIN-2015-03844 (C. Kinnard) and RGPIN-2015-05319 (E. Lévesque), the Canada Research Chair program, grant number 231380 (C. Kinnard) and the Centre de Recherche sur les interactions Bassins Versants Écosystèmes Aquatiques (RIVE) (H. Mohammadzadeh Khani). Logistical support was provided by the Polar Continental Shelf Program (Natural Resources Canada). Support from the Community of Pond Inlet, Parks Canada and the Centre d'Études Nordiques (CEN) is acknowledged. We thank Prof. Gilles Gauthier for his logistical management of the research camp, and Maria Peter, Matthieu Loyer, Denis Sarrazin and Audrey Roy for their participation in fieldwork.

Supplementary materials

Table S1-1 Hourly meteorological data available from the permanent SILA weather station network (station locations are shown in figure 1-1).

Meteorological stations	Longitude and Latitude	Altitude (m)	Air Temperature	Soil Temperature	Snow depth
BYLOSIL	X = 73° 09' 07.9" Y = 79° 59' 18.9"	24	2004-2018	2004-2018	2004-2018
BYLJACK	X = 73° 08' 25" Y = 79° 55' 17"	312	2001-2018	2006-2018	-------
BYLCAMP	X = 73° 09' 21.6" Y = 79° 57' 24.8"	24	1993-2018	1993-2018	2001-2018

Table S1-2 Details on logger location and their number in terms of their location and data retrieval.

year/location	Polygons		Hummocks		flat ground	recovered data
	Rim	Center	top	bottom		
2017	7	7	18	18	50	93
2018	7	7	18	18	31	81

Table S1-3 Estimated and observed SOD and SDD for the validation period at Bylocamp station. n/a indicates years with missing data at the meteorological station due to sensor malfunction and mm/dd represent month and day of year. Delta refers to difference between observed and estimated SOD and SDD.

	SOD			SDD		
Hydrological year	Estimated (mm/dd)	Observed (mm/dd)	Delta (day)	Estimated (mm/dd)	Observed (mm/dd)	Delta (day)
2008-2009	09-12	09-14	-2	06-12	06-10	+2
2010-2011	09-09	09-07	+2	06-15	n/a	-
2011-2012	09-02	09-05	-3	06-17	06-14	+3
2012-2013	09-15	09-17	-2	06-16	n/a	n/a
2013-2014	09-02	09-05	-3	06-13	06-14	-1
2014-2015	09-10	09-09	+1	06-15	n/a	n/a
2015-2016	09-01	n/a	n/a	06-17	n/a	n/a
2016-2017	09-03	09-06	-3	06-21	06-20	+1
2017-2018	09-08	09-09	-1	06-21	06-23	-2
Mean			-1.38			0.60
RMSE			2.26			1.78

Table S1-1 Biplot scores of RDA for constraining variables.

Variables	RDA1	RDA2	RDA3
Altitude	0.34	-0.22	0.578
Slope	0.59	0.09	0.43
WE	0.01	-0.17	-0.26
Solar Radiation	-0.22	0.09	-0.01
Soil texture B	0.18	-0.19	0.01
Soil texture C	-0.21	-0.13	0.12
Soil texture D	0.15	0.16	0.27
Soil texture E	-0.08	-0.08	-0.53
Soil texture O	0.05	-0.16	0.01
Vegetation type B	0.08	0.18	-0.18
Vegetation type C	-0.02	-0.29	0.11
Vegetation type D	0.22	0.15	-0.27
Vegetation type E	-0.24	-0.37	0.17
Vegetation cover	-0.19	0.15	-0.26
Moss thickness	-0.11	-0.15	0.21
Soil moisture July	0.38	0.14	-0.29
SOD	0.13	0.28	-0.52
Snow depth (SD)	0.84	-0.26	-0.28

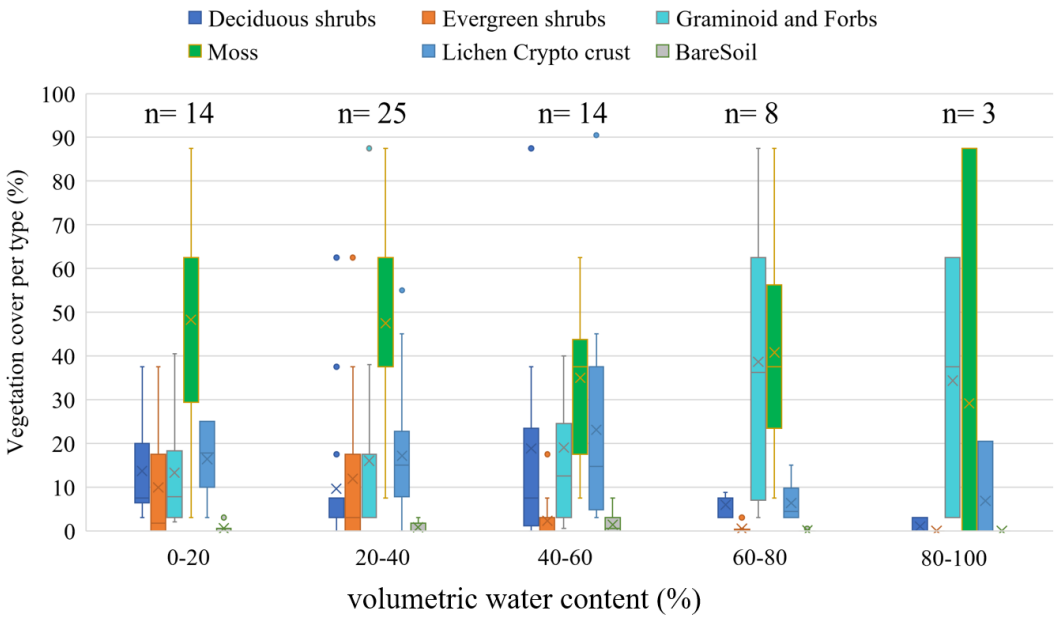

Figure S1-1 Vegetation coverage for each type regarding different level of soil moisture.

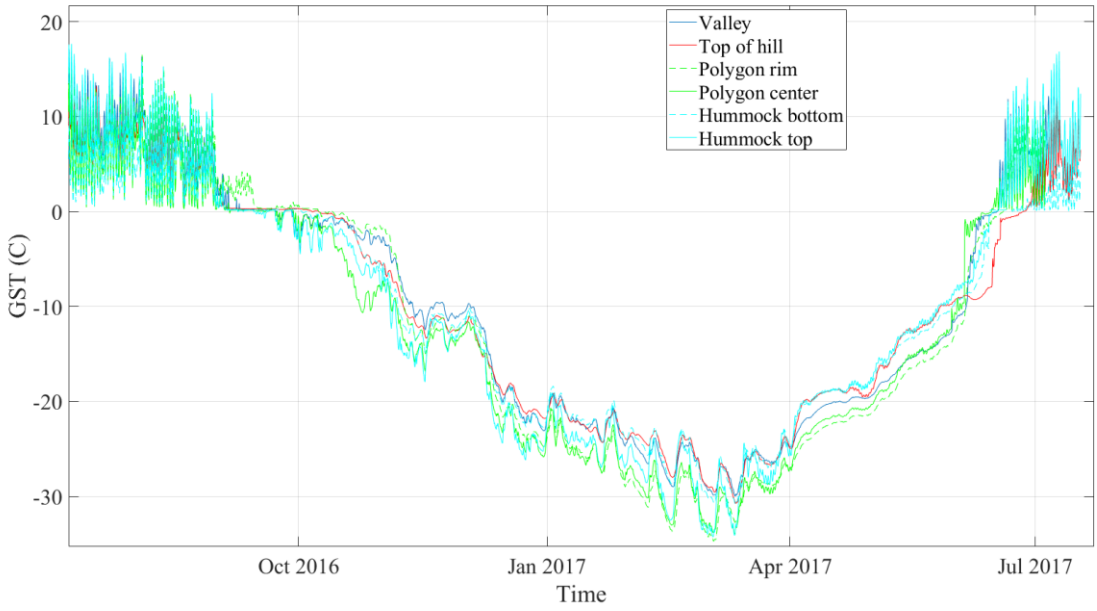

Figure S1-2 The time series of ground surface temperature for different landforms.

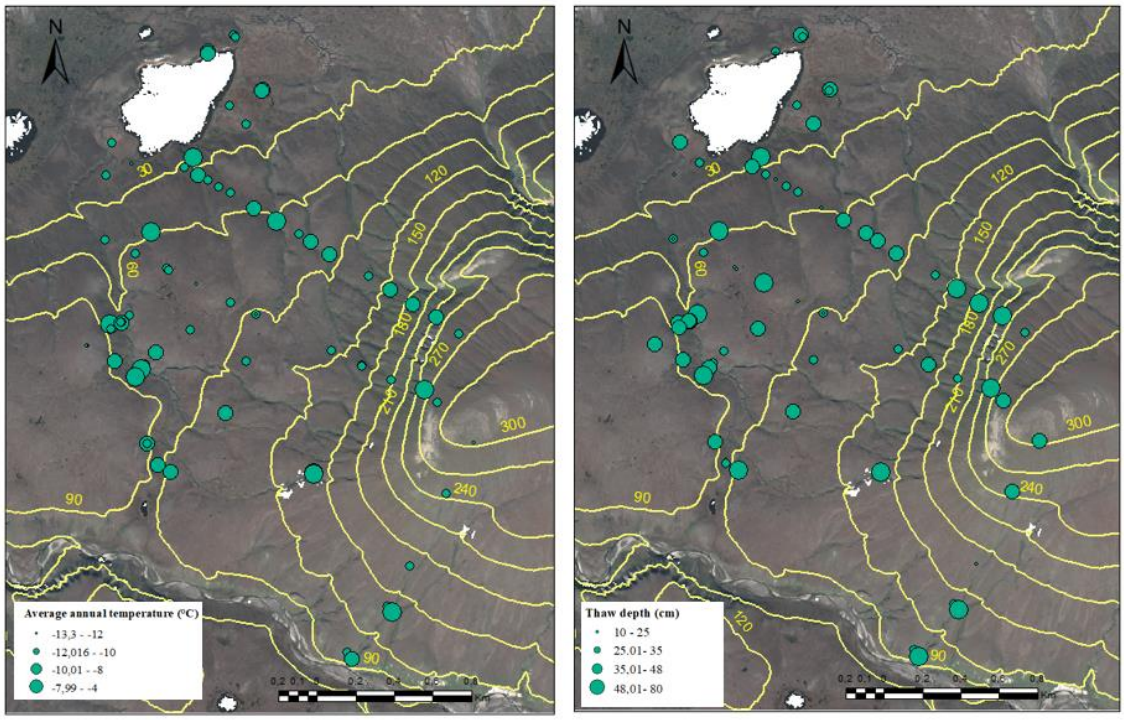

Figure S1-3 The spatial variation of ground surface temperature and thaw depth across the study area.

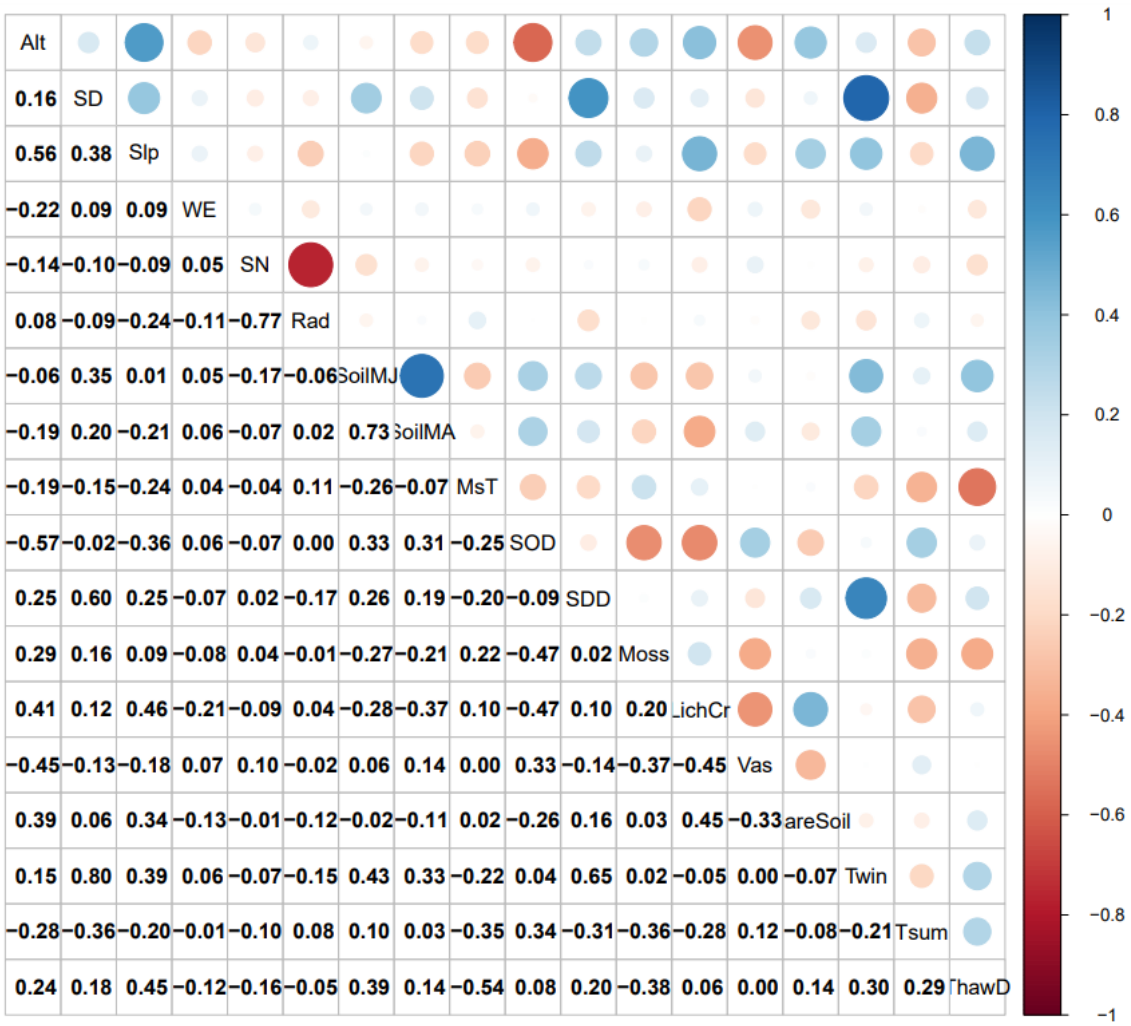

Figure S1-4 Correlation matrix of all variables (n: 65) at the site level scale. Soil type (S) are: Sa: gravely soil, Sb: sandy soil, Sc: sandy loam soil, Sd: loamy soil, Se: clay soil, So: peat soil. Snow cover indices are snow onset date (SOD), snow disappearance date (SDD) and snow depth (SD). Moss thickness (MsT), moss cover (Moss), vascular plants (Vas). Topographic parameters include solar radiation (Rad), northern exposure (SN), and eastern exposure (WE).

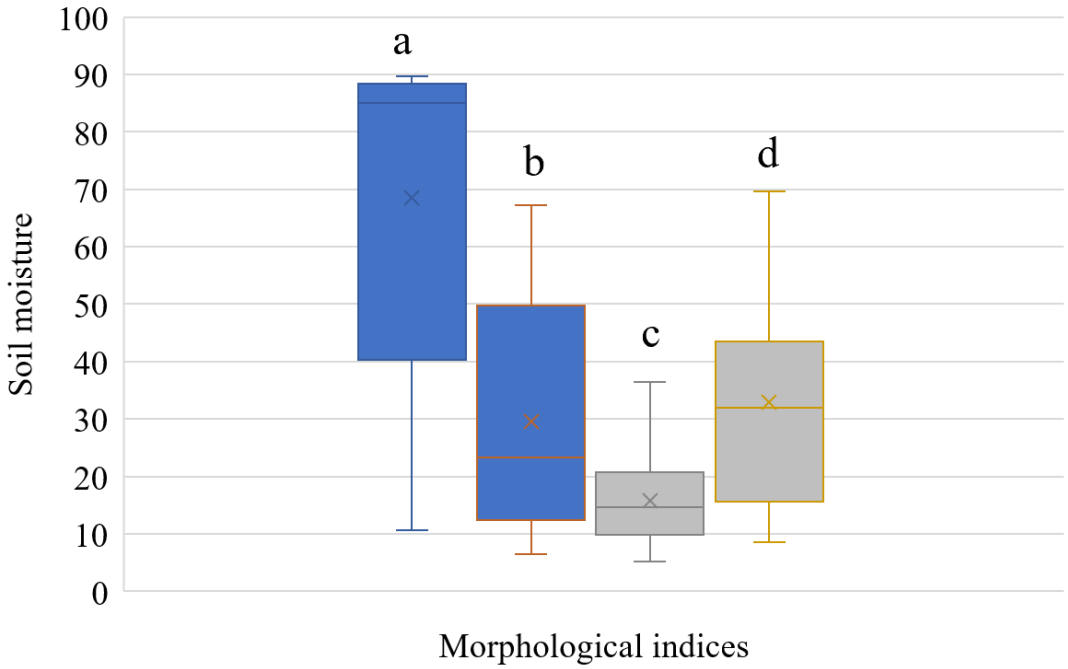

Figure S1-5 Difference in soil moisture between sheltered location (bottom) and exposed location (top). (a) hummocks' bottom; (b) hummocks' top; (c) polygons' rim; (d) polygons' center.

Appendix S1

In addition to end of winter snow depth measurements, snow onset date (SOD) and the snow disappearance date (SDD) were estimated at each micrologger based on the 3-hourly GST records, following the methods from Staub and Delaloye (2016). SOD is defined as the first day of winter with continuous snow on the ground, which was detected from the attenuation of the daily cycle in GST caused by the insulation of the overlying snow, using an optimized variance threshold (Staub and Delaloye, 2016; Way and Lewkowicz, 2017). The SDD was inferred when GST remained positive for several days following the spring zero-curtain period (ZC) (Staub and Delaloye, 2016), i.e. when the thawing of ground ice consumes latent heat and delays soil warming (P. J. Williams and Smith, 1989). The SOD and SDD extraction methods were first calibrated during the 2001-2008 period at the Bylocamp meteorological station, where snow depth is continuously recorded. The hourly GST data from the Bylocamp station was first resampled to 3-hourly to match the sampling interval of the microloggers. The GST daily variance threshold used to identify SOD was optimized by minimising the mean squared error (MSE) between the calculated SOD and that inferred from the snow depth record at Bylocamp (0.1°C). A 1 cm snow depth threshold was applied on the snow depth record to determine snow presence at the station. For SDD, the number of consecutive days with positive GST following the spring zero-curtain period was also optimised against the observed snow disappearance date at the station. The calibrated SOD and SDD methods were validated on the later period (2009-2018) at the Bylocamp station, and then applied to all micro-loggers. The SOD and SDD were further used to define the summer and winter periods in the statistical analyses.

References

Aalto, J., Scherrer, D., Lenoir, J., Guisan, A. and Luoto, M. (2018) 'Biogeophysical controls on soil-atmosphere thermal differences: Implications on warming Arctic ecosystems', Environmental Research Letters, 13(7). doi: 10.1088/1748-9326/aac83e.

Apaloo, J., Brenning, A. and Bodin, X. (2012) 'Interactions between seasonal snow cover, ground surface temperature and topography (Andes of Santiago, Chile, 33.5°S)', Permafrost and Periglacial Processes. Wiley-Blackwell, 23(4), pp. 277–291. doi: https://doi.org/10.1002/ppp.1753.

Barrere, M., Domine, F., Decharme, B., Morin, S., Vionnet, V. and Lafaysse, M. (2017) 'Evaluating the performance of coupled snow-soil models in SURFEXv8 to simulate the permafrost thermal regime at a high Arctic site', Geoscientific Model Development, 10(9), pp. 3461–3479. doi: https://doi.org/10.5194/gmd-10-3461-2017.

Belshe, E. F., Schuur, E. A. G., Bolker, B. M. and Bracho, R. (2012) 'Incorporating spatial heterogeneity created by permafrost thaw into a landscape carbon estimate', Journal of Geophysical Research: Biogeosciences, 117(1), pp. 1–14. doi: https://doi.org/10.1029/2011JG001836.

Biskaborn, B., Smith, S. L., Noetzli, J. et al. (2019) 'Permafrost is warming at a global scale', Nature Communications, 10(2019), pp. 1–11. doi: https://doi.org/10.1038/s41467-018-08240-4.

Ter Braak, C. J. F. (1994) 'Canonical community ordination. Part I: basic theory and linear methods', Ecoscience, 1(2), pp. 127–140. doi: https://doi.org/10.1080/11956860.1994.11682237.

Braun-Blanquet, J. (1932) Plant sociology; the study of plant communities. Fisrt. Edited by G. D. Fuller and H. S. Conard. New York and London: Bibliolife DBA of Bibilio Bazaar II LLC.

Burt, R. (2009) 'Soil Survey Field and Laboratory Methods Manual', United States Department of Agriculture, Natural Resources Conservation Service, Soil Surve(1), p. 487. Available at: https://www.nrcs.usda.gov/wps/PA_NRCSConsumption/download?cid=stelprdb1244466&ext=pdf.

CEN (2021) ‘CEN: Climate station data from Bylot Island in Nunavut, Canada, http://www.cen.ulaval.ca/nordicanad/dpage.aspx?doi= 45039SL-EE76C1BDAADC4890.’

Chapin, F. S., Sturm, M., Serreze, M. C. et al. (2005) ‘Role of Land-Surface Changes in Arctic Summer Warming’, 657(2005), pp. 657–660. doi: 10.1126/science.1117368.

Clayton, L. K., Schaefer, K., Battaglia, M. J. et al. (2021) ‘Active layer thickness as a function of soil water content’, Environmental Research Letters, 16(5). doi: 10.1088/1748-9326/abfa4c.

Cohen, J. (1977) Statistical Power Analysis for the Behavioral Sciences. Academic. New York. 473 p.

Crawley, M. J. (2010) The R Book. Second, Auction Theory. Second. Cambridge, England, 976 p: Wiley. doi: 10.1016/b978-0-12-374507-1.00050-9.

Davis, E., Trant, A., Hermanutz, L., Way, R. G., Lewkowicz, A. G., Siegwart Collier, L., Cuerrier, A. and Whitaker, D. (2021) ‘Plant–Environment Interactions in the Low Arctic Torngat Mountains of Labrador’, Ecosystems. Springer US, 24(5), pp. 1038–1058. doi: 10.1007/s10021-020-00577-6.

Duclos, I., Lévesque, E., Gratton, D. and Bordeleau, P.-A. (2006) Vegetation mapping of Bylot Island and Sirmilik national park. Iqaluit, Nunavut. 101p.

Ellis, C. J., Rochefort, L., Gauthier, G. and Pienitz, R. (2008) ‘Paleoecological evidence for transitions between contrasting landforms in a polygon-patterned high arctic wetland’, Arctic, Antarctic, and Alpine Research, 40(4), pp. 624–637. doi: 10.1657/1523-0430(07-059)[ELLIS]2.0.CO;2.

Elmendorf, S. C., Henry, G. H.R., Hollister, R. D. et al. (2012) ‘Global assessment of experimental climate warming on tundra vegetation: Heterogeneity over space and time’, Ecology Letters, 15(2), pp. 164–175. doi: https://doi.org/10.1111/j.1461-0248.2011.01716.x.

Fisher, J. P. ., Estop-Aragones, C., Thierry, A., Charman, D., Wolfe, S. A., Hartley, I. P. and Murton, J. B. (2016) ‘The influence of vegetation and soil characteristics on active-layer thickness of permafrost soils in boreal forest’, Global Change Biology, 22, pp. 3127–3140. doi: https://doi.org/10.1111/gcb.13248.

Fortier, D. and Allard, M. (2005) ‘Frost-cracking conditions, Bylot Island, eastern Canadian Arctic archipelago’, Permafrost and Periglacial Processes. Wiley-Blackwell, 16(2), pp. 145–161. doi: https://doi.org/10.1002/ppp.504.

Gagnon, C. A., Cadieux, M.-C., Gauthier, G., Lévesque, E., Reed, A. and Berteaux, D. (2010) Analyses and reporting on 15 years of biological monitoring from Bylot Island, Sirmilik national park of Canada.

Garibaldi, M. C., Bonnaventure, P. P. and Lamoureux, S. F. (2021) 'Utilizing the TTOP model to understand spatial permafrost temperature variability in a High Arctic landscape, Cape Bounty, Nunavut, Canada', Permafrost and Periglacial Processes, 32(1), pp. 19–34. doi: 10.1002/ppp.2086.

Gelman, A. and Hill, J. (2018) Data Analysis Using Regression and Multilevel/Hierarchical Models. Edited by R. M. Alvarez, N. L. Beck, and L. L. Wu. Cambridge University Press. 625 pp.

Gisnås, K, Westermann, S., Schuler, T. V, Litherland, T., Isaksen, K., Boike, J., Etzelmüller, B. and Gisnås, Kjersti (2014) 'A statistical approach to represent small-scale variability of permafrost temperatures due to snow cover', The Cryosphere, 8, pp. 2063–2074. doi: https://doi.org/10.5194/tc-8-2063-2014.

Goodrich, L. E. (1982) 'The influence of snow cover on the ground thermal regime', Canadian geotechnical journal, 19(4), pp. 421–432. doi: 10.1029/2004RG000157.

Gouttevin, I., Langer, M., Löwe, H., Boike, J., Proksch, M. and Schneebeli, M. (2018) 'Observation and modelling of snow at a polygonal tundra permafrost site : spatial variability and thermal implications', The Cryosphere, 12, pp. 3693–3717. doi: https://doi.org/10.5194/tc-12-3693-2018.

Grünberg, I., Wilcox, E. J., Zwieback, S., Marsh, P. and Boike, J. (2020) 'Linking tundra vegetation, snow, soil temperature, and permafrost', Biogeosciences, 17(16), pp. 4261–4279. doi: 10.5194/bg-17-4261-2020.

Gubler, S., Fiddes, J., Keller, M. and Gruber, S. (2011) 'Scale-dependent measurement and analysis of ground surface temperature variability in alpine terrain', The Cryosphere, pp. 431–443. doi: https://doi.org/10.5194/tc-5-431-2011.

Heijmans, M. M., Magnússon, R. I., Lara, M. J. et al. (2022) 'Tundra vegetation change and impacts on permafrost', Nature reviews earth & environment, 3, pp. 68–84.

Hrbáček, F., Cannone, N., Kňažková, M., Malfasi, F., Convey, P. and Guglielmin, M. (2020) 'Effect of climate and moss vegetation on ground surface temperature and the active layer among different biogeographical regions in Antarctica', Catena, 190(February). doi: 10.1016/j.catena.2020.104562.

Van Huissteden, J. (2020) Thawing Permafrost:Permafrost Carbon in a Warming Arctic. First. Cham, Switzerland: Springer Nature Switzerland AG, 432 p. doi: https://doi.org/10.1007/978-3-030-31379-1_6.

International Permafrost Association (2008) 'Report from the International Permafrost Association: state of permafrost in the first decade of the 21st century', Permafrost and Periglacial Processes, 136(January), pp. 107–136. doi: 10.1002/ppp.

Jan, A. and Painter, S. L. (2020) 'Permafrost thermal conditions are sensitive to shifts in snow timing', Environmental Research Letters, 15(8), pp. 1–12. doi: 10.1088/1748-9326/ab8ec4.

Jing-Yi, Z. (2018) 'Snow cover influences the thermal regime of active layer in Urumqi River Source , Tianshan Mountains , China', Journal of mountain Science, 15, pp. 2622–2636. doi: https://doi.org/10.1007/s11629-018-4856-y.

Lacelle, D., Lapalme, C., Davila, A. F., Pollard, W., Marinova, M., Heldmann, J. and McKay, C. P. (2016) 'Solar Radiation and Air and Ground Temperature Relations in the Cold and Hyper-Arid Quartermain Mountains, McMurdo Dry Valleys of Antarctica', Permafrost and Periglacial Processes, 27(2), pp. 163–176. doi: 10.1002/ppp.1859.

Lara, M. J., Nitze, I., Grosse, G., Martin, P. and David McGuire, A. (2018) 'Reduced arctic tundra productivity linked with landform and climate change interactions', Nature: Scientific Reports, 8(1), pp. 1–10. doi: https://doi.org/10.1038/s41598-018-20692-8.

Legendre, P., Birks, H. J. B., Lotter, A. F., Juggins, S. and Springer, S. (2012) From Classical to Canonical Ordination. Edited by S. J. Birks H., Lotter A., Juggins S. Dordrecht: Springer. doi: https://doi.org/10.1007/978-94-007-2745-8_8.

Legendre, P., Oksanen, J. and ter Braak, C. J. F. (2011) 'Testing the significance of canonical axes in redundancy analysis', Methods in Ecology and Evolution, 2, pp. 269–277. doi: 10.1111/j.2041-210X.2010.00078.x.

Marti, R., Gascoin, S., Berthier, E., De Pinel, M., Houet, T. and Laffly, D. (2016) 'Mapping snow depth in open alpine terrain from stereo satellite imagery', Cryosphere, 10(4), pp. 1361–1380. doi: 10.5194/tc-10-1361-2016.

Maxwell, J. B. (1982) The climate of the Canadian Arctic Islands and adjacent waters. Environment Canada, Atmospheric Environment Service, 589 p.

Mohammadzadeh Khani, H., Kinnard, C. and Lévesque, E. (2022) 'Historical Trends and Projections of Snow Cover over the High Arctic: A Review', Water. MDPI AG, 14(4), p. 587. doi: 10.3390/W14040587.

Nakagawa, S., Johnson, Paul C D and Schielzeth, H. (2017) 'The coefficient of R2 determination and intra-class correlation coefficient from generalized linear mixed-effects models revisited and expanded', Journal of royal society InterfaceInterface, 14, pp. 1–11. doi: http://dx.doi.org/10.1098/rsif.2017.0213.

Nelson, F. E., Anisimov, O. A. and Shiklomanov, N. I. (2002) 'Climate change and hazard zonation in the circum-arctic permafrost regions', Natural Hazards, 26(3), pp. 203–225. doi: 10.1023/A:1015612918401.

O'Donnell, J. A., Romanovsky, V. E. and Harden, J. W. (2009) 'The Effect of Moisture Content on the Thermal Conductivity of Moss and Organic Soil Horizons From Black Spruce Ecosystems in Interior Alaska', soil science, 174(12), pp. 646–651.

Park, H., Fedorov, A. N., Zheleznyak, M. N., Konstantinov, P. Y. and Walsh, J. E. (2015) 'Effect of snow cover on pan-Arctic permafrost thermal regimes', Climate Dynamics, 44(9–10), pp. 2873–2895. doi: 10.1007/s00382-014-2356-5.

Perreault, N., Lévesque, E., Fortier, D. and Lamarque, L. J. (2016) 'Thermo-erosion gullies boost the transition from wet to mesic tundra vegetation', Biogeosciences, 13(4), pp. 1237–1253. doi: 10.5194/bg-13-1237-2016.

Pinheiro, J. C. and Bates, D. M. (2000) Mixed-Effects Models in S and S-Plus. New York: Springer Science & Business Media. 528 p.

Porada, P., Ekici, A. and Beer, C. (2016) 'Effects of bryophyte and lichen cover on permafrost soil temperature at large scale', Cryosphere, 10, pp. 2291–2315. doi: 10.5194/tc-10-2291-2016.

Pouliot, R., Rochefort, L. and Gauthier, G. (2009) 'Moss carpets constrain the fertilizing effects of herbivores on graminoid plants in arctic polygon fens', Botany, 87(12), pp. 1209–1222. doi: 10.1139/B09-069.

Riseborough, D., Shiklomanov, N., Etzelmüller, B., Gruber, S. and Marchenko, S. (2008) 'Recent Advances in Permafrost Modelling', Permafrost and Periglacial Processes, 19, pp. 137–156. doi: 10.1002/ppp.615.

Rixen, C., Høye, T. T., Macek, P. et al. (2022) 'Winters are changing: snow effects on Arctic and alpine tundra ecosystems', Arctic Science, (February). doi: 10.1139/as-2020-0058.

Rowell, D. L. (1994) Soil science: Methods and applications. New York: Wiley. 350p.

Shean, D. E., Alexandrov, O., Moratto, Z. M., Smith, B. E., Joughin, I. R., Porter, C. and Morin, P. (2016) 'An automated, open-source pipeline for mass production of digital elevation models (DEMs) from very-high-resolution commercial stereo satellite imagery', ISPRS Journal of Photogrammetry and Remote Sensing. International Society for Photogrammetry and Remote Sensing, Inc. (ISPRS), 116, pp. 101–117. doi: 10.1016/j.isprsjprs.2016.03.012.

Slater, A. G. and Lawrence, D. M. (2013) 'Diagnosing present and future permafrost from climate models', Journal of Climate, 26(15), pp. 5608–5623. doi: 10.1175/JCLI-D-12-00341.1.

Smith, M. W. and Riseborough, D. W. (2002a) 'Climate and the Limits of Permafrost : A Zonal Analysis', 15(June 2001), pp. 1–15. doi: 10.1002/ppp.410.

Smith, M. W. and Riseborough, D. W. (2002b) 'Climate and the Limits of Permafrost : A Zonal Analysis', Permafrost and Periglacial Processes, 15(June 2001), pp. 1–15. doi: 10.1002/ppp.410.

Smith, S. (2010) Trends in permafrost conditions and ecology in northern Canada. Canadian Biodiversity: Ecosystem Status and Trends 2010, Technical Thematic Report No. 9. Ottawa, ON.

Smith, S. L., Burgess, M. M., Riseborough, D. and Nixon, F. M. (2005) 'Recent trends from Canadian permafrost thermal monitoring network sites', Permafrost and Periglacial Processes, 16(1), pp. 19–30. doi: 10.1002/ppp.511.

Smith, S. L., O'Neill, H. B., Isaksen, K., Noetzli, J. and Romanovsky, V. E. (2022) 'The changing thermal state of permafrost', Nature reviews earth & environment, 3, pp. 10–23.

Smith, S. L., Romanovsky, V. E., Lewkowicz, A. G., Burn, C. R., Allard, M., Clow, G. D., Yoshikawa, K. and Throop, J. (2010) 'Thermal state of permafrost in North America: A contribution to the international polar year', Permafrost and Periglacial Processes, 21(2), pp. 117–135. doi: https://doi.org/10.1002/ppp.690.

Staub, B. and Delaloye, R. (2016) 'Using near-surface ground temperature data to derive snow insulation and melt indices for mountain permafrost applications',

Permafrost and Periglacial Processes, 28, pp. 237–248. doi: https://doi.org/10.1002/ppp.1890.

Sturm, M., Douglas, T., Racine, C. and Liston, G. E. (2005) 'Changing snow and shrub conditions affect albedo with global implications', Journal of Geophysical Research, 110(G1), pp. 1–13. doi: 10.1029/2005jg000013.

Sturm, M. and Holmgren, J. (1994) 'Effects of microtopography on texture, temperature and heat flow in Arctic and sub-Arctic snow', Annals of Glaciology, 19, pp. 63–68. doi: 10.1017/s0260305500010995.

Turetsky, M. R., Bond-Lamberty, B., Euskirchen, E., Talbot, J., Frolking, S. and Mcguire, A. D. (2012) 'The resilience and functional role of moss in boreal and arctic ecosystems', New Phytologist, 196, pp. 49–67. doi: https://doi.org/10.1111/j.1469-8137.2012.04254.x.

Vonk, J. E., Tank, S. E., Bowden, W. B. et al. (2015) 'Reviews and syntheses: Effects of permafrost thaw on Arctic aquatic ecosystems', Biogeosciences, 12(23), pp. 7129–7167. doi: 10.5194/bg-12-7129-2015.

Voortman, B. R., Bartholomeus, R. P., van Bodegom, P. M., Gooren, H., van der Zee, S. E. A. T. M. and Witte, J. P. M. (2014) 'Unsaturated hydraulic properties of xerophilous mosses: Towards implementation of moss covered soils in hydrological models', Hydrological Processes, 28(26), pp. 6251–6264. doi: 10.1002/hyp.10111.

Way, R. G. and Lewkowicz, A. G. (2017) 'Environmental controls on ground temperature and permafrost in Labrador, northeast Canada', Permafrost and Periglacial Processes. Wiley-Blackwell, 29(2), pp. 73–85. doi: 10.1002/ppp.1972.

Williams, M., Zhang, Y., Estop-Aragonés, C., Fisher, J. P., Xenakis, G., Charman, D. J., Hartley, I. P., Murton, J. B. and Phoenix, G. K. (2020) 'Boreal permafrost thaw amplified by fire disturbance and precipitation increases', Environmental Research Letters, 15(11). doi: 10.1088/1748-9326/abbeb8.

Williams, P. J. and Smith, M. W. (1989) The frozen rarth-fundamentals of geocryology. New York: Cambridge University Press.

Woo, M. (2012) Permafrost Hydrology. Berlin Heidelberg: Springer New York. 574 p. doi: 10.1007/978-3-642-23462-0.

Yi, Y., Kimball, J. S., Chen, R. H., Moghaddam, M., Reichle, R. H. and Mishra, U. (2018) 'Characterizing permafrost active layer dynamics and sensitivity to

landscape spatial heterogeneity in Alaska', The Cryosphere, 12, pp. 145–161. doi: https://doi.org/10.5194/tc-12-145-2018.

Zhang, T. (2005) 'Influence of seasonal snow cover on the ground thermal regime: an overview', Reviews in Geophysics, 43, pp. 1–23. doi: https://doi.org/10.1029/2004RG000157.

Zhang, T. Frauenfeld, O. W., Serreze, M. C. et al. (2005) 'Spatial and temporal variability in active layer thickness over the Russian Arctic drainage basin', Journal of Geophysical Research D: Atmospheres, 110(16), pp. 1–14. doi: 10.1029/2004JD005642.

Zoltai, S. C. and McCormick, K. J. (1983) A natural resource survey of Bylot Island and adjacent Baffin Island, Northwest Territories.

Zuur, A. F., Ieno, E. N., Walker, N. J., Saveliev, A. A. and Smith, G. M. (2010) Mixed effects models and xxtensions in ecology with R, Journal of the Royal Statistical Society: Series A (Statistics in Society). 574 p: Springer New York. doi: 10.1111/j.1467-985x.2010.00663_9.x.

CHAPTER II

FINE SCALE DISTRIBUTED SNOW COVER MODELING IN A HIGH ARCTIC TUNDRA LANDSCAPE USING PHYSICALLY BASED GEOTOP MODEL

Hadi Mohammadzadeh Khani[1-2*], Christophe Kinnard[1-2], Esther Lévesque[1-2]

[1] Research Centre for Watershed-Aquatic Ecosystem Interactions (RIVE), University of Québec at Trois-Rivières, Québec, Canada.

[2] Centre for Northern Studies (CEN), Québec City, Québec, Canada

[*]Corresponding author: Hadi.Mohammadzadeh.Khani@uqtr.ca

Abstract

In the complex terrain of the High Arctic tundra environment, the interactions between wind, topography, and snowfall result in snow cover with non-uniform depth distributions. However, hydrological or meteorological models typically disregard the mechanisms involved in blowing snow. A physically based hydrological model (GEOtop) is used to perform a snow cover sensitivity and simulate the evolution of snow depth over topographically varied terrain and perform a sensitivity analysis in Bylot Island, Canada. In this study, an improved version of the blowing snow detection algorithm developed for GEOtop3.0 was used to compute the blowing snow sublimation and transport rates over the irregular terrain typical of the High Arctic tundra environment. The model performance is tested by statistical and graphical comparison of simulated snow cover metrics. An extensive model validation was carried out using a suite of *in situ* observations including manual, automatic, and UAV (Unmanned Aerial Vehicle) snow depth measurements at the site. The model outputs consist of the spatial and temporal changes in snow cover conditions due to different factors such as precipitation, transportation by saltation and suspension, and sublimation. The study highlights the dependence of model parameterization on the period (snow accumulation and ablation) while also revealing that blowing snow mechanisms and landscape patterns govern the regional distribution and overall accumulation of snow water equivalent over winter. The model is found to simulate closely the observed snow-depth distribution patterns and the interannual variability at the point and the catchment scale (NSE= 0.81 and 0.68 respectively). It is demonstrated that the end-of-winter snow depth can be more accurately represented by taking into account subgrid-scale snow-cover heterogeneity over complex Arctic terrain. Also, blowing snow activating in the model resulted in cumulative seasonal sublimation differences ranging from 15% to 30% of seasonal snowfall over the period of 2016-2018. Improvements in wind-blowing snow process understanding will be the basis for improved short-term forecast and climate projections in snow-covered regions.

Keywords: The High Arctic, tundra environment, physically based hydrological model, GEOtop, wind-blowing snow, Bylot Island.

2.1 Introduction

In the High Arctic tundra environment, where cold and dry conditions prevail with limited vegetation growth (Bliss *et al.*, 1973) and the snow cover lasts for a long period on the ground (Williams and Smith, 1989; Woo, 2012; Brown *et al.*, 2021), the combination of wind and snowfall play an important role in determining the winter snow distribution (Liston and M. Sturm, 1998). In the windswept, treeless and irregular terrain typical of the High Arctic, snow redistribution and relocation are largely governed by topography and wind at the hillslope scale (Pomeroy *et al.*, 1997; Liston and M. Sturm, 1998; Assini and Young, 2012). The snow redistribution due to wind transport typically occurs at the hillslope scale (< 100 meters) and tends to accumulate snow on the lee of topographic disturbances such as ridges, while also exhibiting a tendency to erode snow predominantly from flat areas where an adequate fetch to establish wind erosion exists (Pomeroy *et al.*, 1997; Bruland *et al.*, 2004; Clark *et al.*, 2011). In return, the spatial variability of the snow cover at the hillslope scale has been shown to significantly affect vegetation growth and animal habitats in the Arctic tundra environment (Fraser *et al.*, 2011; Bilodeau *et al.*, 2013). The spatial heterogeneity of the snow cover is an important driver of near-surface permafrost temperatures (Gisnås *et al.*, 2014; Mohammadzadeh Khani, *et al.*, 2023). For example, Mohammadzadeh Khani *et al.* (2023) found that the spatial heterogeneity of snow depth led to large (up to 9 °C) differences in winter ground surface temperatures across a tundra landscape (< 100 meters) on Bylot Island, Arctic Canada. Yet, the spatial distribution of snow cover at the hillslope or smaller scales is often not well modeled, which can lead to substantial uncertainties in snow cover representations (Bennett *et al.,* 2022). This is particularly problematic when using snow cover models to estimate the impacts of changing snow cover on the water cycle and ecosystems processes in cold regions.

Blowing snow is an important process in exposed tundra landscapes (Pomeroy and Jones, 1996; Pomeroy *et al.*, 1997). The sublimation of blown snow particles returns moisture to the atmosphere, and horizontal snow transport leads to spatial variations in snow depth that generate a patchy snow cover and strong heterogeneities in snowpack characteristics (Essery and Pomeroy, 2004). For these reasons, physically based, spatially distributed process models of snow cover are required to calculate snowpack evolution in

heterogeneous landscapes prone to blowing snow transport and to accurately model meltwater fluxes within distributed hydrological models. Robust, physically based hydrological models account for shortwave and longwave radiation, shading, and turbulent fluxes of sensible and latent heat to simulate snow cover conditions at high spatial and temporal resolutions (Mott *et al.*, 2011; Krogh *et al.*, 2017; Bui *et al.*, 2020). Several physically-based hydrological models have been developed for cold climate regions such as CATchment HYdrology (CATHY) (Paniconi and Putti, 1994), HydroGeosphere (Therrien, 1996), TopoFlow (Schramm *et al.*, 2007), DMHS (deterministic modeling hydrological system) (Vinogradov *et al.*, (2011), and the Hydrograph model (Semenova *et al.*, 2013). Yet, these models do not include explicit representations of snow cover processes such as wind-blowing snow. In fact, few snow cover and hydrological models are snowdrift-permitting, i.e. that include a blowing snow routine. For example, the Prairie Blowing Snow Model (PBSM) (Pomeroy *et al.*, 1993), PIEKTUK (Déry and Yau, 1999), and SnowModel (Liston and Elder, 2006) are well-known snow cover evolution models that represent blowing snow processes but they are not coupled to a hydrological model. More recently, Vionnet *et al.* (2021) introduced a multi-scale snow redistribution model and highlighted the need for further improvements of snowdrift-permitting models for large-scale applications, in particular the representation of subgrid topographic effects on snow transport. The Cold Regions Hydrological Model (CRHM, (Pomeroy *et al.*, 2007, 2022)) is a physically based, semi-distributed hydrological model which includes blowing snow processes based on PBSM (Pomeroy *et al.*, 2007, 2022b). While CHRM has been extensively used to diagnose cold region hydrological processes including blowing snow redistribution (e.g., Krogh *et al.,* 2017; Aygün *et al.,* 2020), this semi-distributed model requires a careful delineation of the hydrological representative units (HRUs) and prescribing redistribution weight factors for blowing snow, which are not easy to constrain (MacDonald *et al.*, 2009). In fact there are only a few models that have a grid based scheme for description of snow processes in complex terrain. GEOtop is a grid-based, physically-based distributed hydrological model platform that is capable of simulating the heat and water budgets at and below the soil surface (Endrizzi *et al.*, 2014; Engel *et al.*, 2017). It integrates a multilayer snowpack model and a three-dimensional representation of various hydrological processes, including those that occur in permafrost and seasonally freezing

grounds. The model calculates the energy balance for snow, soil, glacier, and vegetated surfaces in complex terrains and targets small catchments. GEOtop comprehensively considers the interplay between topography and radiation, which sets it apart from many existing hydrological models (Endrizzi *et al.*, 2014). GEOtop has been applied in different cold regions to simulate snow cover conditions. For example, Pullens *et al.* (2018) used GEOtop 2.0 model to assess the water and energy budget and simulate snow cover evolution in a peatland catchment of the Alps. Engel *et al.* (2017) evaluated the capability of the GEOtop 2.0 snow module to simulate snowpack evolution at the point scale and snow cover area over an alpine catchment in Italy. GEOtop 3.0 is the latest version of the GEOtop model, which includes a blowing snow parameterization (Bortoli *et al.*, 2018). To our knowledge, the developed blowing snow routine within the GEOtop 3.0 model has not yet been tested against snow field measurements in the Arctic.

The purpose of this study is thus to evaluate the ability of the GEOtop 3.0 snow model, including its untested blowing snow module, to simulate the spatiotemporal evolution of the snow cover in a High Arctic tundra landscape over a 15-year period. A parameter sensitivity analysis was first conducted to identify the most sensitive snow cover model parameters at both the point (weather station) and spatial scale. Next, an extensive model validation was carried out using a suite of in situ observations including manual, automatic, and UAV (Unmanned Aerial Vehicle) snow depth measurements at the site. The impact of blowing snow processes on model performance and on the reconstructed snow cover variability are assessed, and the limitations of the model for High Arctic tundra landscapes are presented and discussed.

2.2 Methodology

2.2.1 Study domain

This research study was carried out in a High Arctic tundra environment in the Qarlikturvik Valley of Bylot Island, off the northern coast of Baffin Island in Nunavut, Canada (Figure 2-1). The 7.3 km^2 study area ranges in elevation from 20 to 350 m a.s.l, extending from a low-lying wetland, into a mesic hillslope and up to a xeric hilltop, named Jack Mountain.

The ground surface is dominated by mineral-earth hummocks, water tracks, and small ravines on mesic slopes and by low center polygons traversed by thermokarst ravines in the humid valley lowlands, which are underlain by a thick (approximately 400 m) continuous permafrost (Maxwell, 1982; Fortier and Allard, 2004, 2005). According to the Köppen-Geiger climate classification the climate in Bylot Island is High Arctic, with cold temperatures, dry winter season, and cold summers (Beck *et al.*, 2018).

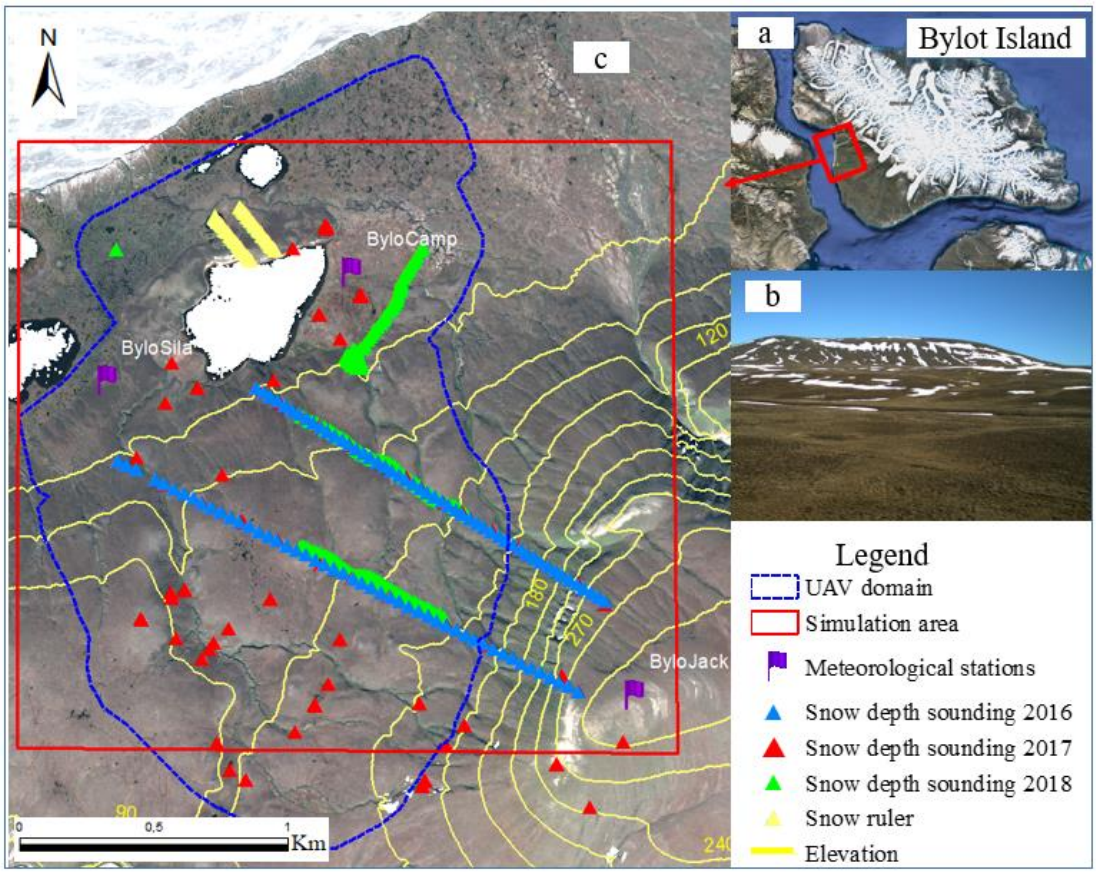

Figure 2-1 Map of the study area in Bylot Island, Nunavut, Canada. (a) Location of study area on Bylot Island, Arctic Canada (b) View of the site, looking towards the southeast, Jack Mountain in the background; (c) modeling domain and network of snow depth and meteorological observations; background map: satellite Image by Pléiades © CNES 2016 Distribution Airbus DS.

The annual mean temperature at the Bylocamp weather station (Table 2-1), operated by Centre d'Études Nordiques (CEN) was -15.1°C for the period 1981-2010. The average annual precipitation is slightly below 200 mm/year, mostly (76%) falling as snow (Fortier and Allard, 2005). The snowfall season normally starts in early September and ends in mid-

June. The annual average winter snow depth normally reaches 35 to 45 cm, however with pronounced spatial variability due topographic variability of the terrain and winter snow drifting (Exposed areas have 5-25 cm and sheltered up to 2-3 m in ravines) (Fortier and Allard, 2004; Gagnon *et al.*, 2010; Mohammadzadeh Khani, *et al.*, 2023). The prostrate vegetation is relatively diverse for this latitude, with more than 166 vascular plant species and a rich bryophyte flora (Duclos *et al.,* 2006).

2.2.2 Meteorological data

Three permanent weather stations are operated at the site since the early 1990s by CEN (SILA network), two (Bylocamp and Bylosila) in the valley (elevation 20 m a.s.l.) and one (Bylojack), on the adjacent Jack Mountain (elevation 314 m a.s.l.) (Figure 2-1, Table 2-1). Weather station data was retrieved through the NordicanaD online data repository (CEN, 2021). The meteorological variables used to force the GEOtop model included hourly air temperature, relative humidity, wind speed and direction, total precipitation, and incoming solar radiation. Table 2-1 describes the availability of each variable at each weather station.

Table 2-1 On-site hourly meteorological data available from the permanent weather station of the SILA network (see station locations on Figure 2-1). P: Total precipitation, Ta: 2 m air temperature, RH: relative humidity, WS: wind speed at 2 m height, WD: wind direction, SD: snow depth, S: incoming solar radiation. Hourly and daily precipitation data from the Pond Inlet station were also used.

Meteorological station	Latitude and longitude (°)	Elevation (m)	Operation start	Meteorological variables
Bylosila	73.15, -79.98	24	1994	T_a, WS, WD, SW
Bylojack	73.14, -79.90	312	2001	T_a, WS, WD
Bylocamp	73.15, -79.95	24	2004	T_a, P, SD, WS, WD, RH
Pond Inlet	72.69, -77.97	55	1975	P, RH

Hourly wind speed and direction and air temperature were recorded at the three meteorological stations since 2002. Snow depth (SD) was measured with an ultrasonic gauge (Campbell Scientific SR50) at the Bylocamp station with an hourly interval between

2002 and 2019. However there were years with missing data (due to sensor malfuctioniong or disturbance by animal) which were excluded from analyses in this study. Hourly precipitation is recorded since 2011 at the Bylocamp with a Geonor total precipitation gauge. A single-Alter shield was installed around the Geonor in July 2016. The precipitation record suffers from several large gaps due to gauge malfunctioning and disruption by animals, e.g. from February-May 2014, June-July 2015 and January-April 2017. As such, we also relied on precipitation measured at the Pond Inlet Environment Canada weather station (id: 43223) located at the Pond Inlet airport on Baffin Island (72.69° N, 77.95° W; almost 80 km southeast from the Bylocamp station). The precipitation data from Pond Inlet was well correlated with the Bylocamp station over the period 1995–2004 and thus was used to fill the missing data at Bylocamp using linear regression transfer functions (see section 2.2.4 and Figure S2-1). Incoming solar radiation was recorded using a CNR1 net radiometer at the Bylosila station since July 2009. Relative humidity (RH) data is recorded at the Bylocamp station since July 1993.

2.2.3 Snow depth data

Snow depth is monitored annually since 1995 at two permanent snow ruler transects, each comprised of 50 points and installed close to the CEN research camp (Figure 2-1) (Gauthier *et al.,* 2013). In addition, the late-winter snow depth was measured using a graduated snow probe during three consecutive seasons (2016-2018) across the study area. In 2017, each sampling location represented a spatial average of five measurements, taken at and 1 m away from the center point in a cross pattern, to account for microscale snow depth variability around the reference point, in the context of a dedicated observational study on snow-soil-vegetation interactions (Mohammadzadeh Khani, *et al.*, 2023). In 2016 and 2018 only one measurement was done per sampling location, which was targeted to validate high-resolution UAV-based snow depth maps (Loyer and Kinnard, 2018). A detailed (mean ground sampling distance – GSD = 2.3 cm) map of the maximum snow accumulation was derived in 2018 from UAV photogrammetric surveys, following previously established methodologies (e.g. Revuelto *et al.,* 2021). A Sensefly EbeePlus UAV equipped with a survey grade double frequency GNSS receiver was used for this

purpose. The images were geo-tagged with centimeter-level accuracy using a FOIF A30 GNSS base station and Post-Processed Kinematic (PPK) techniques. A set of 43 ground control points georeferenced to sub centimeter accuracy with a FOIF A30 rover GNSS was used to further improve the direct georeferencing. Snow-on (17th May 2018) and snow-off (11th July 2018) digital elevation models (DEMs) were produced in the Pix4d mapper software and differenced to obtain the snow depth map. Validation against the manual snow depth measurements yielded root mean square errors (RMSE) of 4.38 cm over the snow ruler transects and 7.05 cm on the snow soundings.

2.2.4 Preprocessing of model forcings

The cumulative Geonor bucket weight from the Bylosila station was converted to hourly precipitation rates using the segmented neutral aggregating filter (NAF-SEG, Ross *et al.,* 2020). The NAF-SEG is an automated technique that implements the NAF to process multi-day precipitation time series in successive 24 h segments using overlapping moving windows. The use of 24 h windows automates the identification and removal of evaporation, minimizing the negative biases in total precipitation from evaporation (Ross *et al.* 2020). Before applying the NAF-SEG filter, the cumulative bucket precipitation weight was smoothed using a robust local 2nd order polynomial moving regression to get rid of diurnal noise. Hourly precipitation events with relative humidity less than 60% were considered noise and set to zero. The hourly precipitation rates were corrected for wind undercatch as a function of air temperature and wind speed following Kochendorfer *et al.* (2017) (Equation 2.1).

$$CE = e^{-a(WS)(1-tan^{-1}(b(T_a))+c)} \quad (2.1)$$

Where *WS* is wind speed, T_a is the air temperature (°C), and *a*, *b*, and *c* are coefficients optimized by Kochendorfer *et al.* (2017). Different coefficient values were used for the no-Alter (2011-2016) vs. with-Alter (2016-2019) correction (Kochendorfer *et al.,* 2017). Prior to filling in the missing precipitation data from the Bylocamp record, the daily and hourly precipitation data from the Pond Inlet station (station ID: 43223) were first corrected for

wind undercatch using the same procedure. Daily precipitation was then disaggregated into 24 uniform hourly values, and used for infilling when hourly values were unavailable. Linear regression models were developed between the Bylocamp and Pond Inlet stations and used to fill in missing values for the period modeling period, September 2005 to September 2019 (Figure S1). Any remaining missing values after infilling from the Pond Inlet station were filled using a linear regression model between the Bylocamp station and the Canadian Precipitation Analysis product (CaPA) (Lespinas *et al.,* 2015). The 6-hourly CaPA precipitation data was disaggregated into 6 uniform hourly values. The gap-filled, undercatch-corrected mean annual precipitation at Bylocamp was 266 mm/yr for the period of 2005-2019. A large gap in RH data was found from September to December 2014, which was filled with RH data from Pond Inlet using linear regression.

GEOtop calculates the incoming solar radiation (SW_{in_calc}) based on calculated top-of-the atmosphere solar radiation (SW_{toa}) and atmospheric (τ_a) and cloud (τ_c) transmissivity (equation 2.2), before modifying for topographic effects.

$$SW_{in\_calc} = SW_{toa} * \tau_a * \tau_c \tag{2.2}$$

The cloud transmissivity is calculated at a reference weather station based on the ratio between the observed incoming solar radiation (SW_{in_obs}) and the calculated clear-sky solar radiation ($SW_{toa} * \tau_a$). Since this ratio cannot be calculated during the long polar night, the cloud transmissivity at Bylocamp was calculated beforehand and provided as input to GEOtop. For daytime, τ_c was calculated as $SW_{in}/(SW_{toa} * \tau_a)$ and for nighttime when SW_{in} observations are absent, using the formulation from Kimball (1928) (Equation 2.3):

$$\tau_c = 1 - kc \tag{2.3}$$

Which approximates the cloud transmissivity as a function of cloud cover fraction (c), varying from 0 (clear sky) to 1 (overcast sky). Since cloud cover was not measured at the site, hourly cloud cover from the ERA5 reanalysis (Hersbach *et al.,* 2023) was used. The

global value for the coefficient k is 0.71 (Kimball, 1928), and so was adjusted for the local conditions by fitting k to daytime cloud transmissivity values derived from solar radiation observations after replacing SW_{in_calc} by SW_{in_obs} in equation 2.2, yielding $k = 0.77$.

2.2.5 Model configuration

GEOtop 3.0 was used in this study, which is the latest version of the GEOtop model and notably includes a blowing snow parametrization (Bortoli *et al.,* 2018). The GEOtop model computes the energy and water balance on a digital elevation model (DEM). The spatial distribution of meteorological forcing follows the MicroMet model (Liston and Elder, 2006), using prescribed lapse rates combined with optimal spatial interpolation methods (Barnes, 1964).

In GEOtop snow cover processes are computed as: (i) the heat equation, (ii) snow metamorphism, (iii) water percolation and (iv) accumulation (Endrizzi *et al.,* 2014). The mass and energy exchanges between the atmosphere and snowpack are calculated at each grid cell of the DEM and the heat equation ignores lateral gradients. The boundary condition at the snowpack surface is given by the surface heat flux while the heat flux at the soil-snow interface is estimated from an effective thermal conductivity defined at the interface and the temperature gradient determined using the temperatures of the top soil layer and the lowest snow layer (Zanotti *et al.*, 2004; Endrizzi *et al.*, 2014; Engel *et al.*, 2017). The snow discretization process within GEOtop serves the purpose of achieving precise representation of thermal gradients within the snowpack and minimizing unnecessary memory allocation. A dynamic layer-accounting scheme is used to discretize the snowpack. The snowpack is categorized into an upper, middle and lower section. The upper and lower regions are characterized by relatively large vertical thermal gradients, which arise due to interactions with the atmosphere and the underlying soil, respectively. Conversely, the middle section exhibits weaker vertical gradients. The actual number of layers depends on the total mass of snowpack, and is distributed in a manner that primarily emphasizes the upper and lower sections of the snowpack. Four parameters control the snow layering scheme, which are the snow mass (SWE) in the upper and bottom regions,

the maximum admitted mass for a single layer, and the maximum number of layers admitted in the middle region (Endrizzi *et al.*, 2014). GEOtop encompasses the comprehensive representation of snow densification processes, capturing both rapid initial snow transformation (destructive metamorphism) and the gradual compaction induced by the snow own weight (overburden). These processes are characterized using empirical equations initially proposed by Anderson (1976) and subsequently refined by Jordan et al. (1999). Densification is an integral part of the model, taking into account various scenarios. For instance, densification is observed when liquid water begins to refreeze, resulting in the filling of empty pore spaces with new ice. Conversely, a snow layer may experience a reduction in density due to the percolation process, where the total water volume within the layer decreases without a corresponding change in volume. Furthermore, the model accounts for snow densification resulting from wind-induced loads. This aspect of the model captures the surface snowpacking process, leading to a gradual resistance against drifting, as elucidated by Liston *et al.* (2007). Constructive metamorphism leading to new shapes of the snow crystals, like hoar layers, is currently not represented. Water percolation (rain and melt) in the snowpack is accounted for, including refreezing (Endrizzi *et al.*, 2014; Engel *et al.*, 2017). A simplified snow gravitational routine allows for representing snow avalanching, following Gruber (2007). A full description of how the GEOtop model accounts for the processes i-iv can be found in Endrizzi *et al.* (2014), while the blowing snow transport module is outlined in details in section 2.2.6.

2.2.6 Blowing snow transport in GEOtop 3.0

Blowing snow transport and sublimation is parameterized following Essery *et al.* (1999), Liston and. Sturm, (1998), and (Liston *et al.,* 2007), who adapted the original formulation of the Prairie blowing snow model (PBSM) of Pomeroy *et al.* (1993) . In GEOtop 3.0 the calculations for mean particle mass are modified to estimate horizontal blowing snow fluxes, sublimation rates and latent heat flux due to blown snow sublimation. In the absence of melting, the rate of change in snow mass S at a point is:

$$\frac{dS}{dt} = S_f - q_s - \nabla q_t \tag{2.4}$$

Where S_f represents the rate of snowfall, q_s the local sublimation and ∇q_t is the net rate of snow ablation or deposition due to transport. The vector q_t is parallel to the local wind direction (Essery *et al.*, 1999).

Equilibrium blowing snow transport and sublimation fluxes, $\mathrm{Q}_{s,t}(\mathrm{x},\mathrm{y})$, were calculated at each gridcell following PBSM (Pomeroy et al., 1993), based on wind speed, air temperature and humidity measurements interpolated to the model grid and a threshold wind speed for snow transport (u^*_t), which varies according to the density of the surface snow layer, following Liston (2007). PBSM has been developed for homogeneous fetches of 300 m or greater. Hence an ad hoc scheme similar to that used by Liston and Sturm (1998) and Essery et al. (1999) is used to account for the downwind development of blowing snow in response to spatial variations in wind speed, which vary according to topography and vegetation (Figure 2-2). Under these non-equilibrium conditions, the local blowing snow sublimation (q_s) and transport (q_t) follow equation 2.5:

$$q_{s,t}(\mathrm{x},\mathrm{y}) = \frac{\mathrm{Q}_{s,t}(\mathrm{x},\mathrm{y}) + q_{s,t}(\mathrm{x},\mathrm{y}+\Delta\mathrm{xy}) * \frac{F}{\mu\Delta\mathrm{xy}}}{1 + \frac{F}{\mu\Delta\mathrm{xy}}} \tag{2.5}$$

Where $Q_{S,T}$ is the fully developed sublimation and transport flux for a 1000 m fetch calculated by PBSM, $\Delta\mathrm{xy}$ is the distance between the gridcell and the neighboring upwind gridcell, equal to the grid resolution (10 m), F (m) is the equilibrium-fetch distance, assumed to be somewhere between the 300 m and 1000 m (Pomeroy et al., 1993; Liston and Sturm, 1998), and μ is a non-dimensional scaling constant set to 3 (Essery et al., 1999, Liston and Sturm., 1998). Equation 2.5 is applied separately for each orthogonal component of the wind, i.e., along the east-west (x) and south-north (y) directions, by adjusting the sign of $\Delta\mathrm{xy}$ depending on the wind direction; the two orthogonal flux values are then summed.

A different value for the equilibrium flux F can be used when fluxes are increasing or decreasing downwind, to account for snow transport or snow deposition:

$$F = \begin{cases} F_{up}, & \mathrm{Q}_{s,t}(\mathrm{x},\mathrm{y}) - q_{s,t}(\mathrm{x},\mathrm{y}-\Delta\mathrm{xy}) \geq 0 \\ F_{down}, & \mathrm{Q}_{s,t}(\mathrm{x},\mathrm{y}) - q_{s,t}(\mathrm{x},\mathrm{y}-\Delta\mathrm{xy}) < 0 \end{cases}$$

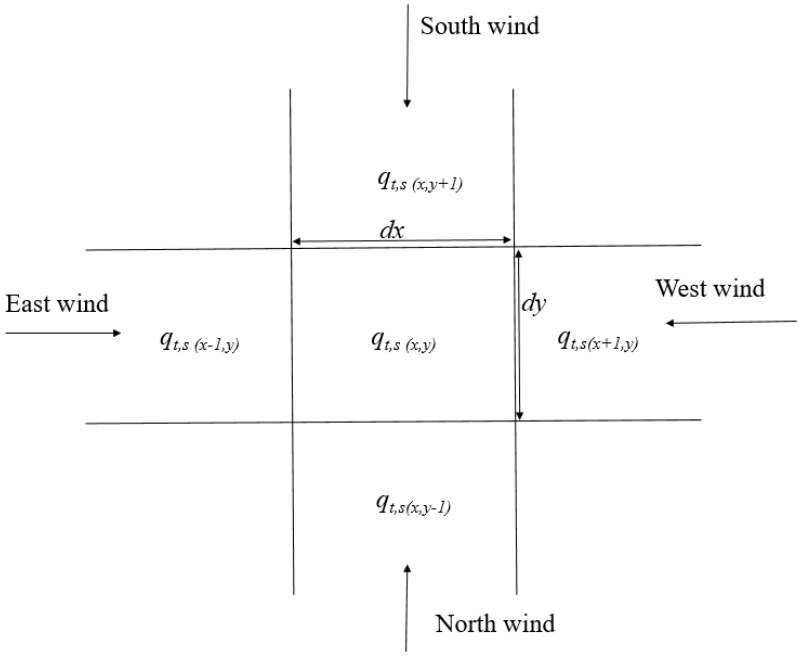

Figure 2-2 A schematic illustration for blowing snow calculation in GEOtop, modified based on Liston and Sturm (1998) and Essery et al. (1999).

The flux divergence term for snow transport (∇q_t) is calculated at each gridcell from the upwind (q_{up}) and downwind (q_{down}) fluxes for each orthogonal component of the wind calculated from equation 2.5:

$$\nabla q_t = \frac{q_{up} - q_{down}}{dx} + \frac{q_{up} - q_{down}}{dy} \tag{2.6}$$

The GEOtop 3.0 model also considers the gravitational movement of snow on steep slopes. Snow accumulation, either from snowfall or from blowing snow transport, is redistributed downslope according to the DEM slope values, for slopes between 30 and 80 degrees,

following Gruber (2007). In the current study, less than 1% of the simulation area had slopes in this range.

2.2.7 GEOtop model configuration and parameterization

A high-resolution (3 m) DEM built from Pleiades stereo images acquired on 28 July 2016 was used to extract topographic inputs to the GEOtop model. The DEM was generated using the Ames Stereo Pipeline (Shean *et al.,* 2016) using the same configuration as a previous study in the Pyrenees Mountains in Europe (Marti *et al.,* 2016). In this study, the snow cover simulations and sensitivity analyses were performed at 3m resolution (3 meters). However, given the high computational cost of running the model at this resolution, simulations were also performed on a 10 m grid in order to evaluate the model sensitivity to DEM resolution. Topographic indices (slope, aspect and skview) were derived for both model resolutions. The local horizon heights and angles used for the calculation of direct solar radiation are calculated internally by the GEOtop model from the input DEM.

In this study, the model parameterization was performed using the deduction, induction, and abduction (DIA) approach (Pomeroy *et al.*, 2013). As such, some parameters were initially prescribed using results from previous studies at the Bylot site and the remaining parameters were derived from other regions with similar hydrological characteristics. Eventually, parameters that could not be determined using filed measurement or from other regions were calibrated (see section 2.2.8).

An hourly temperature lapse rate was calculated for the modeling period 2005-2019 between the Bylocamp and Bylojack stations, respectively located at the lowest and highest points of the modeling domain. The precipitation lapse rate was set to zero due to the small elevation range. The temperature thresholds to distinguish between snowfall and rainfall were set to -1°C (for snow) and 3°C (for rain) based on the air temperature and humidity range at the site (Jennings *et al.,* 2018). In this range (between -1°C and 3°C), the precipitation may fall as a mix of rain and snow, or it may change from rain to snow (or *vice versa*) as it travels through different layers of the atmosphere. The specific conditions,

such as the altitude and humidity, play a role in determining the precipitation type. Soil properties (e.g., the thermal and hydraulic conductivity) were defined based on the literature for each observed soil type (Table S2-1). The initial soil surface temperature was set to 0°C according to surface soil temperature recorded in the Bylocamp station. The vegetation effect on the snow cover is not considered due to the fact that the vegetation is very short (shorter than 5 cm).

Incoming longwave radiation was parameterized since only limited measurements were available at the site. GEOtop includes different parameterizations for the incoming longwave radiation; the parameterization from Dilley and O'Brien (1998) was found to give adequate results against the sparse measurements at the Bylosila station (Figure S2-2). The downward clear sky long-wave irradiance is estimated from air temperature and water vapor pressure (Dilley and O'Brien, 1998). For cloudy skies, GEOtop uses the method of Crawford and Duchon (1999) which proposed a direct relation between the shortwave radiation cloud transmissivity (τ_c) and cloud emissivity (ε_c):

$$\varepsilon_c = \tau_c + (1 - \tau_c) * \varepsilon_a \tag{2.10}$$

The equation provides a linear interpolation between the clear-sky emissivity value (ε_a) and the black-body emissivity (1) for a completely overcast. Turbulent fluxes of sensible (H) and latent heat (LE) in GEOtop are calculated with the flux–gradient relationship following Garratt (1994). A correction for air stability and instability was applied on the turbulent fluxes based on the Monin–Obukhov similarity theory (Monin and Obukhov, 1954).

The visible albedo for snow-free conditions was set to 0.15 based on measured soil albedo at the Bylosila station, deemed representative of a typical tundra surface at the site. To account for the snow albedo decay process in GEOtop several parameters are required including a maximum (fresh snow) and minimum (ground snow-free) albedo. Due to the shallow and patchy nature of the snowpack in the High Arctic, the extinction depth of snow albedo was used, which controls the transition from the snowpack albedo to the ground albedo (e.g. Gubler *et al.,* 2013; Engel *et al.,* 2017). Once the snow depth reaches the

extinction depth, the albedo is interpolated between the snow albedo and that of the bare ground below with an exponential term, approximating the extinction of radiation penetration in the snowpack (Tarboton and Luce, 1996). An initial fresh snow density of 100 kg/m^3 was used, typical of tundra environments (Ménard *et al.,* 2014; Krogh *et al.,* 2017). A maximum of 11 layers was selected to discretize the snowpack, following the suggestion to use at least 10 layers by the model developers.

2.2.8 Parameter sensitivity analysis and calibration

Manual sensitivity analysis was performed at both point (station) and spatial scales for the uncertain model parameters, i.e., those that could not be prescribed based on previous studies or ancillary information at the site (Table 2-2).

Table 2-2 Model parameters selected for sensitivity analysis and calibration. The calibrated value for each parameter is highlighted in bold.

Parameter	Symbol	Unit	Default	Parameter range			
Precipitation input							
Snow correction factor	SCF	-	1	0.8	**1.2**	1.4	1.6
Snow parameters							
Extinction depth of snow albedo	EA	mm	10	0	**70**	100	200
Albedo of fresh snow (VIS)	AV	-	0.9	0.85	0.9	**0.95**	0.98
Albedo of fresh snow (NIR)	AN	-	0.65	0.6	0.65	**0.67**	0.7
Snow ageing coefficient	AF	-	0.2	0.05	0.15	**0.25**	0.25
Irreducible water saturation in snow	IW	-	**0.02**	0.03	0.04	0.05	0.07
Snow aerodynamic roughness	SR	mm	0.1	1	**2**	5	10
Blowing snow							
Fetch-up	F_{up}	m	**1000**	300	500	700	1200
Fetch-down	F_{down}	m	**100**	50	200	300	500

Sensitivity analysis is a useful tool to highlight parameters that significantly influence the model response (Saltelli *et al.*, 1995). Sensitivity analysis was performed at the finest DEM resolution (3 m) for a single hydrological year (Sept. 2016 to Aug. 2017), due to

computational constraints. The default parameter values in GEOtop were used for the base model configuration, except for those parameters that were prescribed based on previous studies or ancillary information as described in section 2.2.7. A one-at-a-time sensitivity test was performed, i.e., by varying each parameter within its sensitivity range while keeping the others to their default value. The parameter ranges used for sensitivity analyses were based on a previous sensitivity analysis by Engel *et al.* (2017) in the Alps. Four parameter combinations were tested per parameter, yielding a total of 36 model iterations. The sensitivity analysis was first conducted at the point scale, then at spatial scale (the simulation domain is highlighted in Figure 2-1) both during the accumulation and melt periods in order to examine how the parameters affect differently the accumulation and melting processes (e.g., Raleigh *et al.,* 2015). The performed model sensitivity at point and spatial scales was assessed by computing the relative change between the simulated snow depth using the modified parameter and that simulated using the default parameters.

Model calibration was done at the Bylocamp station where continuous snow depths measurements are available. The calibration focused on the parameters that had been identified as influential during the model sensitivity analysis. The calibration process was split into two phases: first by calibrating sensitive parameters during the accumulation period, followed by calibration of sensitive parameters during the ablation period. A sequential (incremental) approach was adopted, starting with the parameter deemed most sensitive, and continuing towards the least sensitive parameter. This calibration sequence was applied separately to each period. In each iteration, adjustments were made to the parameter values to iteratively converge towards the observed snow depth value at the Bylocamp station. The parameter interval employed for model calibration corresponds to the identical range as delineated in the sensitivity analysis (Table 2-2). The parameter value yielding the highest value of the Nash-Sutcliffe Efficiency (Nash and Sutcliffe,1970), calculated from the comparison between simulated and observed snow depth, was selected as optimal.

2.2.9 Model validation

Following the sensitivity and calibration analysis, GEOtop was run at an hourly step from 1st September 2005 to 1st September 2019, corresponding to the entire available forcing data. The simulated snow depths were validated against the continuous snow depth record at Bylocamp for 2005-2015. Spatially-distributed snow soundings (2016-2018) and the 2018 UAV snow depth map were used to validate the GEOtop snow depth spatial simulations. Two methods were used to compare the simulated snow depth raster maps with the in-situ observations: (i) bilinear interpolation of the raster snow depth within a 3x3 pixel window centered on the observation; (ii) using the best nearest neighbor within the 3x3 window. Method (ii) was used because a small spatial (± 1 pixel) mismatch was often seen between the simulated and observed snow depth patterns, and so a ±1 pixel tolerance was allowed around the measurement to find the nearest most similar simulated snow depth. The snow cover meltout date simulated by GEOtop was further validated against the snow ruler observations during 2016-2018, using a 1cm threshold on snow depth to determine snow presence and calculate the snow meltout date. The Nash-Sutcliffe efficiency (NSE), the root mean square error (RMSE), the coefficient of correlation (R) and the percent bias (PBIAS) were used to assess model performance against observations (Equations 2.11-2.14).

$$PBIAS = 100 * \frac{\sum_{i=1}^{n}(\mathrm{SD}_s - \mathrm{SD}_o)}{\sum_{i=1}^{n}\mathrm{SD}_o} \tag{2.11}$$

$$NSE = 1 - \frac{\sum_{i=1}^{n}(\mathrm{SD}_s - \mathrm{SD}_o)}{\sum_{i=1}^{n}\left(\mathrm{SD}_o - \overline{\mathrm{SD}_o}\right)} \tag{2.12}$$

$$RMSE = \sqrt{\frac{1}{n}\sum_{i=1}^{n}(\mathrm{SD}_s - \mathrm{SD}_o)^2} \tag{2.13}$$

$$R = \frac{\frac{1}{n}\sum_{i=1}^{n}\left(\mathrm{SD}_s - \overline{\mathrm{SD}_s}\right)\left(\mathrm{SD}_o - \overline{\mathrm{SD}_o}\right)}{\sqrt{\frac{1}{n}\sum_{i=1}^{n}\left(\mathrm{SD}_s - \overline{\mathrm{SD}_s}\right)}\sqrt{\frac{1}{n}\sum_{i=1}^{n}\left(\mathrm{SD}_o - \overline{\mathrm{SD}_o}\right)}} \quad (2.14)$$

Where n is the number of observations, SD_o is the observed snow depth value, SD_s is the simulated snow depth value, $\overline{\mathrm{SD}_o}$ is the average observed snow depth value, and $\overline{\mathrm{SD}_s}$ is the average simulated snow depth value. The Nash-Sutcliffe Efficiency (NSE) metric is widely utilized in the field of hydrology to assess the ratio of the residual variance to the variance of the observations. An NSE score of 1 suggests that the model simulations are an ideal match to the observations, whereas an NSE score of 0 means that the explanatory power of the model is similar to that of the average of observations (Moriasi *et al.*, 2007). The root mean squared error (RMSE) is a weighted metric for quantifying the divergence between the observation and simulation data, in which an RMSE score of 0 denotes a perfect prediction by the model. The correlation coefficient (R) ranges from -1 to +1 and evaluates the strength and directionality of the association between the predictions and observations. The percentage bias (PBIAS) is a proportional measure of the systematic error in the model. A positive PBIAS indicates a model overestimation, whereas a negative value indicates an underestimation.

2.2.10 Snow cover sensitivity to blowing snow processes and model resolution

To investigate the effect of blowing snow transport on the snow depth simulation, the simulations were run with (BS-enabled) and without (BS-disabled) the blowing snow scheme. Also, because the accurate representation of the snow distribution in complex terrains is contingent on the spatial scale of the model employed (Schlögl *et al.*, 2016; Baba *et al.*, 2019), the sensitivity of the model performance to model resolution was examined by comparing the 10m and 3m model runs against snow depth measurements.

2.3 Results

2.3.1 Sensitivity analysis and model calibration

The sensitivity analysis showed that the model was more sensitive to uncertain parameters overall during the melting period than during the accumulation period at the Bylocamp station (Figure 2-3). The parameter sensitivity at the spatial scale during the melt period is also pronounced, but less than at the point (Bylocamp) scale. During snow accumulation, the snow correction factor (SCF) is by far the most sensitive parameter, followed by the extinction depth of snow albedo (EA) at both spatial and point scales. Both the fetch-up (F_{up}) and fetch-down (F_{down}) parameters showed a relatively moderate sensitivity at point scale and a relatively weak sensitivity at the spatial scale. The remaining parameters are comparatively insensitive (Figure 2-3).

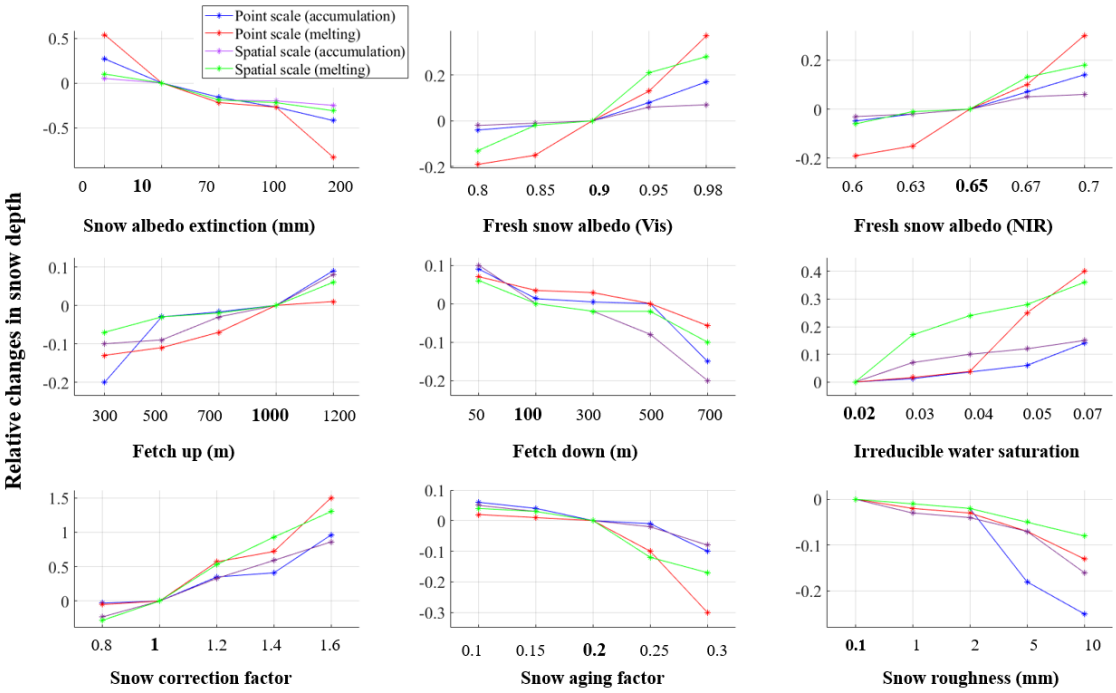

Figure 2-3 Results of sensitivity analyses of GEOtop model parameters for the snow accumulation (10th Sept. 2017 to 1st May 2017) and melting (10th May 2017 to 31th May 2017) periods. The sensitivity is measured as the relative changes in simulated mean snow depth compared to the default model parameter, at the point (Bylocamp station) and spatial scale for hydrological year 2017. The default value for each parameter is highlighted in

bold along the x-axis. Note the non-linear scaling of the x-axis and the different limits on the y axis.

In the melting season, the snow correction factor was also the most important parameter affecting snow depth at the point scale, even surpassing the sensitivity during the snow accumulation season. Snow albedo extinction, fresh snow albedo (both at NIR and Vis wavelengths) and irreducible water saturation were found to be the next most important parameters that significantly affect the snow cover dynamic during the melting season. The snow aging coefficient and snow aerodynamic roughness showed a moderate sensitivity. At the spatial scale, the most critical metric is by far the snow correction factor (SCF), followed by the snow albedo extinction depth, fresh snow albedo and irreducible water saturation while the other parameters were comparatively insensitive.

The calibration process was executed independently for each distinct period, with a focus on the most influential parameter for that specific phase. During the snow accumulation period, the initial step involved calibrating the snow correction factor, succeeded by adjustments to the extinction depth of snow albedo (EA), fetch-up (Fup), and fetch-down. Conversely, in the melt period, calibration commenced with the fresh snow albedo (both NIR and Vis wavelengths) and irreducible water saturation, followed by fine-tuning of the snow aging coefficient and snow aerodynamic roughness. Notably, when calibrating the model for the melting season, parameters that were both highly sensitive and successfully calibrated during the accumulation period were maintained within their optimal ranges.

The albedo values of fresh snow for the visible and near-infrared bands were calibrated to 0.95 and 0.67, respectively. The snow aging coefficient, which significantly influenced the simulated snow depth during melting, was calibrated to 0.25. A better estimation of snow depth was achieved when the snow albedo extinction was set to 70 mm. The snow surface aerodynamic roughness was set to 2 mm after calibration. The irreducible water saturation for snow (the ratio of the capillarity-hold water to ice content in the snow) was calibrated to 0.02. The range of fetch-up (Fup) and fetch-down (Fdown) parameters were calibrated to 1000 and 100 meters respectively.

2.3.2 Model validation

The simulated snow depth at the Bylocamp station over the historical period, using the calibrated parameters (Table 2-2) showed a reasonably good agreement with observations (Figure 2-4, Table 2-3). The model performance metrics decreased somewhat during the validation period, but were still considered good ($0.65 < NSE < 0.75$) based on Moriasi *et al.* (2007) (Table 2-3).

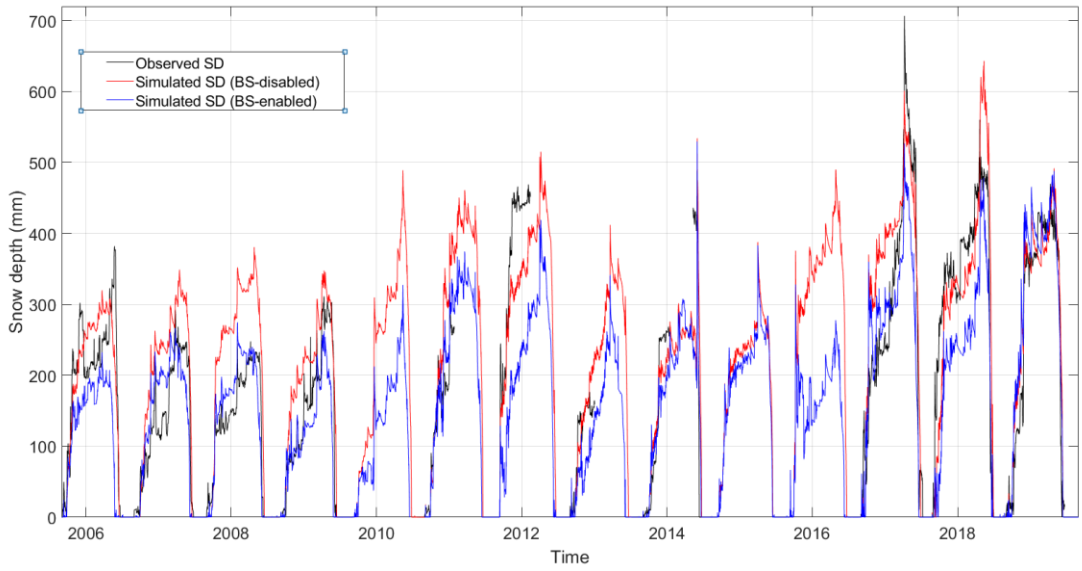

Figure 2-4 Observed (black) and simulated (blue: with blowing snow transport, red: without blowing snow transport) snow depth at the Bylocamp station at a 3 m model resolution. The period 2016-2018 was used for model calibration and 2005-2015 for model validation.

The simulated snow depth at the Bylocamp station exhibits a slight negative bias during the calibration period (2016-2018) and a slight positive bias during validation (2005-2015). The magnitude of the bias is greater during validation than during calibration (Table 2-3). The simulated snow depth displays similar interannual variability to the recorded snow depth, with no evidence of anomalous behavior during validation (Figure 2-5). As such, the correlation coefficient (R) and the Nash-Sutcliffe coefficient (NSE) were high during calibration ($R = 0.91$, $NSE = 0.81$), reflecting the good temporal synchronicity and small errors between the simulated and observed SD, but decreased somewhat during validation

(R = 0.86, NSE = 0.70). Ignoring of the blowing snow routine in the simulation resulted in a large underestimation of snow depth (BIAS = -33.59%) and a decrease in NSE during validation (0.52), despite a high correlation between observed and simulated snow depths (R = 0.90).

Table 2-2 Calibration and validation metrics for simulated daily snow depth at the Bylocamp station on a 3 m model resolution grid

	Calibration (2016-2018)	Validation (2005-2015)	
	BS-enabled	BS-enabled	BS-disabled
PBIAS (%)	-5.97	14.38	-33.59
RMSE (mm)	16.07	18.54	42.75
R (-)	0.91	0.86	0.90
NSE (-)	0.81	0.70	0.52

The spatial model validation during the period 2016-2018 showed a lower accuracy compared to the points-scale validation (Table 2-4), but the results were still satisfactory (NSE > 0.5). The best nearest neighbor interpolation method yielded better validation metrics (NSE = 0.68) than the bilinear interpolation method (NSE = 0.17), against the recorded snow depth data, showing that small spatial offsets (± 1 pixel) between modelled and observed snow depth can significantly degrade model validation when comparing points observations with fine-scale, gridded simulated snow depths. Hence, the best nearest neighbor interpolation method was used thereafter for model validation.

Table 2-3 Validation metrics for simulated snow depths against spatial manual snow depth surveys across the model domain at 3 and 10 m spatial resolution. –BS refers to model simulation with blowing snow processes disabled.

Error metrics	2016			2017			2018		
	BS 3m	-BS 3m	BS 10m	BS 3m	-BS 3m	BS 10m	BS 3m	-BS 3m	BS 10m
PBIAS (%)	7.1	17.1	14.4	4.1	21.8	14.2	5.6	-9.6	6.7
RMSE (mm)	30.3	68.1	61.1	18.5	98	65.8	26.7	44.7	31.7
R (-)	0.78	-0.19	0.58	0.86	-0.23	0.73	0.77	-0.24	0.59
NSE (-)	0.49	-0.03	0.21	0.68	-0.04	0.31	0.52	-0.03	0.26

Deactivating blowing snow resulted in a significant degradation in model performance (Table 2-4). This shows that the blowing snow scheme greatly improved the spatial representation of the snow cover due to snow redistribution by wind and blowing snow sublimation. The best performance was found in 2017 (R = 0.86 and NSE = 0.68) compared to 2016 (R = 0.77, NSE = 0.49) and 2018 (R = 0.78, NSE = 0.52), respectively. This can partly be ascribed to the fact that the manual snow depth surveys in 2017 were spatially more extensive, covering a larger landscape gradient (Figure 2-1). Also, the snow depth observations in 2017 were averages of five measurements within a 1 m radius from the center point, thus reducing the uncertainties due to measurements and microscale spatial variability. The 2018 UAV snow depth map captured highly heterogeneous snow depth patterns across the landscape, including deeper snow depth in ravines and channels, and shallower depth over flat terrain (Figure 2-5c and f). The higher resolution (3 m) simulation seems to have adequately reproduced the main erosion and snowdrift patterns (Figure 2-5b).

The moderate correlation between the simulated and UAV SD map (R = 0.67) confirms that the spatial variability is reasonably well reproduced by GEOtop. However, small spatial misalignments of snowdrift features deteriorated the error metrics, yielding only moderate spatial model skill (NSE = 0.32). The mean relative error (bias) is -10%, showing an underestimation by the model, while ignoring blowing snow instead led to a positive bias (17%), showing a significant snow depth overestimation by the model. The coefficient of variation (CV) of the simulated snow depth map was much higher (0.38) than that when BS was disabled at a 3m resolution (CV = 0.07); however, UAV snow depth demonstrated a higher CV (CV = 0.58) than simulated, showing that the spatial heterogeneity was still underestimated by the model even after accounting for BS processes. It should also be noted that the gridded UAV snow depths were aggregated (averaged) from 2.3 cm resolution raw grids, thus capturing microscale variability not simulated at either 3m or 10m by GEOtop. Increasing the model resolution from 3 to 10m degraded the spatial representation of the snow cover (CV= 0.28), but the main snowdrift patterns were still captured with deeper snow in sheltered depositional areas and shallower depth in exposed, eroded areas (Figure 2-5e).

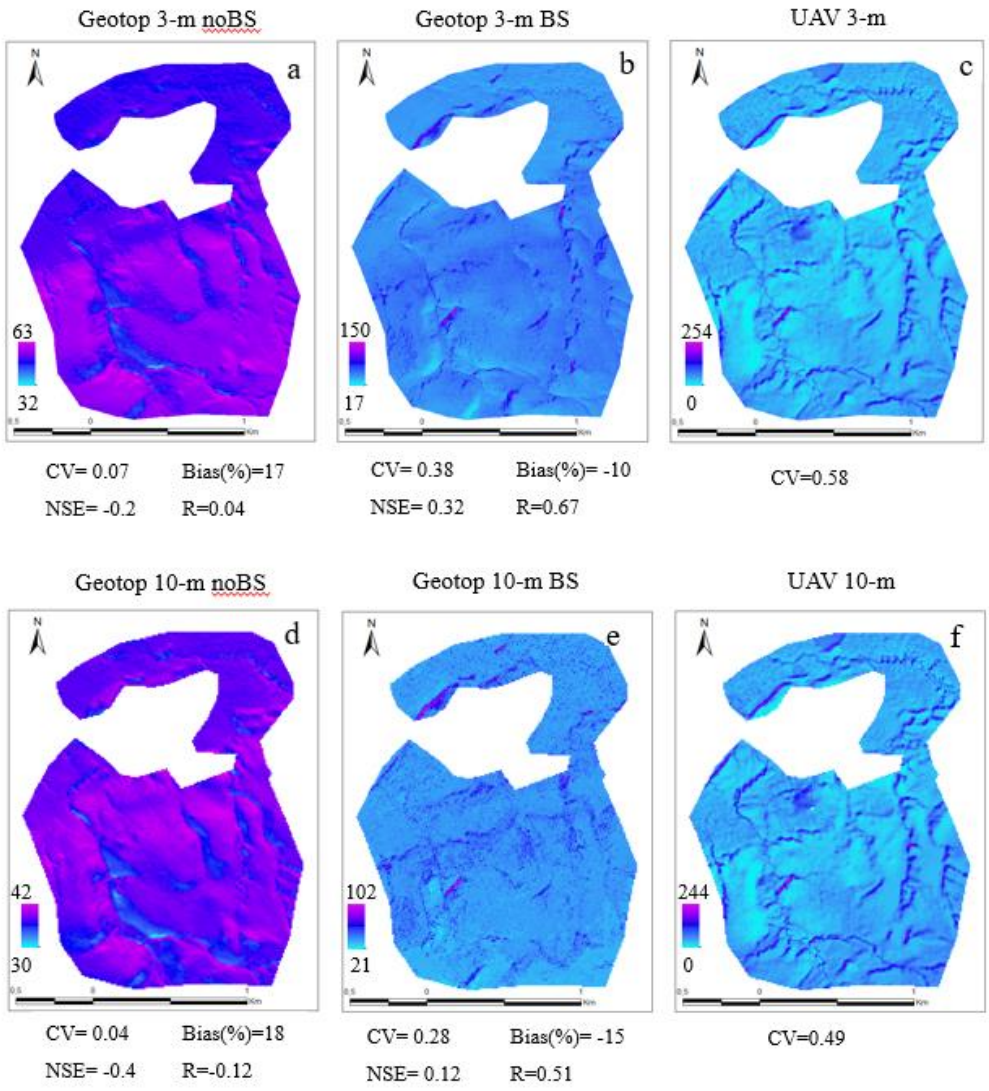

Figure 2-5 Simulated (a, b, d and e) and measured (c and f) snow depth at two different resolutions (a-c: 3m, d-f: 10m) on May 15th, 2018. (a) Simulated SD with BS disabled at 3 m resolution; (b) Simulated SD with BS enabled at 3 m resolution; (c) UAV SD map aggregated at 3 m resolution; (d) Simulated SD with BS disabled at 10 m resolution; (e) Simulated SD with BS enabled at 10 m resolution, and (f) UAV SD map aggregated at 10 m resolution. The statistical values (CV, Bias, NSE, and R) are relative to the UAV snow depth map.

In order to better understand if, and how, the unaccounted spatial heterogeneity relates to microtopography, the simulated and manual snow depth were compared by the main morphology types (Figure 2-6). The correlation between predicted and observed snow depth accuracy was higher (higher R) in the deposition areas (ice wedge polygons, ravines and water tracks) in comparison to hummocky surfaces, which are typically more exposed and windswept.

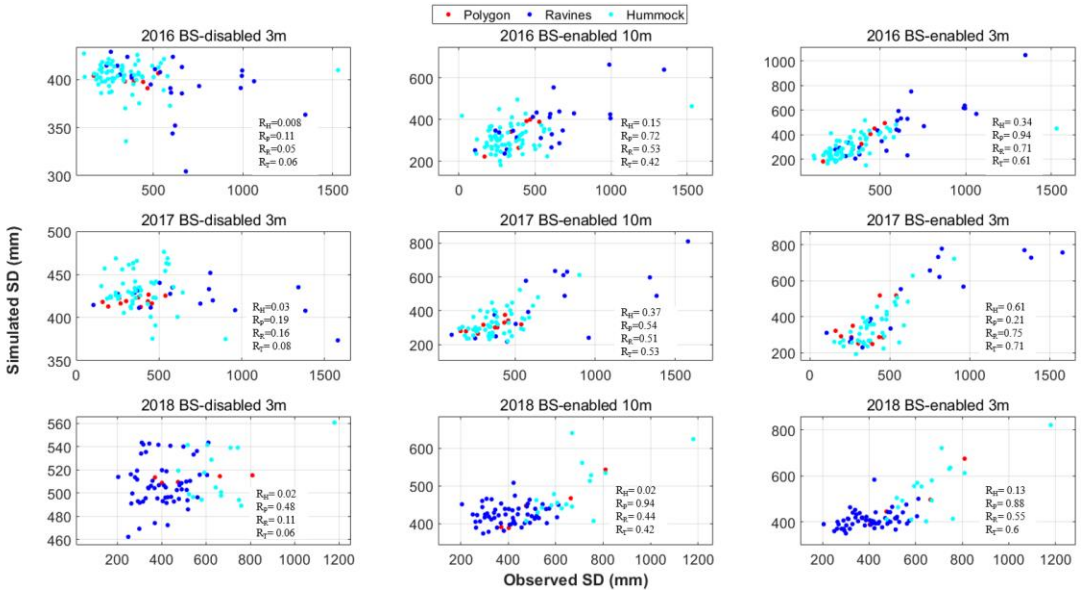

Figure 2-6 Observed vs. simulated snow depth over the modelled domain over three consecutive years. Points are colored by the dominant landform type, with corresponding correlation coefficients between simulated and observed snow depth: hummocky surfaces (RH), ice wedge polygons (RP), ravines/water tracks (RR) and all morphologies combined (RT).

The activation of blowing snow processes had only a minimal impact on the snowmelt pattern at the snow ruler network (Figure 2-7). The results showed that simulated snow depth is almost less than observed snow depth at transects when BS enabled. During 2017 and 2018 a snow accumulation event is not captured by either models (BS enabled/disabled) which is most probably due to the undercatch of precipitation. The visual pattern in Figure 2-7 indicates that the model, whether with or without blowing snow processes, was sufficiently capable of simulating the snowmelt slope across the observed snow depth in snow transects.

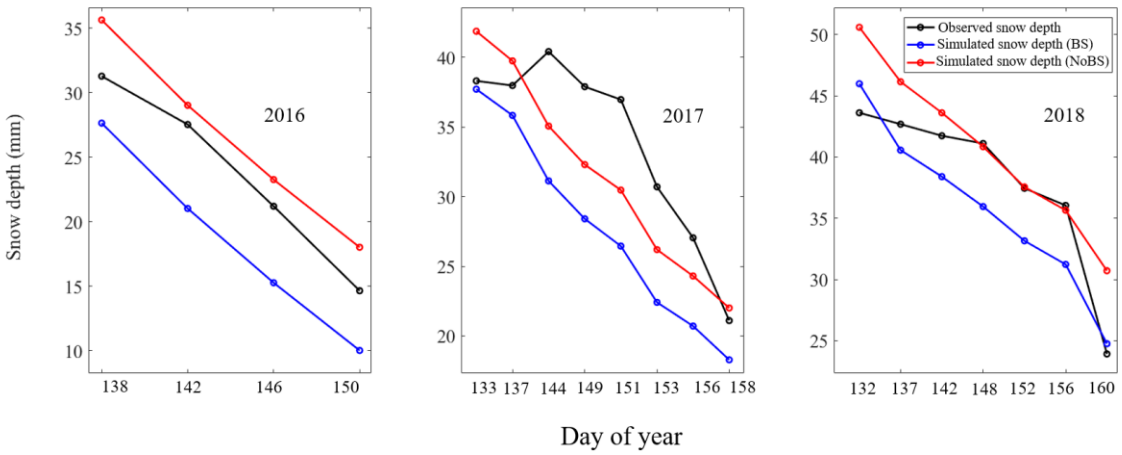

Figure 2-7 Average snow depth (mm) over 50 points at the snow ruler transects for three consecutive years at 3 meters resolution. The black line represents measured snow depth, while blue and red lines indicate simulated SD in the presence and absence of the wind respectively.

2.3.3 Simulated mass balance

The spatially averaged simulated cumulative mass fluxes and daily SWE evolution for the 2016-2018 validation period is presented in Figure 2-8. The simulated snowpack starts accumulating in the first week of September and remains on the ground until the first week of June. Blowing snow at Bylocamp station started in early October and increased when snowfall occured (Figure 2-8a). The mean SWE exhibited large inter-annual variability (±24 mm), which mostly resulted from the high interannual variability of snowfall (±38mm). Snowmelt was the largest outflux at approximately 140 mm year−1, representing approximately 68% of the mean annual snowfall. Snowpack sublimation reached an average of 14 mm year−1, which is approximately 8.9 % of the mean annual snowfall. Overall, total sublimation losses from both snowpack and blowing snow reached 41 mm year−1 (22.5 % of annual snowfall). The rate of snow erosion dominated the snow transport in the simulated study area.

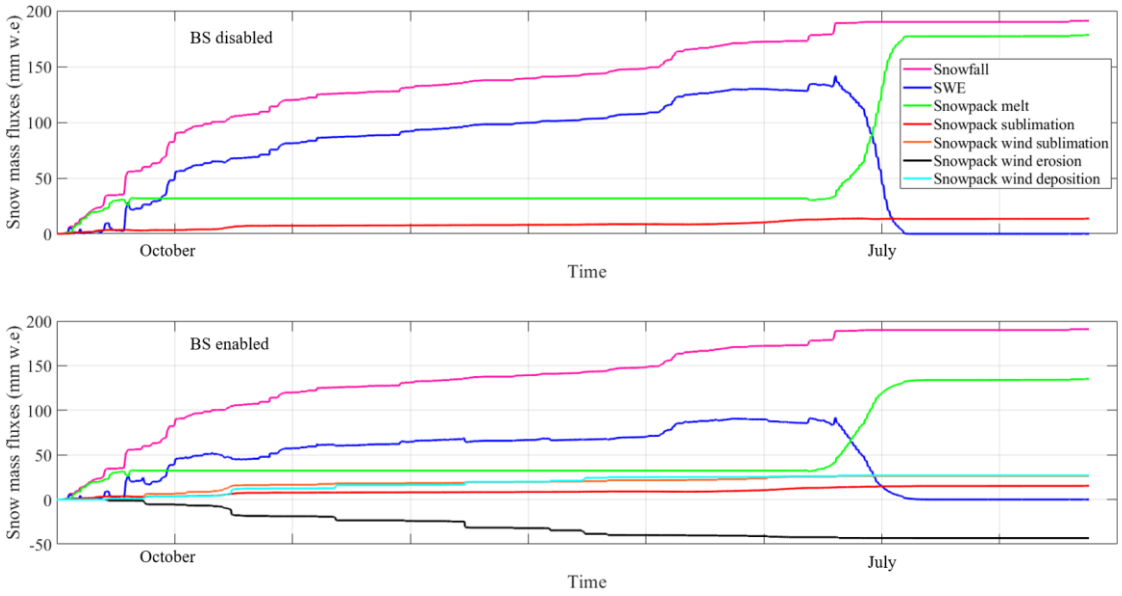

Figure 2-8 Simulated cumulative snow mass fluxes at the spatial scale between the years 2016-2018 when BS is enabled and when BS is disabled.

Exclusion of blowing snow processes significantly affected snow cover metrics (Figure 2-8). The differences in snow phenologies were most pronounced in the fall and spring when most precipitation events occured (Mohammadzadeh Khani *et al.*, 2023), which enhanced blowing snow sublimation during high snow transport events during snowfall. SWE showed a substantial variability between the two model configurations (BS-enabled/disabled), with the mean maximum SWE reaching 91 mm over the validation period (2016-2018) when blowing snow was enabled, and 145 mm when blowing snow was disabled. Removing blowing snow processes led to a corresponding increase of snow cover duration up to 10 days compared to the BS-enabled simulation during the validation (Figure 2-8b).

2.4 Discussion

2.4.1 Model parameterization

Regardless of model selection, the uncertainty in the determination of model parameters is a major cause of error in hydrological modeling (Devak and Dhanya, 2017). This makes

parameterization as important as having an appropriate model structure and accurate external forcings (Luo and Schuur, 2020). In this study model parameterization relied on prior knowledge of Arctic hydrology, field research in the region, and calibration against snow depth observations. The sensitivity analysis showed that the model parameterization was highly dependent on the season, i.e., some model parameters were more sensitive during the snow accumulation than the ablation period, and vice-versa. The snow correction factor had the largest influence on the simulated winter snow depth both at the point and spatial scales. This influence carried over to the melting period, since snow depth evolution during melting is reliant on the pre-melt snow accumulation. The even higher sensitivity of the snow correction factor observed during ablation implies a positive feedback of winter snow accumulation on melting via other parameters, such as the albedo extinction depth, i.e. lower accumulation causes the snow to reach more quickly its extinction depth in the spring. The high sensitivity to the snow correction factor is unsurprising, as accurate snowfall is the main requirement for an accurate snow cover simulation, as found in previous studies in the Arctic (Pomeroy and Jones, 1996; Franz and Karsten, 2013; Krogh, Pomeroy and Marsh, 2017) and in the alpine areas (Engel *et al.,* 2017; Voordendag *et al.,* 2021). It points to the already recognized necessity, and challenge, of obtaining quality winter precipitation data, reliable undercatch corrections, and realistic spatialization procedures (Mair *et al.*, 2016; Freudiger *et al.*, 2017; Kochendorfer *et al.*, 2017). A higher parameter sensitivity was observed at the point scale than at the spatial scale (Figure 2-3). This could be explained by the fact that the relative changes in mean snow depth were spatially averaged, so that locally high or low values compensate each other and reduce the sensitivity range. This is similar to study by Engel *et al.* (2017) that observed a wider range of snow depth sensitivity to parameter ranges at the point scale compared to the spatial scale.

The calibrated snow albedo extinction depth in this study (7 cm) is less than reported in other regions, for example 20 cm by Engel *et al.* (2017) in the Alps and 10 cm by Baker *et al.* (1991) in Minnesota, USA. The lower snow albedo extinction depth at the Bylot island site can be due to fact that snow cover is denser in tundra environment, due to the presence of a thick wind slab (Dominé *et al.*, 2002; Domine *et al.*, 2018). The greater snowpack

density facilitates energy exchanges between the atmosphere and the ground surface (DeWalle and Rango, 2008). As a result, the current study calibrated a reduced snow depth extinction to account for this phenomenon compared to previous studies. The fresh snow albedo also was found to be a significant parameter affecting snow depth during the melting season. This is in line with the study by Xue *et al.* (2003) in the Arctic region emphasizing that a proper snow albedo is essential throughout the ablation period which can impact the timing and amount of both the SWE and runoff. However the fresh snow albedo calibrated in this study (0.95) was slightly higher than that reported by Krog *et al.* (2003) for Havikpak Creek area (0.9), a low Arctic tundra environment. The variation in albedo observed in these two studies can likely be attributed to disparities in the physical characteristics of the snow cover (Warren *et al.*, 2006). Regarding the fetch parameters that control the redistribution of snow in the landscape, optimal values of 1000 meters for fetch-up (F_{up}) and 100 meters for fetch-down (F_{down}) were found during the snow accumulation season. The calibrated fetch-up in this study is in the same range of values as applied in other studies for open terrain of the Arctic region (Pomeroy and Jones, 1996; Pomeroy *et al.*, 1997; Krogh *et al.*, 2017). In this study, fetch down parameter was calibrated to 100 meters which contributed to a more accurate representation of snowpack dynamics but also holds promise for improving the understanding of snow-driven processes, such as snowmelt, sublimation, and snowpack energy balance.

2.4.2 Impact of blowing snow processes on model skill

Our results show that calculating snow accumulation only based on winter precipitation is insufficient. Instead, blowing snow processes and landscape conditions control the spatial distribution and overall accumulation of snow depth during the winter. This is in agreement with prior studies in open terrains of the Arctic and Antarctic that showed that winter precipitation alone is insufficient to calculate snow accumulation and that blowing snow processes and landscape govern the spatial distribution and total accumulation of snow water equivalent over the winter (Pomeroy *et al.*, 1997; Déry and Yau, 2002; Liston and Elder, 2006a; Palm *et al.*, 2017). Including wind-blown snow in the simulation led to a more than 43% decrease in maximum SWE simulated at the Bylocamp station, compared

to when blowing snow was excluded (Figure 2-8). This is similar to the study by Pomeroy and Li (2000) who found that blowing snow processes were responsible for removing 48% to 58% of snowfall in Prairies environments. However this is less than the study by Frezzotti *et al.* (2002) that found over certain parts of Antarctica, where persistent katabatic winds prevail, blowing snow sublimation was found to remove up to 85% of the solid precipitation and much higher than study by Chung *et al.* (2011) that reported that blowing snow resulted in a loss of approximately 6% of the annual precipitation over 324 days from 1997 to 1998 across the Arctic Ocean (SHEBA). Our results was also higher than study by (Gascoin *et al.*, 2013) that found that inclusion of blowing snow processes led to 18% of the total ablation over the whole study area of the Dry Andes (Chili).

While previous studies have used distributed blowing snow models to document the effect of topography and vegetation on snowdrift patterns (Pomeroy and Jones, 1996; Liston and Elder, 2006a; Musselman *et al.*, 2015; Bennett *et al.*, 2022), few studies have validated extensively snowdrift-permitting models at fine spatial scales (less than 10m). The inclusion of blowing snow processes into the GEOtop model yielded substantial and favorable improvements in model performance, particularly in its agreement with UAV-derived and manually snow depth measurements. Prior to the inclusion of blowing snow processes, the Nash-Sutcliffe Efficiency (NSE) were -0.2 (against UAV-derived) to 0.07 (against manual). However, post-inclusion, the NSE increased significantly to 0.32 and 0.52 respectively. The model exhibited an overestimation of maximum snow depths when blowing snow (BS) was disabled (Table 2-4). This overestimation can be attributed to a notable unaccounted mass loss due to blowing snow sublimation. The inclusion of blowing snow improved the model accuracy and resulted in reduced bias values. Our result is same as the study by Gascoin *et al.* (2013) that under both condition (BS enabled/disabled) overestimated the snow depth in the Dry Andes of Chile. However our result was against a study by Marsh *et al.* (2020) that found an underestimation of SWE across a tundra valley. Despite this lingering positive bias, the model satisfactorily represented the spatial pattern of accumulation observed from UAV mapping, albeit with subdued spatial heterogeneity (CV = 0.38) compared to the UAV map (CV = 0.58). These results are in line with those by Marsh *et al.* (2020) who found that including blowing snow processes in their simulation

increased the coefficient of variation of snow depth from 0.04 to 0.31, better matching the observed CV (0.41).

2.4.3 Effect of model resolution and landscape morphology on model skill

The current study demonstrated that coarsening the model resolution from 3m to 10m did not affect greatly the snow patterns at the hillslope scale, but impacted variability at the microscale (Figure 2-5). Our results showed that a coarser model resolution can lead to locally erroneous simulated snow depth conditions. For instance, when simulated snow depth using the 10m DEM, flat areas had deeper snow and deposition areas shallower snow depth compared to simulated snow depth using the 3m DEM. This agrees with the study by Schlögl et al. (2016) who tested the sensitivity of snow simulation to model resolution in Switzerland. They concluded that the flattening of the topography at coarser resolution led to SWE being overestimated by up to 10% during the ablation period, which causes the amount of snow melting to be underestimated. This is also similar to study by Sohrabi *et al*. (2019) indicated that model accuracy is substantially reduced with model scales coarser than 50 m.

The association of snow cover depth with periglacial morphology was examined by comparing observed snow depth around 3 periglacial landform (Hummocks, polygons and ravines) against simulated snow depth at 2 different model resolutions (3 and 10 meters). The analysis was made of scatterplots and correlations between snow depth and individual topographic variables. The findings of this study revealed the model varying capacity for accurate simulation, with more favorable outcomes observed in larger landscape areas, such as polygons, compared to smaller features like hummocks (Figure 2-6). The pronounced differences in correlation between different morphological types and snow depth distribution suggest that the presence of specific periglacial morphology, such as deposition areas, may act as a controlling factor in snow distribution and depth accuracy and call for a need to include surface morphology as a further parameterization. These findings demonstrate a resemblance to a previous investigation conducted in a sub-Arctic watershed of the Seward Peninsula, Alaska, which revealed that a simple model developed

using topographic information alone correlate strongly with local snow depth variation (Shirley *et al.*, 2023). Additionally, our results underscored the sensitivity of the model ability to reproduce snow patterns within periglacial morphology to the model resolution (Figure 2-6). Notably, a substantial decline in the correlation between simulated and observed snow depths, from 0.7 to 0.5, was observed around ravine landforms when the model resolution was coarsened from 3 meters to 10 meters. These findings are in line with a previous investigation conducted in the Upper Kuparuk watershed, Alaska, which revealed that subgrid-scale snow-cover heterogeneity over complex Arctic terrain provides a better representation of the end-of-winter snow water equivalent (Déry *et al.,* 2004). These fining are crucial because several study reported the importance of spatial variability of snow accumulation on ground surface temperature and the thickness of permafrost active layer (e.g., Sturm and Holmgren, 1994; Smith *et al.*, 2010; Gouttevin *et al.*, 2018). For example, Mohammadzadeh Khani *et al.* (2023) reported a significant difference of ground surface temperature (up to 3.9°C) over a distance of less than one meter due to the large heterogeneity in snow depth resulting from blowing snow over at the Bylot island study site.

2.4 Conclusion

The physically based, distributed hydrological model GEOtop was used for the first time to estimate the snow cover evolution and assess the effect of blowing snow processes and fine-scale topography on the heterogeneity of snow cover in a High Arctic tundra environment. Prior to model calibration a sensitivity analysis was conducted to identify the most important parameters that affect snow depth during both snow accumulation and snow ablation. Also, the sensitivity of the model performance to the DEM spatial resolution and landscape morphology type was also examined. The model results were compared to an extensive snow depth observation dataset at the point and spatial scales. The sensitivity analysis showed that some model parameters were more sensitive during the accumulation or ablation season, which required to use a sequential calibration procedure to tune the uncertain model parameters. Also, the model parameters showed a stronger sensitivity at point scale compared to spatial scale. Changing the model resolution from 3 m to 10 m

caused an increase in the model bias and erroneous due to the flattening of the topography with coarser resolution. An observable impact of periglacial morphology on model performance became evident when simulating snow depth across various landform types. Model was able to perform better across the fine scale morphological indices while it was struggling when simulation snow depth around small scale features. The blowing snow enabled GEOtop model allowed for a realistic representation of the snow cover, allowing to reliably diagnose the snow cover and snow mass balance evaluation in a tundra landscape. Inclusion of blowing snow processes in the model allowed to better simulate the snow cover heterogeneity across the complex terrain of tundra environment. Also, not considering the wind effect led to a false estimation of snow mass fluxes. The physically based nature of the model allows for its application in a wide variety of climates and makes it particularly apt to address issues of changing climate. This could be very useful, i.e. in order to study climate change effects on flora and fauna.

Supplementary materials

Table S2-1 Defined soil characteristics for the simulation. Dz: soil layer thickness, Kh: lateral hydraulic conductivity, Kv: normal hydraulic conductivity, TC: thermal conductivity, res: residual water content soil hydraulic property representing the minimum water content in the soil, fc: Field capacity, sat: Theta saturated (thetas) is the saturated water content soil hydraulic property representing the maximum water content in the soil. , a: Alpha, n: N parameters of Van Genuchten, and SS: soil Specific Storativity.

Dz	Kh	Kv	TC	res	fc	sat	a	n	SS
280	1.00E-07	1.00E-07		0	0.03	0.4	0.004	1.1	1.00E-06

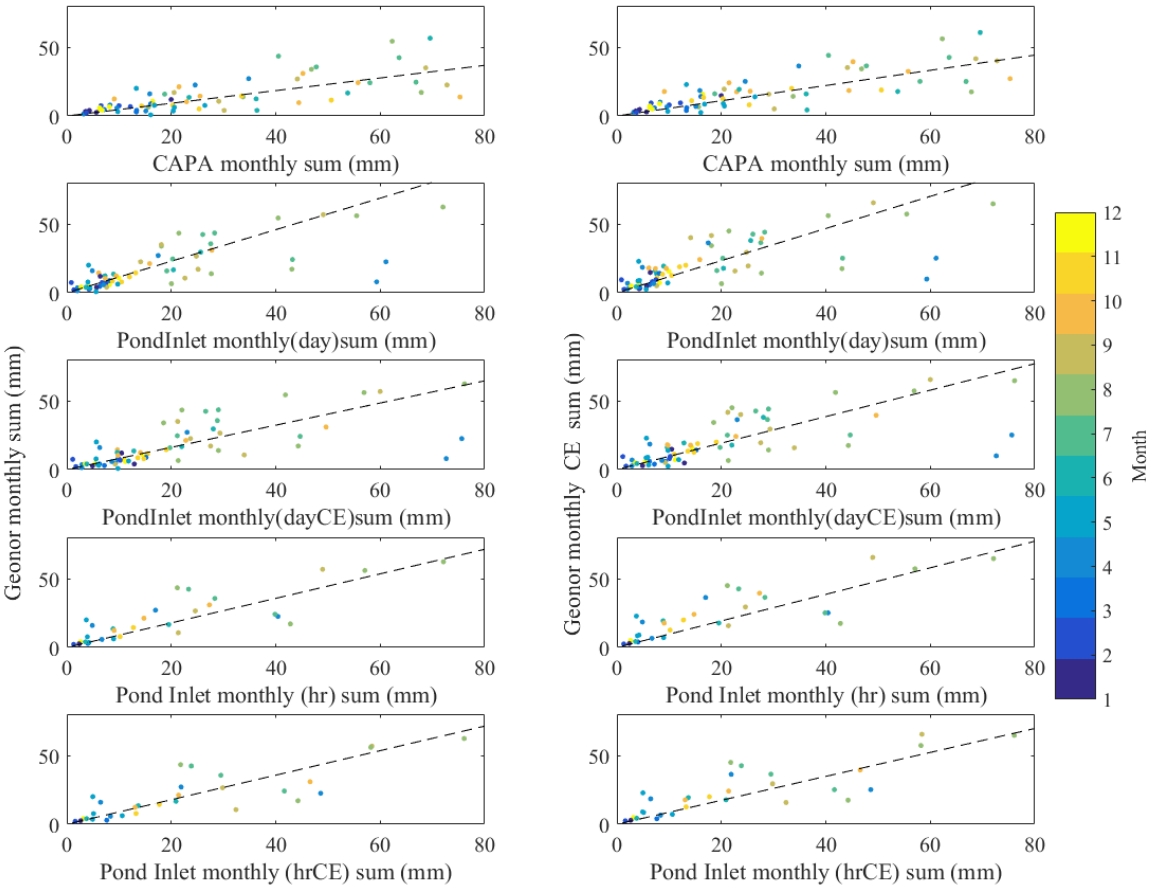

Figure S2-1 Correlation between monthly precipitation in Bylocamp station and reference data (Including daily and hourly precipitation data of Pond Inlet station and CAPA data).

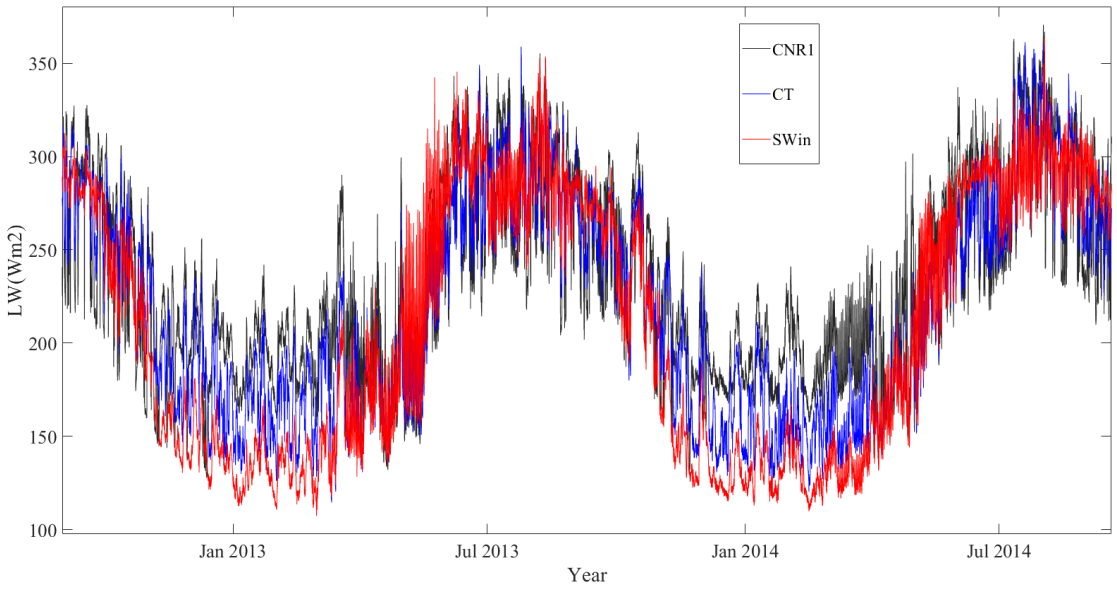

Figure S2-2 Simulated incoming longwave radiation by two different input data, including cloud transmissivity (blue line, CT) and incoming shortwave radiation (red line, SWin) versus recorded incoming longwave radiation by CNR1 at Bylosila station (black line). CT refers to the method that instead of incoming solar radiation the model was run by cloud transmissivity.

References

Benson, C. S. and Sturm, M. (1993) 'Structure and wind transport of seasonal snow on the Arctic slope of Alaska', Annals of Glaciology, 18, pp. 261–267. doi: 10.3189/s0260305500011629.

Biskaborn, B., Smith, S. L., Noetzli, J. et al. (2019) 'Permafrost is warming at a global scale', Nature Communications, 10(2019), pp. 1–11. doi: https://doi.org/10.1038/s41467-018-08240-4.

Bliss, L. C., Courtin, G. M., Pattie, D. L., Riewe, R. R., Whitfield, D. W. A. and Widden, P. (1973) 'Arctic tundra ecosystems', Annual Review of Ecology and Systematics, 4, pp. 359–399. doi: 10.1146/annurev.es.04.110173.002043.

Brown, R. D. and Robinson, D. A. (2011) 'Northern Hemisphere spring snow cover variability and change over 1922-2010 including an assessment of uncertainty', The Cryosphere, 5, pp. 219–229. doi: 10.5194/tc-5-219-2011.

Assini, J. and Young, K. L. (2012) 'Snow cover and snowmelt of an extensive High Arctic wetland : spatial and temporal seasonal patterns', Hydrological Sciences Journal, 57, pp. 738–755. doi: 10.1080/02626667.2012.666853.

Aygün, O., Kinnard, C., Campeau, S. and Krogh, S. A. (2020) 'Shifting hydrological processes in a Canadian agroforested catchment due to a warmer and wetter climate', Water (Switzerland), 12(3). doi: 10.3390/w12030739.

Baba, M. W., Gascoin, S., Kinnard, C., Marchane, A. and Hanich, L. (2019) 'Effect of digital elevation model resolution on the simulation of the snow cover evolution in the High Atlas', Water Resources Research, 55(7), pp. 5360–5378. doi: 10.1029/2018WR023789.

Baker, D. G., Skaggs, R. H. and Ruschy, D. L. (1991) 'Snow depth required to mask the underlying surface', Journal of Applied Meteorology and Climatology, pp. 387–392.

Barnes, S. L. (1964) 'A technique for maximizing details in numerical weather map analysis', Journal of Applied Meteorology and Climatology, pp. 396–409.

Beck, H. E., Zimmermann, N. E., McVicar, T. R., Vergopolan, N., Berg, A. and Wood, E. F. (2018) 'Present and future köppen-geiger climate classification maps at 1-km resolution', Scientific Data, 5, pp. 1–12. doi: 10.1038/sdata.2018.214.

Bennett, K. E. et al. (2022) 'Spatial patterns of snow distribution in the sub-Arctic', Cryosphere, 16(8), pp. 3269–3293. doi: 10.5194/tc-16-3269-2022.

Bilodeau, F., Gauthier, G. and Berteaux, D. (2013) 'The effect of snow cover on lemming population cycles in the Canadian High Arctic', Oecologia, 172, pp. 1007–1016. doi: 10.1007/s00442-012-2549-8.

Bliss, L. C., Courtin, G. M., Pattie, D. L., Riewe, R. R., Whitfield, D. W. A. and Widden, P. (1973) 'Arctic tundra ecosystems', Annual Review of Ecology and Systematics, 4, pp. 359–399. doi: 10.1146/annurev.es.04.110173.002043.

Bortoli, E., Bertoldi, G., Cordano, E., Sartori, A. and Cozzini, S. (2018) 'GEOTOP 3.0: Towards a modern software engineering for integrated hydrologic models', in Atti del XXXVI Convegno Nazionale di Idraulica e Costruzioni Idrauliche. Ancona, Italy. doi: 10.1002/2016WR019191.

Brown, R., Marsh, P., Dery, S. and Yang, D. (2021) 'Snow cover—Observations, processes, changes and impacts. In Arctic Hydrology, Permafrost and Ecosystems', in Arctic Hydrology, Permafrost and Ecosystems, pp. 61–99.

Bruland, O., Liston, G. E., Vonk, J., Sand, K. and Killingtveit, A. (2004) 'Modelling the snow distribution at two high arctic sites at Svalbard, Norway, and at an alpine site in central Norway', Nordic Hydrology, 35(3), pp. 191–208. doi: 10.2166/nh.2004.0014.

Bui, M. T., Lu, J. and Nie, L. (2020) 'A review of hydrological models applied in the permafrost-dominated Arctic region', Geosciences (Switzerland). MDPI AG, 10(10), pp. 1–27. doi: 10.3390/GEOSCIENCES10100401.

CEN (2021) 'CEN: Climate station data from Bylot Island in Nunavut, Canada, http://www.cen.ulaval.ca/nordicanad/dpage.aspx?doi= 45039SL-EE76C1BDAADC4890.'

Chung, Y. C., Bélair, S. and Mailhot, J. (2011) 'Blowing snow on arctic sea ice: Results from an improved sea ice-snow-blowing snow coupled system', Journal of Hydrometeorology, 12(4), pp. 678–689. doi: 10.1175/2011JHM1293.1.

Clark, M. P., Hendrikx, J., Slater, A. G., Kavetski, D., Anderson, B., Cullen, N. J., Kerr, T., Örn Hreinsson, E. and Woods, R. A. (2011) 'Representing spatial variability of snow water equivalent in hydrologic and land-surface models: A review', Water Resources Research, 47(7). doi: 10.1029/2011WR010745.

Crawford, T. M. and Duchon, C. E. (1999) 'An improved parameterization for estimating effective atmospheric emissivity for use in calculating daytime downwelling longwave radiation', Journal of Applied Meteorology, 38(4), pp. 474–480. doi: 10.1175/1520-0450(1999)038<0474:AIPFEE>2.0.CO;2.

Déry, S. J., Crow, W. T., Stieglitz, M. and Wood, E. F. (2004) 'Modeling snow-cover heterogeneity over complex Arctic terrain for regional and global climate models', Journal of Hydrometeorology, 5(1), pp. 33–48. doi: 10.1175/1525-7541(2004)005<0033:MSHOCA>2.0.CO;2.

Déry, S. J. and Yau, M. K. (1999) ‘A bulk blowing snow model’, Boundary-Layer Meteorology, 93(2), pp. 237–251. doi: 10.1023/A:1002065615856.

Déry, S. J. and Yau, M. K. (2002) ‘Large-scale mass balance effects of blowing snow and surface sublimation’, Journal of Geophysical Research Atmospheres, 107(23), pp. 1–8. doi: 10.1029/2001JD001251.

Devak, M. and Dhanya, C. T. (2017) ‘Sensitivity analysis of hydrological models: Review and way forward’, Journal of Water and Climate Change, 8(4), pp. 557–575. doi: 10.2166/wcc.2017.149.

DeWalle, D. R. and Rango, A. (2008) Principles of Snow Hydrology. Cambridge: Cambridge University Press.

Dilley, A. C. and O’Brien, D. M. (1998) ‘Estimating downward clear sky long-wave irradiance at the surface from screen temperature and precipitable water’, Quarterly Journal of the Royal Meteorological Society, 124(549), pp. 1391–1401. doi: 10.1256/smsqj.54902.

Domine, F., Belke-Brea, M., Sarrazin, D., Arnaud, L., Barrere, M. and Poirier, M. (2018) ‘Soil moisture, wind speed and depth hoar formation in the Arctic snowpack’, Journal of Glaciology, 64(248), pp. 990–1002. doi: 10.1017/jog.2018.89.

Dominé, F., Cabanes, A. and Legagneux, L. (2002) ‘Structure, microphysics, and surface area of the Arctic snowpack near Alert during the ALERT 2000 campaign’, Atmospheric Environment, 36(15–16), pp. 2753–2765. doi: 10.1016/S1352-2310(02)00108-5.

Duclos, I., Lévesque, E., Gratton, D. and Bordeleau, P.-A. (2006) Vegetation mapping of Bylot Island and Sirmilik national park. Iqaluit, Nunavut. 101p.

Endrizzi, S., Gruber, S., Dall’Amico, M. and Rigon, R. (2014) ‘GEOtop 2.0: Simulating the combined energy and water balance at and below the land surface accounting for soil freezing, snow cover and terrain effects’, Geoscientific Model Development, 7(6), pp. 2831–2857. doi: 10.5194/gmd-7-2831-2014.

Engel, M., Notarnicola, C., Endrizzi, S. and Bertoldi, G. (2017) ‘Snow model sensitivity analysis to understand spatial and temporal snow dynamics in a high-elevation catchment’, Hydrological Processes. Wiley-Blackwell, 31(23), pp. 4151–4168. doi: 10.1002/hyp.11314.

Essery, R., Li, L. and Pomeroy, J. (1999) ‘A distributed model of blowing snow over complex terrain’, Hydrological Processes, 13, pp. 2423–2438. doi: 10.1002/(SICI)1099-1085(199910)13:14/15<2423::AID-HYP853>3.0.CO;2-U.

Essery, R. and Pomeroy, J. (2004) ‘Vegetation and topographic control of wind-blown snow distributions in distributed and aggregated simulations for an Arctic tundra

basin', Journal of Hydrometeorology, 5, pp. 735–744. doi: 10.1175/1525-7541(2004)005<0735:VATCOW>2.0.CO;2.

Fortier, D. and Allard, M. (2004) 'Late Holocene syngenetic ice-wedge polygons development, Bylot Island, Canadian Arctic Archipelago', Canadian Journal of Earth Sciences, 41, pp. 997–1012. doi: https://doi.org/10.1139/e04-031.

Fortier, D. and Allard, M. (2005) 'Frost-cracking conditions, Bylot Island, eastern Canadian Arctic archipelago', Permafrost and Periglacial Processes. Wiley-Blackwell, 16(2), pp. 145–161. doi: https://doi.org/10.1002/ppp.504.

Fraser, R. H., Olthof, I., Ere, M., Deschamps, A. and Pouliot, D. (2011) 'Detecting long-term changes to vegetation in northern Canada using the Landsat satellite image archive', Environ. Res. Lett, 6, pp. 45502–9. doi: 10.1088/1748-9326/6/4/045502.

Freudiger, D., Kohn, I., Seibert, J., Stahl, K. and Weiler, M. (2017) 'Snow redistribution for the hydrological modeling of alpine catchments', Wiley Interdisciplinary Reviews: Water, 4(5), pp. 1–16. doi: 10.1002/WAT2.1232.

Frezzotti, M., Gandolfi, S. and Urbini, S. (2002) 'Snow megadunes in Antarctica: Sedimentary structure and genesis', Journal of Geophysical Research Atmospheres, 107(18), p. ACL 1-1-ACL 1-12. doi: 10.1029/2001JD000673.

Gagnon, C. A., Cadieux, M.-C., Gauthier, G., Lévesque, E., Reed, A. and Berteaux, D. (2010) Analyses and reporting on 15 years of biological monitoring from Bylot Island, Sirmilik national park of Canada.

Garratt, J. R. (1994) 'Atmospheric Boundary Layer.', Earth-Science, 37, pp. 89–134. doi: 10.1201/9781439847121-c2.

Gascoin, S., Lhermitte, S., Kinnard, C., Bortels, K. and Liston, G. E. (2013) 'Wind effects on snow cover in Pascua-Lama, Dry Andes of Chile', Advances in Water Resources. Elsevier Ltd, 55, pp. 25–39. doi: 10.1016/j.advwatres.2012.11.013.

Gauthier, G., Bêty, J., Cadieux, M.-C., Legagneux, P., Doiron, M., Chevallier, C., Lai, S., Tarroux, A. and Berteaux, D. (2013) 'Long-term monitoring at multiple trophic levels suggests heterogeneity in responses to climate change in the Canadian Arctic tundra.', Philosophical transactions of the Royal Society. The Royal Society, 368(1624), p. 20120482. doi: 10.1098/rstb.2012.0482.

Gisnås, K, Westermann, S., Schuler, T. V, Litherland, T., Isaksen, K., Boike, J., Etzelmüller, B. and Gisnås, Kjersti (2014) 'A statistical approach to represent small-scale variability of permafrost temperatures due to snow cover', The Cryosphere, 8, pp. 2063–2074. doi: https://doi.org/10.5194/tc-8-2063-2014.

Gouttevin, I., Langer, M., Löwe, H., Boike, J., Proksch, M. and Schneebeli, M. (2018) 'Observation and modelling of snow at a polygonal tundra permafrost site : spatial

variability and thermal implications', The Cryosphere, 12, pp. 3693–3717. doi: https://doi.org/10.5194/tc-12-3693-2018.

Gubler, S., Endrizzi, S., Gruber, S. and Purves, R. S. (2013) 'Sensitivities and uncertainties of modeled ground temperatures in mountain environments', Geosci. Model Dev, 6, pp. 1319–1336. doi: 10.5194/gmd-6-1319-2013.

Hersbach, H., Bell, B., Berrisford, P., Biavati, G., Horányi, A., Muñoz Sabater, J., Nicolas, J., Peubey, C., Radu, R., Rozum, I., Schepers, D., Simmons, A., Soci, C., Dee, D., Thépaut, J.-N. (2023) ERA5 hourly data on single levels from 1940 to present. Copernicus Climate Change Service (C3S) Climate Data Store (CDS). doi: 10.24381/cds.adbb2d47.

Jennings, K. S., Winchell, T. S., Livneh, B. and Molotch, N. P. (2018) 'Spatial variation of the rain-snow temperature threshold across the Northern Hemisphere', Nature Communications. Springer US, 9(1), pp. 1–9. doi: 10.1038/s41467-018-03629-7.

Kimball, H. H. (1928) 'Amount of solar radiation that reaches the surface of the earth on the land and sea and methods by which it is measured', Monthly Weather Review, 56, pp. 393–398.

Kochendorfer, J. et al. (2017) 'Analysis of single-Alter-shielded and unshielded measurements of mixed and solid precipitation from WMO-SPICE', Hydrology and Earth System Sciences, 21(7), pp. 3525–3542. doi: 10.5194/hess-21-3525-2017.

Krogh, S. A., Pomeroy, J. W. and Marsh, P. (2017) 'Diagnosis of the hydrology of a small Arctic basin at the tundra-taiga transition using a physically based hydrological model', Journal of Hydrology. Elsevier, 550, pp. 685–703. doi: 10.1016/J.JHYDROL.2017.05.042.

Lespinas, F., Fortin, V., Roy, G., Rasmussen, P. and Stadnyk, T. (2015) 'Performance evaluation of the canadian precipitation analysis (CaPA)', Journal of Hydrometeorology, 16(5), pp. 2045–2064. doi: 10.1175/JHM-D-14-0191.1.

Liston, G. E. and Elder, K. (2006a) 'A distributed snow-evolution modeling system (snowmodel)', Journal of Hydrometeorology, 7(6), pp. 1259–1276. doi: 10.1175/JHM548.1.

Liston, G. E. and Elder, K. (2006b) 'A meteorological distribution system for high-resolution terrestrial modeling (MicroMet)', Journal of Hydrometeorology, 7(2), pp. 217–234. doi: 10.1175/JHM486.1.

Liston, G. E., Haehnel, R. B., Sturm, M., Hiemstra, C. A., Berezovskaya, S. and Tabler, R. D. (2007) 'Instruments and methods simulating complex snow distributions in windy environments using SnowTran-3D', Journal of Glaciology, 53(181), pp. 241–256. doi: 10.3189/172756507782202865.

Liston, G. E. and Sturm, M. (1998) 'A snow-transport model for complex terrain', Journal of Glaciolog, 44(148). Available at: https://www.cambridge.org/core/services/aop-cambridge-core/content/view/E69A94C3326F3E2194D6AB3BC94D9CBC/S0022143000002021a.pdf/snowtransport_model_for_complex_terrain.pdf.

Liston, G. E. and Sturm, M. H. (1998) 'A snow-transport lD.odel for cotnplex terrain', JournalofGlaciolog)I, 44(148). Available at: https://www.cambridge.org/core/services/aop-cambridge-core/content/view/E69A94C3326F3E2194D6AB3BC94D9CBC/S0022143000002021a.pdf/snowtransport_model_for_complex_terrain.pdf (Accessed: 30 April 2018).

Loyer, M. and Kinnard, C. (2018) 'Spatial variability of snow and its impact on tundra vegetation: the case of Bylot Island, Canadian Arctic', in AGU Fall Meeting, pp. C13I-1236.

Luo, Y. and Schuur, E. A. G. (2020) 'Model parameterization to represent processes at unresolved scales and changing properties of evolving systems', Global Change Biology, 26(3), pp. 1109–1117. doi: 10.1111/gcb.14939.

MacDonald, M. K., Pomeroy, J. W. and Pietroniro, A. (2009) 'Parameterizing redistribution and sublimation of blowing snow for hydrological models: tests in a mountainous subarctic catchment', Hydrological Processes, 23, pp. 2570–2583. doi: 10.1002/hyp.

Mair, E., Leitinger, G., Della Chiesa, S., Niedrist, G., Tappeiner, U. and Bertoldi, G. (2016) 'A simple method to combine snow height and meteorological observations to estimate winter precipitation at sub-daily resolution', Hydrological Sciences Journal. Taylor & Francis, 61(11), pp. 2050–2060. doi: 10.1080/02626667.2015.1081203.

Marsh, C. B., Pomeroy, J. W., Spiteri, R. J. and Wheater, H. S. (2020) 'A Finite Volume Blowing Snow Model for Use With Variable Resolution Meshes', Water Resources Research, 56(2), pp. 1–28. doi: 10.1029/2019WR025307.

Marti, R., Gascoin, S., Berthier, E., De Pinel, M., Houet, T. and Laffly, D. (2016) 'Mapping snow depth in open alpine terrain from stereo satellite imagery', Cryosphere, 10(4), pp. 1361–1380. doi: 10.5194/tc-10-1361-2016.

Maxwell, J. B. (1982) The climate of the Canadian Arctic Islands and adjacent waters. Environment Canada, Atmospheric Environment Service, 589 p.

Ménard, C. B., Essery, R., Pomeroy, J., Marsh, P. and Clark, D. B. (2014) 'A shrub bending model to calculate the albedo of shrub-tundra', Hydrological Processes, 28(2), pp. 341–351. doi: 10.1002/hyp.9582.

Mohammadzadeh Khani, H., Kinnard, C. and Lévesque, E. (2023) 'Fine scale distributed snow cover modeling in a High Arctic tundra landscape using the physically based GEOtop model', Cryosphere.

Mohammadzadeh Khani, H., Kinnard, C., Lévesque, E. and Gascoin, S. (2023) 'Fine scale environment control on ground surface temperature and active-layer thickness in a High Arctic tundra landscape', Permafrost and Periglacial Processes, pp. 1–14. doi: 10.1002/ppp.2203.

Monin, A. S. and Obukhov, A. M. (1954) 'Basic laws of turbulent mixing in the surface layer of the atmosphere', Contributions of the Geophysical Institute of the Slovak Academy of Sciences, 20, pp. 163–187.

Moriasi, D. N., J. G. Arnold, M. W. V. L., Bingner, R. L., Harmel, R. D. and Veith, T. L. (2007) 'Model evaluation guidelines for systematic quantification of accuracy in watershed simulations', American Society of Agricultural and Biological Engineers, 50, pp. 885–900.

Mott, R., Egli, L., Grünewald, T., Dawes, N., Manes, C., Bavay, M. and Lehning, M. (2011) 'Micrometeorological processes driving snow ablation in an Alpine catchment', Cryosphere, 5(4), pp. 1083–1098. doi: 10.5194/tc-5-1083-2011.

Musselman, K. N., Pomeroy, J. W., Essery, R. L. H. and Leroux, N. (2015) 'Impact of windflow calculations on simulations of alpine snow accumulation, redistribution and ablation', Hydrological Processes. doi: 10.1002/hyp.10595.

Nash, J.E.; Sutcliffe, J. . (1970) 'River flow forecasting through conceptual models part I—A discussion of principles', Journal of Hydrology, 10, pp. 280–290. doi: 10.1080/00750770109555783.

Palm, S. P., Kayetha, V., Yang, Y. and Pauly, R. (2017) 'Blowing snow sublimation and transport over Antarctica from 11 years of CALIPSO observations', The Cryosphere, 11, pp. 2555–2569. doi: 10.5194/tc-11-2555-2017.

Paniconi, C. and Putti, M. (1994) 'A comparison of Picard and Newton iteration in the numerical solution of multidimensional variably saturated flow problems', Water Resources Research. Wiley-Blackwell, 30(12), pp. 3357–3374. doi: 10.1029/94WR02046.

Pomeroy, J. W. et al. (2022a) 'The cold regions hydrological modelling platform for hydrological diagnosis and prediction based on process understanding', Journal of Hydrology, 615(May). doi: 10.1016/j.jhydrol.2022.128711.

Pomeroy, J. W. et al. (2022b) 'The cold regions hydrological modelling platform for hydrological diagnosis and prediction based on process understanding', Journal of Hydrology, 615(November). doi: 10.1016/j.jhydrol.2022.128711.

Pomeroy, J. W., Fang, X., Shook, K. and Whitfield, P. H. (2013) 'Predicting in ungauged basins using physical principles obtained using the deductive, inductive, and abductive reasoning approach', Environmental Science, pp. 41–62.

Pomeroy, J. W., Gray, D. M., Brown, T., Hedstrom, N. R., Quinton, W. L., Granger, R. J. and Carey, S. K. (2007) 'The cold regions hydrological model: A platform for basing process representation and model structure on physical evidence', Hydrological Processes, 21(19), pp. 2650–2667. doi: 10.1002/hyp.6787.

Pomeroy, J. W., Gray, D. M. and Landine, P. G. (1993) 'The Prairie Blowing Snow Model: characteristics, validation, operation', Journal of Hydrology, 144(1–4), pp. 165–192. doi: 10.1016/0022-1694(93)90171-5.

Pomeroy, J. W. and Jones, H. G. (1996) 'Wind-blown snow: Sublimation, transport and changes to Polar snow', in Processes of chemical exchange between the atmosphere and polar Snow. Berlin, Germany, pp. 453–490. doi: 10.1007/978-3-642-61171-1_19.

Pomeroy, J. W. and Li, L. (2000) 'Prairie and arctic areal snow cover mass balance using a blowing snow model', Journal of Geophysical Research Atmospheres, 105(D21), pp. 26619–26634. doi: 10.1029/2000JD900149.

Pomeroy, J. W., Marsh, P. and Gray, D. M. (1997) 'Application of a distributed blowing snow model to the arctic', Hydrological Processes, 11(11), pp. 1451–1464. doi: 10.1002/(sici)1099-1085(199709)11:11<1451::aid-hyp449>3.0.co;2-q.

Pullens, J. W. M., Sottocornola, M., Kiely, G., Gianelle, D. and Rigon, R. (2018) 'Assessment of the water and energy budget in a peatland catchment of the Alps using the process based GEOtop hydrological model', Journal of Hydrology, 563, pp. 195–210. doi: 10.1016/j.jhydrol.2018.05.041.

Revuelto, J., Alonso-Gonzalez, E., Vidaller-Gayan, I., Lacroix, E., Izagirre, E., Rodríguez-López, G. and López-Moreno, J. I. (2021) 'Intercomparison of UAV platforms for mapping snow depth distribution in complex alpine terrain', Cold Regions Science and Technology, 190. doi: 10.1016/j.coldregions.2021.103344.

Ross, A., Smith, C. D. and Barr, A. (2020) 'An improved post-processing technique for automatic precipitation gauge time series', Atmospheric Measurement Techniques, 13(6), pp. 2979–2994. doi: 10.5194/amt-13-2979-2020.

Saltelli, A., Andres, T. H. and Homma, T. (1995) 'Sensitivity analysis of model output. Performance of the iterated fractional factorial design method', Computational Statistics and Data Analysis, 20(4), pp. 387–407. doi: 10.1016/0167-9473(95)92843-M.

Schlögl, S., Marty, C., Bavay, M. and Lehning, M. (2016) 'Sensitivity of Alpine3D modeled snow cover to modifications in DEM resolution, station coverage and

meteorological input quantities', Environmental Modelling and Software, 83, pp. 387–396. doi: 10.1016/j.envsoft.2016.02.017.

Schramm, I., Boike, J., Bolton, R. W. and Hinzman, L. D. (2007) 'Application of TopoFIow, a spatially distributed hydrological model, to the Imnavait Creek watershed, Alaska', Journal of Geophysical Research: Biogeosciences, 112(4), pp. 1–14. doi: 10.1029/2006JG000326.

Semenova, O., Lebedeva, L. and Vinogradov, Y. (2013) 'Simulation of subsurface heat and water dynamics, and runoff generation in mountainous permafrost conditions, in the Upper Kolyma River basin, Russia', Hydrogeology Journal, 21(1), pp. 107–119. doi: 10.1007/s10040-012-0936-1.

Shean, D. E., Alexandrov, O., Moratto, Z. M., Smith, B. E., Joughin, I. R., Porter, C. and Morin, P. (2016) 'An automated, open-source pipeline for mass production of digital elevation models (DEMs) from very-high-resolution commercial stereo satellite imagery', ISPRS Journal of Photogrammetry and Remote Sensing. International Society for Photogrammetry and Remote Sensing, Inc. (ISPRS), 116, pp. 101–117. doi: 10.1016/j.isprsjprs.2016.03.012.

Shirley, I., Uhlemann, S., Peterson, J., Bennett, K., Hubbard, S. S. and Dafflon, B. (2023) 'Disentangling the effect of geomorphological features and tall shrubs on snow depth variation in a sub-Arctic watershed using UAV derived products', (May), pp. 1–23. Available at: https://doi.org/10.5194/egusphere-2023-968.

Smith, S. L., Romanovsky, V. E., Lewkowicz, A. G., Burn, C. R., Allard, M., Clow, G. D., Yoshikawa, K. and Throop, J. (2010) 'Thermal state of permafrost in North America: A contribution to the international polar year', Permafrost and Periglacial Processes, 21(2), pp. 117–135. doi: https://doi.org/10.1002/ppp.690.

Sturm, M. and Holmgren, J. (1994) 'Effects of microtopography on texture, temperature and heat flow in Arctic and sub-Arctic snow', International Glaciological Society Effects, 19, pp. 63–68. doi: https://doi.org/10.3189/1994AoG19-1-63-68.

Tarboton, D. G. and Luce, C. H. (1996) 'Utah energy balance snow accumulation and melt model (UEB)', (March).

Therrien, R. (1996) 'Three-dimensional analysis of variably-saturated flow and solute transport in discretely-fractured porous media', Journal of Contaminant Hydrology, 3542(95), pp. 1–44.

Vinogradov, Y. B., Semenova, O. M. and Vinogradova, T. A. (2011) 'An approach to the scaling problem in hydrological modelling: The deterministic modelling hydrological system', Hydrological Processes, 25(7), pp. 1055–1073. doi: 10.1002/hyp.7901.

Vionnet, V., Marsh, C. B., Menounos, B., Gascoin, S., Wayand, N. E., Shea, J., Mukherjee, K. and Pomeroy, J. W. (2021) 'Multi-scale snowdrift-permitting modelling of

mountain snowpack', Cryosphere, 15(2), pp. 743–769. doi: 10.5194/tc-15-743-2021.

Voordendag, A., Réveillet, M., MacDonell, S. and Lhermitte, S. (2021) 'Snow model comparison to simulate snow depth evolution and sublimation at point scale in the semi-arid Andes of Chile', Cryosphere, 15(9), pp. 4241–4259. doi: 10.5194/tc-15-4241-2021.

Warren, S. G., Brandt, R. E. and Grenfell, T. C. (2006) 'Visible and near-ultraviolet absorption spectrum of ice from transmission of solar radiation into snow', Applied Optics, 45(21), pp. 5320–5334. doi: 10.1364/AO.45.005320.

Williams, J. P. and Smith, M. W. (1989) The Frozen Earth-Fundamentals of Geocryology, … of the American Astronomical Society. doi: 10.1017/CBO9780511564437.

Woo, M. (2012) Permafrost Hydrology. Berlin Heidelberg: Springer New York. 574 p. doi: 10.1007/978-3-642-23462-0.

Xue, Y., Sun, S., Kahan, D. S. and Jiao, Y. (2003) 'Impact of parameterizations in snow physics and interface processes on the simulation of snow cover and runoff at several cold region sites', Journal of Geophysical Research: Atmospheres, 108(22). doi: 10.1029/2002jd003174.

Zanotti, F., Endrizzi, S., Bertoldi, G. and Rigon, R. (2004) 'The GEOtop snow model', in 61st Eastern snow conference, pp. 87–100. Available at: http://citeseerx.ist.psu.edu/viewdoc/download?doi=10.1.1.571.599&rep=rep1&type=pdf (Accessed: 26 September 2018).

CHAPTER III

BLOWING SNOW TRANSPORT PROCESSES MODULATES THE CLIMATE SENSITIVITY OF SNOW COVER IN A CANADIAN HIGH ARCTIC TUNDRA ENVIRONMENT

Hadi Mohammadzadeh Khani[1-2*], Christophe Kinnard[1-2], Esther Lévesque[1-2]

[1] Research Centre for Watershed-Aquatic Ecosystem Interactions (RIVE), University of Québec at Trois-Rivières, Québec, Canada.

[2] Centre for Northern Studies (CEN), Québec City, Québec, Canada

[*]Corresponding author: Hadi.Mohammadzadeh.Khani@uqtr.ca

Abstract

The snow cover in the Arctic tundra is highly heterogeneous, due to wind-driven snow redistribution into topographic depressions. While several global and regional models have projected future changes in snow cover in response to projected climate change for the 21st century, such models either ignore blowing snow processes, or do so inadequately. This study evaluates the impact of blowing snow processes on the climate sensitivity of snow cover in a Canadian High Arctic tundra environment at a fine scale (10 meters). The physically-based, distributed hydrological GEOtop model was forced with historical and perturbed climate under the Representative Concentration Pathway (RCP) 8.5, with and without considering blowing snow processes. Including blowing snow processes significantly modified the climate sensitivity of the snow cover. Nonetheless, the extent of this modification exhibited a dependency on the specific climate scenario under consideration. The influence of blowing snow processes on the climate sensitivity of snow cover condition was overall decreased under warmer scenarios while slight changes in snow cover metrics were observed under colder climate scenarios. Considering blowing snow led to shorter snow cover duration (SCD) compared to when blowing snow was ignored, by 7 to 21 days, depending on the climate scenario. Blowing snow effects on the climate sensitivity of snow cover duration varied primarily according to temperature, while changes in precipitation mostly modulated blowing snow effects on the climate sensitivity of peak SWE. Blowing-snow transport was also found to decrease in response to projected warming, by 5 to 10% which reduced the spatial heterogeneity of snow cover compared to the present day.

Keywords: High Arctic, blowing snow, climate change, snow spatial variability.

3.1 Introduction

Northern regions have experienced an accelerated rate of warming, much faster than elsewhere, particularly in the Arctic regions (Stuecker *et al.*, 2018; Rantanen *et al.*, 2022). Climate change is significantly influencing the amount, seasonality, and spatial distribution of snow cover, and these changes have a profound impact on the hydrological cycle, ecosystems, and infrastructure of Arctic regions (Bokhorst et al., 2016). Snow is a critically important feature of the Arctic due to its long lasting on the ground (Pomeroy and Brun, 2001; Callaghan *et al.*, 2011; Woo, 2012). Owing to its low thermal conductivity, high albedo, and spatiotemporal variability, the seasonal snow cover plays a significant role in regulating the global radiation balance (Hall, 1988). The snow cover significantly affects Arctic wildlife habitats and movement (Poirier *et al.*, 2019), and northern biomes plant phenology by controlling the growth period and providing key water availability in the spring (Wang *et al.*, 2018). As such, the development of snow conditions will have a significant impact on future biodiversity patterns in Arctic regions (Niittynen *et al.*, 2018). Observational evidence shows that snow cover is changing across Arctic regions (Callaghan *et al.*, 2011; Brown *et al.*, 2017; Mohammadzadeh Khani *et al.*, 2022) in response to atmospheric warming since the 1970s (Serreze and Barry, 2011; Brown *et al.*, 2017; Rantanen *et al.*, 2022) and it is widely acknowledged that snow cover conditions will continue to be modified under warming air temperature and changing precipitation amount, phase and timing in the future (Thackeray *et al.*, 2016; Bintanja and Andry, 2017; Mudryk *et al.*, 2018; McCrystall *et al.*, 2021; Mohammadzadeh Khani *et al.*, 2022). For example, the maximum annual snow water equivalent (SWE) has been projected to increase, but the snow cover duration (SCD) to decrease, over much of the Arctic tundra during the present century (Callaghan *et al.*, 2011; Brown *et al.*, 2017; Mudryk *et al.*, 2018, 2020; Derksen and Mudryk, 2023). There is thus a pressing need to better predict and understand future snow cover conditions, their causes, and their effects on the water cycle and ecosystems of northern regions.

Despite significant advances in continental scale snow cover modeling (e.g., Xu *et al.* 2022) and in our understanding of snow cover impacts on ecosystems and climate feedbacks (Hall, 1988; Ballantyne *et al.*, 1990; Niittynen *et al.*, 2018; Poirier *et al.*, 2019),

numerous uncertainties due to model errors and input data still persist (Largeron *et al.*, 2020). A prevalent challenge in projecting future changes in snow cover conditions and their ecohydrological impacts is the sometimes-formidable spatial heterogeneity of snow cover. The thin snow cover in the open landscapes of the Arctic tundra is constantly redistributed by the wind, which blows snow into topographic depressions, resulting in pronounced snow cover heterogeneity (Pomeroy and Jones, 1996; Sturm *et al.*, 2001; Essery and Pomeroy, 2004). In such areas, a large portion of snowfall can be removed by blowing snow locally, before melting begins (Pomeroy *et al.*, 1997; Déry and Yau, 2001). For example, Pomeroy and Li (2000) calculated that exposed snowpacks can lose from 48 to 58% of the annual snowfall due to blowing snow transport and sublimation at an Arctic tundra plateau in Trail Valley Creek, Canada (Pomeroy and Li, 2000). Inadequate representation of the spatial heterogeneity of snow processes in snow cover and hydrological models can lead to inaccurate predictions of snow cover and runoff (Déry et al., 2004; Castaneda-Gonzalez *et al.*, 2019), and compromise projections under climate change scenarios. As such, measuring and understanding snow cover heterogeneity, and representing it within process-based models represents one of the greatest ongoing challenges in atmospheric and hydrological sciences, which calls for innovative efforts to address this issue (Peters-Lidard *et al.,* 2017).

All large-scale (continental) simulations of snow cover evolution ignore blowing snow (BS) (e.g., Shi and Wang, 2015; Mudryk *et al.*, 2020; Bigalke and Walsh, 2022). As the wind in the exposed tundra locally relocates the snow in different microtopography conditions (Pomeroy and Jones, 1996), the snow cover simulated at larger spatial scales (hillslope to regional) is expected to respond differently to climate change when fine-scale blowing snow processes are considered. Ignoring such small-scale or 'subgrid' processes in regional snow models could lead to biased simulations of snow cover in the Arctic. This research addresses the following questions: (1) Does considering or ignoring BS processes impact the simulated climate sensitivity of snow cover conditions (peak accumulation and timing, snow cover duration)? (2) How does the snow cover spatial variability respond to climate change when BS processes are either considered or ignored? The main purpose of this study is thus to understand how BS processes affect the climate sensitivity of snow

cover in an open Arctic tundra landscape. To this end, a calibrated physically based model (GEOtop) was used to simulate snow cover metrics (peak SWE and its timing, snow cover duration, spatial variability) and snow mass fluxes under climate change scenarios with, and without consideration of blowing snow processes.

3.2 Materials and methods

3.2.1 Study area

The study area is situated on the western coast of Bylot Island (Nunavut, Canada) in a High Arctic tundra landscape (Figure 3-1). The modeling domain encompasses a 7.32 km^2 area which ranges from a valley with wetlands to mesic hillslope and up to a xeric plateau with an elevation ranging from 20 to 350 meters above sea level. Low and high center ice wedge polygons are found in the lower valley underlain by fluvioglacial deposits, while mineral-earth hummocks predominantly cover the mesic hillslopes underlain by glacial till. Exposed tertiary bedrock and thin soils with scattered mudboils are found on the upper plateau (Figure 3-1). The area is underlined by a thick (approx. 400m) and continuous layer of permafrost (Heginbottom, 1995). According to the Köppen-Geiger climate classification the climate at Bylot is High Arctic, with cold temperatures, dry winter seasons, and cold summers (Beck *et al.,* 2018). The mean annual air temperature between 1981 and 2010 was -15.1°C based on the Bylocamp meteorological station (73.15° N, -79.95° W, Figure 3-1). Annual precipitation during the same time period was 191 mm, 76% falling as snow. Snow typically begins to accumulate in September, and lasts until mid-June. The annual average winter snowpack typically reaches between 35 and 45 cm and due to terrain topography and winter snow drifting from prevailing easterly winds, snow accumulation is highly heterogeneous in space (Fortier and Allard, 2004; Gauthier *et al.*, 2013; Mohammadzadeh Khani *et al.*, 2023).

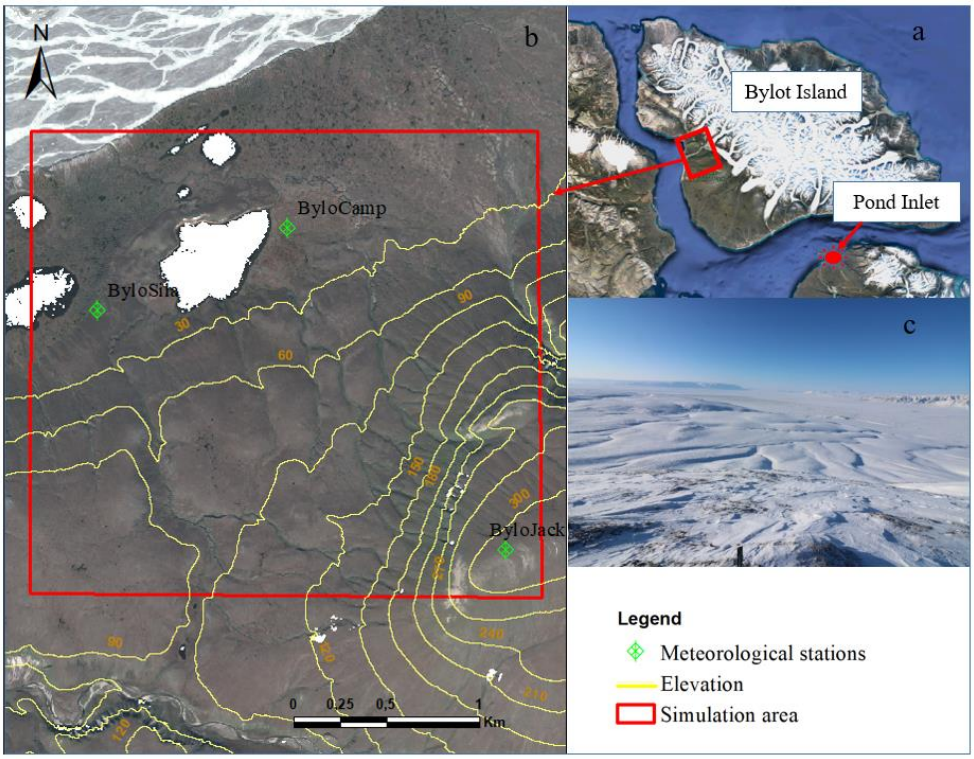

Figure 3-1 Study area and site. a: study location on Bylot Island, Nunavut, Canada, b: study area and spatial modeling domain (red square), and c: photograph of the study area taken on 1st May 2018 from near Bylojack station, looking towards the northwest. Background satellite Image by Pléiades © CNES 2016 Distribution Airbus DS.

With more than 166 vascular plant species and a varied bryophyte flora (Duclos *et al.*, 2006), the prostrate vegetation is relatively diversified for this latitude. Sedges, grasses, and fen mosses are the predominant plant species in the wetland areas, while mosses and prostrate shrubs (<5cm) high) are the dominant plant species in the mesic areas (Ellis *et al.,* 2008; Pouliot *et al.,* 2009; Perreault *et al.,* 2016). The total vegetation cover varied from 34 to 145% with 3–88% for mosses and 3–63% for vascular plants (Mohammadzadeh Khani *et al.*, 2023).

3.2.2 GEOtop model configuration

The GEOtop 3.0 land surface/hydrological model was used to assess the role of blowing snow processes on the snow cover sensitivity to climate change. GEOtop 3.0 is a grid-based modeling platform with a configurable distributed hydrological model that can

simulate the water and heat budgets above and below the soil surface (Zanotti *et al.*, 2004). Most pertinent to this study is its snow module that includes a multi-layer representation of the snowpack that accounts for snow accumulation, melting, refreezing, snowpack sublimation, blowing snow transport and sublimation, and changes in snowpack density due to wind, temperature and compaction (Endrizzi *et al.,* 2014). The GEOtop model has been successfully used in several studies to simulate surface energy balance and hydrological processes in cold environments (e.g., Endrizzi and Marsh, 2010; Gubler *et al.*, 2013; Wani *et al.*, 2021). Engel *et al.* (2017) extensively tested and validated the GEOtop snow module in the European Alps and found the model to perform well in simulating the spatiotemporal snow cover evolution. The GEOtop 3.0 snow module, including its recent blowing snow redistribution and sublimation scheme, was extensively tested by Mohammadzadeh Khani *et al.* (2023) at the Bylot Island research site. Their results demonstrated that incorporating blowing snow processes into the snow cover simulation yielded a much-improved simulation of the spatiotemporal evolution of snow depths at the site. The most important processes and methods included in the GEOtop 3.0 snow cover module are summarized in Table 3-1.

Table 3-1 Processes and methods used in GEOtop 3.0 to simulate the snow cover evolution at Bylot Island.

Method/process	Description
Spatialization of model forcings	Air temperature is distributed using measured lapse rates combined with Barnes's optimal spatial interpolation scheme (Barnes, 1964; Liston and Elder, 2006). Relative humidity (RH) is converted to dewpoint temperature and distributed to the model grid using the same interpolation method for air temperature, before converting back to RH (Liston and Elder, 2006). Measured wind speed and directions from weather stations are distributed to the model grid using Barnes's scheme (1964) and adjusted to the local terrain according to topographic slope and curvature. Due to the small elevation range of the model domain, the precipitation lapse rate was set to zero.
Snowpack energy-balance	Snow accumulation and melt are calculated using an energy-based multi-layer snowpack (Endrizzi *et al.*, 2014). The energy balance

	accounts for various radiation fluxes, sensible and latent heat fluxes, and evaporation in complex topography.
Radiation	Incoming shortwave radiation on a ground surface is the result of the top-of-atmosphere (SWtoa) shortwave radiation, and atmosphere and cloud transmissivities. Incoming longwave radiation is calculated for both clear and cloudy sky, based on air temperature Ta and water vapour pressure. The outgoing longwave radiation emitted by the surface is calculated with the Stefan–Boltzmann law.
Albedo	The parameterization of snow albedo follows Dickinson et al (1993) which includes (i) decaying albedo after fresh snowfalls; (ii) increasing albedo during lower sun angles due to Mie scattering effects on snow grains; (iii) partitioning of the electromagnetic spectrum into visible and near-infrared regions with distinct snow aging coefficients and fresh snow albedo values. The albedo of the snow-free ground varies linearly with the liquid water contents of the top soil layer.
Snow metamorphism	GEOtop encompasses the comprehensive representation of snow densification processes, capturing both rapid initial snow transformation (destructive metamorphism) and the gradual compaction induced by the snow own weight (overburden) using empirical equations initially proposed by Anderson (1976) and subsequently refined by Jordan et al. (1999). Furthermore, the model accounts for snow densification resulting from wind-induced loads, as elucidated by Liston *et al.* (2007).
Blowing snow	The transport of snow by saltation and suspension, and the rate of sublimation of blowing snow are calculated following Pomeroy *et al.* (1993) and Essery *et al.* (1999).
Snowpack discretization	The snowpack is classified into an upper, middle and bottom portion according to the thermal gradients. The total number and thickness of individual layers are dynamically adjusted according to the mass of snow present. The distribution of layers in the snowpack privileges the upper and bottom zones where thermal gradients are steeper (see Mohammadzadeh Khani *et al.* (2023) and Endrizzi *et al.*(2014) for more details).

The GEOtop model was calibrated and validated against station data and snow depth maps (Chapter 2). They obtained reasonable accuracies, as estimated with the Nash-Sutcliffe efficiency (NSE), against manual snow depth and a detailed snow depth map derived from Unmanned Aerial Vehicle (UAV) surveys for simulations made at a 3 m (NSE = 0.49 to

0.56) and 10 m (NSE = 0.20 to 0.32) spatial resolution. Model errors appeared to be mainly caused by uncertain precipitation forcings, while the simulated spatial snow depth patterns correlated well with observations (3m: r = 0.77 to 0.86; 10m: r = 0.58 to 0.73). While a greater overall performance was obtained at 3 m, the computing time was prohibitive for climate change impact assessment, and the main snow drifts spatial patterns were still properly reproduced by the model at 10m spatial resolution. For these reasons, a 10 m model grid was used in this study to explore the impact of blowing snow processes on the climate sensitivity of the snow cover. The 10m model grid was derived by resampling a 2m digital elevation model (DEM) built from Pleiades stereo images acquired on 28 July 2016. Topographic indices (aspect, slope, and skyview factor) were further extracted from the 10m DEM and used as inputs into GEOtop. An hourly temperature lapse rate was calculated from the Bylocamp (elevation = 24 m) and Bylojack (elevation = 312m) (Figure 3-1), over the available 15-year record, 2005-2019. Due to the small elevation range of the model domain, the precipitation lapse rate was set to zero. The GEOtop 3.0 model was used to simulate snow cover evolution at an hourly time step from September 1, 2005 to September 1, 2019, driven by the insitu weather station data interpolated to the model grid (Table 3-2). The model was then forced with the historical forcings perturbed with mean monthly changes in temperature and precipitation projected by ensemble climate models under the RCP8.5 scenario for the end of the century, with and without blowing snow processes considered, as detailed further.

3.2.3 Meteorological data

The available meteorological forcing data for the period 2005–2019 were collected from three automated weather stations of the Centre d'études Nordiques (CEN) ‘SILA’ network and one weather station operated by Environment Canada in Pond Inlet (station id: 43223) (Table 3-2). The distribution of the CEN stations covers the elevation range of the study area, with one station situated on an adjacent hill (Bylojack) and the other two stations located in the valley (Bylocamp and Bylosila) (Figure 3-1). CEN station data was retrieved through the NordicanaD online data repository (CEN, 2021).

Table 3-2 Meteorological data available from the weather stations of the SILA network at hourly steps (see locations in Figure 3-1). P: Total precipitation, Ta: 2 m air temperature, RH: relative humidity, WS: wind speed at 2 m height, WD: wind direction, SD: snow depth, S: incoming solar radiation. Lat and Lon present the geographical location (latitude and longitude) of stations.

Weather stations	Lat (°)	Lon (°)	Elevation (m)	Operation start	Variables
Bylosila	73.15	-79.98	24	1994	T_a, WS, WD, S
Bylojack	73.14	-79.90	312	2001	T_a, WS, WD
Bylocamp	73.15	-79.95	24	2004	T_a, P, SD, WS, WD, RH
Pond Inlet	72.69	-77.97	55	1975	T_a, P, SD, WS, WD, RH

All three SILA meteorological stations have been simultaneously recording hourly wind speed and direction and air temperature since 2002. Hourly snow depth (SD) was recorded between 2015 and 2019 at the Bylocamp station using a Campbell Scientific SR50 ultrasonic gauge. A Geonor precipitation gauge was installed at the Bylocamp station in 2011 to record hourly total precipitation. A single-Alter-shield was installed around the Geonor in July 2016. The precipitation record suffers from several gaps due to gauge malfunctioning and disruption by animals, i.e. from February-May 2014, July 2015 to June 2015 and January-April 2017. As such, we also relied on precipitation measured at the Pond Inlet Environment Canada weather station, located at the Pond Inlet airport on Baffin Island, ~80 km southeast from the study site. Precipitation was corrected for undercatch using the method from Kochendorfer *et al.* (2017), which includes corrections for the Geonor gauge with (>2011)), and without (<2011) the Alter shield. Precipitation gaps were first filled by linear regression against the Pond Inlet station, and against the Canadian Precipitation Analysis System (CaPA) (Lespinas *et al.*, 2015) data when gaps occurred at the Pond Inlet station. Hourly incoming solar radiation is recorded using a CNR1 Net Radiometer at the Bylosila station since July 2009. Relative humidity (RH) data were collected at the Bylocamp station, starting July 1993. A gap in RH data was found for the period of September 2014 to December 2014 which was filled with RH data from Pond Inlet using linear regression. A detailed explanation of the precipitation correction and infilling gap in meteorological data is given in Mohammadzadeh Khani *et al.* (2023).

3.2.4 Climate Sensitivity Analysis

Statistically downscaled projected temperature and precipitation from ensemble climate model projections available for Canada (Cannon *et al.*, 2015) were used for the climate sensitivity experiment. The projections are from an ensemble of 29 members of the Coupled Model Intercomparison Project Phase 5 (Tam *et al.,* 2019). Monthly mean daily temperature and monthly total precipitation from each climate model were downscaled using bias correction constructed analogues with the quantile mapping reordering (BCCAQ) method which is a hybrid of BCCA (Maurer *et al.*, 2010) and QMAP (Gudmundsson *et al.*, 2012). BCCAQ combines quantile-mapping bias correction with a constructed analogues approach using daily large-scale temperature and precipitation fields and regridded them to a common 1.4° grid (Cannon *et al.,* 2015). Downscaled precipitation and temperature were extracted from the gridbox closest to the study site. Each model member simulated the climate for the historical (1950-2005) and future (2006-2100) periods, in response to three emission scenarios representing different atmospheric concentrations of greenhouse gases, i.e. the Representative Concentration Pathways (RCP). Here, monthly air temperature and precipitation projected under the scenario RCP8.5 were used because they most closely resemble the observed emissions pathway over the past decade (Schwalm *et al.*, 2020). The ensemble mean annual temperature has increased continuously from the 1980s onward, while the mean annual precipitation also shows a continuous, but more subdued increase over time (Figures 3-2a and c). The current study considered scenario uncertainties (colored envelopes in panels 3-2a and c) to derive the monthly ‘deltas’ of temperature and precipitation (Table 3-3).

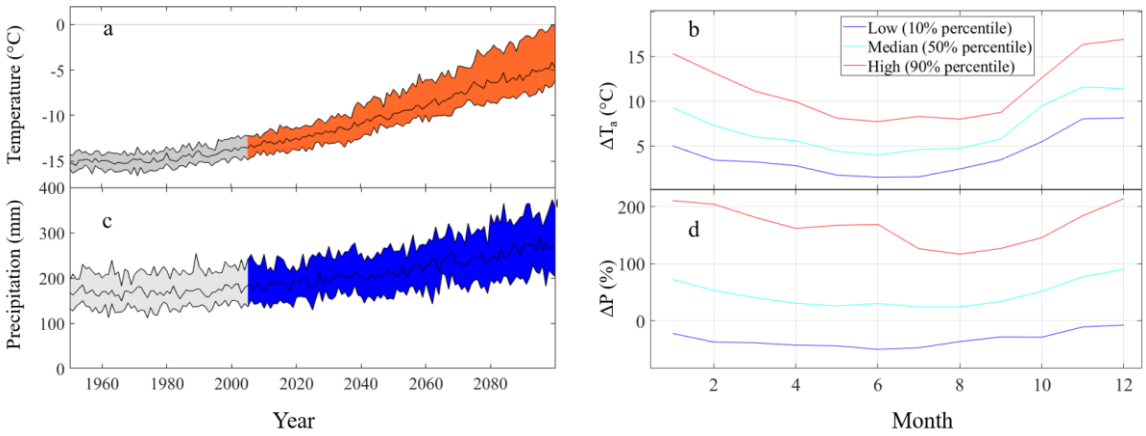

Figure 3-2 Projected air temperature and precipitation at the study site. (a) and (c) Projected mean annual air temperature and total precipitation under RCP 8.5 scenario. Bold black lines represent median values (50th percentile) of the climate model ensemble. The color envelopes correspond to the 10th and 90th percentiles of the model ensemble; (b) mean monthly projected air temperature and (d) mean monthly projected precipitation over the period of 2085-2100. Colors correspond to the level of uncertainty (low, median, and high) of RCP 8.5, as shown at the top of the plot.

Table 3-3 Projected changes in annual precipitation and temperature for the gridbox area close to research camp at Bylot Island under RCP 8.5 scenarios (low, median, and high) for period of 2085-2100. P_T, P_R, and P_S present total precipitation, rainfall, and snowfall, respectively.

Scenario	P_T (mm)	P_R (mm)	P_S (mm)	T_a (°C)	ΔP_T (%)	ΔP_R (%)	ΔP_S (%)	ΔT_a (°C)
Historic	165	69	96	-13.2				
Low	105	51	54	-9.4	-36	-30	-40	3.8
Median	245	157	88	-5.2	48	130	-10	8.0
High	460	336	124	-0.2	179	380	30	13.0

Consistent with the annual air temperature trends (Figure 3-2a), the air temperature increased in all months at the end of century, with the largest increase in temperature (ΔT_a) projected in winter (Figure 3-2b). The mean monthly precipitation was projected to increase under the median and high ensemble percentile while it was projected to decrease under the low percentile scenario (Figure 3-2d). The total annual precipitation was projected to increase significantly at the end of the century under the median and high RCP

8.5 scenarios up to 48% and 179% (Figure 3-3c and Table 3-3). However, the total precipitation was projected to decrease by 36% under the low RCP 8.5 scenario.

Bias correction was used to developed climate projections at the study site, by applying mean monthly change factors to observations (e.g. Navarro-Racines *et al.,* 2020). The mean monthly changes in downscaled temperature (°C) and precipitation (%) calculated between the future (2085-2100) and reference (1995-2010) period of the ensemble (Figure 3.2b, d), were used to perturb the three historical SILA weather station data that serve to force the GEOtop model (Equations 3-1 and 3-2).

$$\Delta Ta_i = Ta_{Fi} - Ta_{Ci} \tag{3-1}$$

$$\Delta P_i = \frac{P_{Fi} - P_{Ci}}{P_{Ci}} \tag{3-2}$$

Where, ΔTa_{Fi} and ΔP_{Fi} are respectively the absolute and relative difference in temperature and precipitation for month i, between the future (F) and current (C) climate periods. The use of relative changes for precipitations ensures that negative precipitation do not occurs after applying the change factors. The median (50th percentile) of the ensemble simulations was used as the most probable scenario, and the 10th and 90th percentiles were used to consider uncertainties in projections. Combining the different percentiles resulted in six different combinations of temperature and precipitation perturbations (Table 3-4).

Table 3-4 Climate scenarios of monthly precipitation and temperature.

Warming scenario (Ta)	Precipitation scenario (P)
Historical (Ta_{hist})	Historical (P_{hist})
Low (Ta_{low})	Low (P_{low})
Low (Ta_{low})	High (P_{high})
Median (Ta_{med})	Median (P_{med})
High (Ta_{high})	Low (P_{low})
High (Ta_{high})	High (P_{high})

The sensitivity of the snow cover metrics to these different scenarios was investigated, focusing on the most likely (median) scenario, but also looking at the extreme scenarios resulting from the uncertainties in the projection ensemble, i.e. the combination of the 'high' and 'low' temperature and precipitation changes. Four snow cover metrics which reflect the phenology of the snow cover and its spatial variability were used to investigate the climate sensitivity of the snow cover: (i) the maximum annual ('peak') snow water equivalent (SWE); (ii) the peak SWE timing (in day of year: DOY); (iii) the snow cover duration (SCD, in days); and (iv) the spatial coefficient of variation (CV) of peak SWE, a commonly-use metric used to characterize the snow cover spatial heterogeneity (e.g., Liston, 2004; Marsh *et al.*, 2020; Dharmadasa *et al.*, 2023). A SWE threshold of 1 mm was used to define snow presence on the ground and calculate the annual SCD. The SCD and CV were calculated at each model gridcell for each simulated year, and then spatially and temporally averaged over the model domain and simulation period. The peak SWE and its timing are spatially and temporally averaged over the model domain and simulation period. The peak SWE map corresponds to day of peak SWE timing. The climate sensitivity of each metric was defined as its difference (Δ) between the future (2085-2100) and the reference (2005-2019) period, for a given scenario. The climate sensitivity of peak SWE was expressed in relative (%) unit, following previous studies (Callaghan *et al.*, 2011; Shi and Wang, 2015; López-Moreno *et al.*, 2017; Mudryk *et al.*, 2020). In addition, the sensitivity of the snow fluxes was also investigated, including snowpack sublimation, blowing snow sublimation, snow melting and blowing snow transport.

3.3 Results

3.3.1 Changes in snow phenology

Under historical conditions, the simulated snowpack starts accumulating in the first week of September and remains on the ground until the last week of June, with a typical SCD of 256 days. Maximum SWE accumulation typically occurred on 15th May, reaching 72 mm (Figure 3-3a).

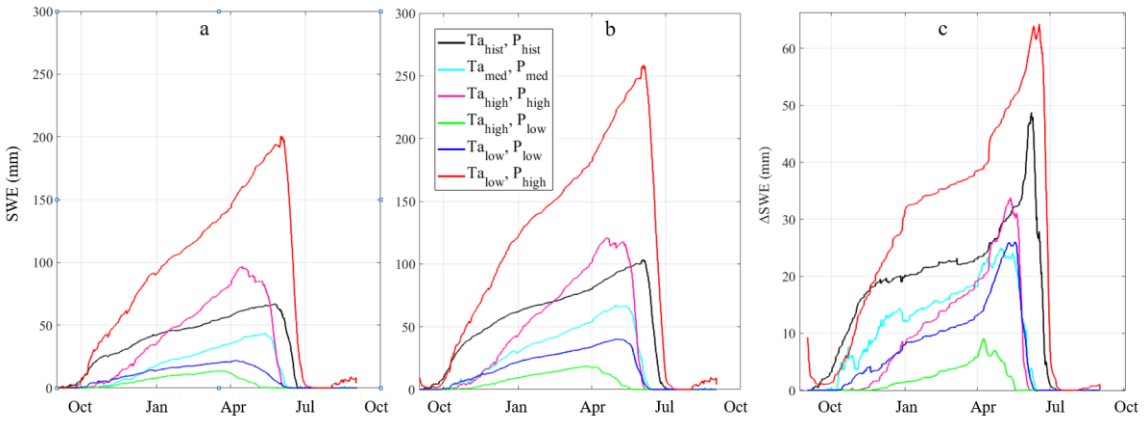

Figure 3-3 Mean seasonal cycle of the spatially-averaged snow water equivalent (SWE) under different climate scenarios. a) Simulations with blowing snow (BS) processes and (b) without blowing snow processes; (c) difference between BS-disabled and BS-enabled simulations, i.e. panel b minus panel a. Ta_{his}, Ta_{low}, Ta_{med}, and Ta_{high} represent air temperature for historical period, low, median, and high scenarios respectively. The same abbreviations are used for precipitation (P).

A marked decrease in peak SWE (-37%) occurs under the most likely climate change scenario (Ta_{med}, P_{med}) compared to the reference period (cyan curve in Figure 3-3a). When looking at the effect of scenario uncertainties, increasing precipitation is seen to cause a considerable increase in peak SWE while temperature warming mainly affects the peak SWE timing (Figure 3-3a). Under the most drastic scenarios, peak SWE increases by 178% under the wettest/coldest scenario (Ta_{low}, P_{high}) and decreases by 78% under the warmest/driest scenario (Ta_{high}, P_{low}), while other scenarios fall in between these two extremes snow phenologies (Figure 3-3a). The typical snow cover duration over the historical period (SCD = 256 days) is seen to decrease under all scenarios, except the coldest/wettest one (Phigh, Ta_low) (Figure 3-3a). Removing blowing snow processes led to a significant increase in simulated peak SWE of 64 mm (23%) and a corresponding increase of SCD by 11 days (SCD = 267 days) compared to the BS-enabled simulation during the reference period (Figure 3-3b, c). The differences in snow phenologies are most pronounced in the fall and spring when most precipitation events occur (Chapter 2), which enhances blowing snow sublimation during high snow transport events during snowfall (Figure 3-3c).

3.3.2 Impact of blowing snow on the climate sensitivity of snow cover metrics

3.3.2.1 Peak SWE

Omitting blowing snow processes caused the climate sensitivity of peak SWE to decrease slightly, from -37.2% to -34%, under the most likely climate scenario (Ta_{med}-P_{med}) (Figure 3-4a). The difference in sensitivity between BS and no-BS varied across the scenarios, with colder and wetter conditions favoring a larger impact of BS on the peak SWE sensitivity and warmer/drier conditions favoring a lower sensitivity. For example, the wettest and coldest scenario (Ta_{low}-P_{high}) led to the largest difference (23%) in SWE sensitivity between BS and no-BS. Whilst under the warmest and wettest scenario (Ta_{high}-P_{high}), ignoring blowing snow processes resulted in a much smaller decrease (7.8%) in peak SWE sensitivity. To the other end of the spectrum, the warmest and driest scenario (Ta_{high}-P_{low}) led to the lowest (2%) difference in sensitivity between BS and no-BS.

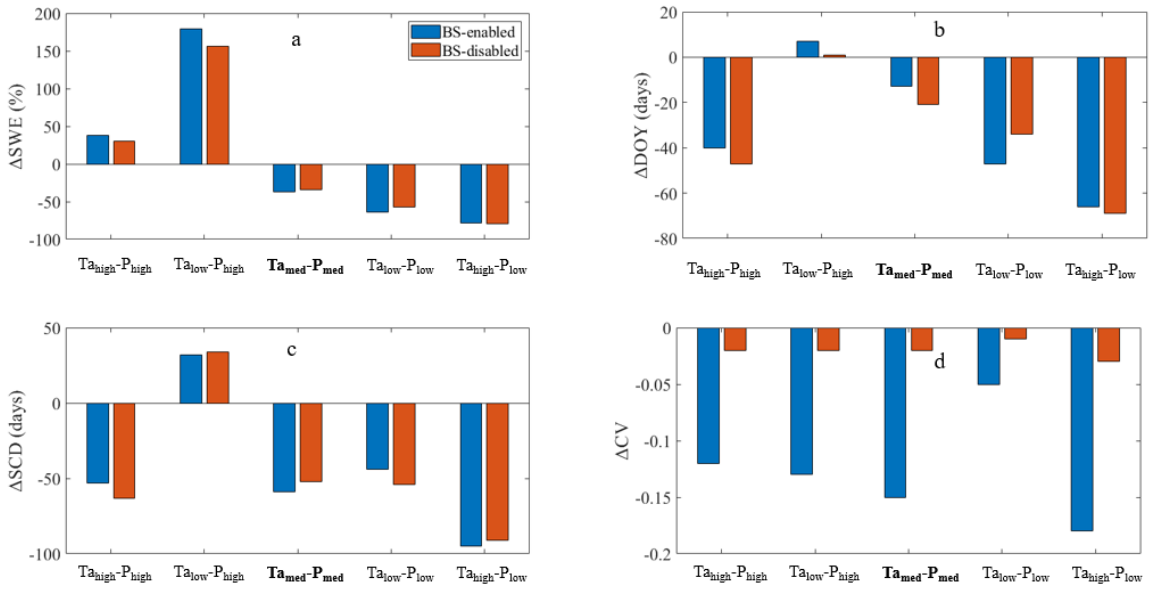

Figure 3-4 Sensitivity of snow cover metrics to climate for the different scenarios. (a) peak SWE; (b) peak SWE timing; (c) snow cover duration (SCD); (d) spatial coefficient of variation (CV). The most probable climate scenario (med) is highlighted in bold.

3.3.2.2 Peak SWE timing

An earlier peak SWE timing was projected for all scenarios but the coldest/wettest (Ta_{low}-P_{high}), for which peak SWE occurred 7 days later than present (Figure 3-4b). In certain scenarios characterized by both elevated temperatures and increased precipitation, it is evident that the duration of snow cover is primarily influenced by the warming factor. For instance, despite the augmented precipitation in both the moderately wet and warm (Ta_{med}-P_{med}) and highly wet and warm (Ta_{high}-P_{high}) scenarios, the peak SWE timing exhibited a reduction by 13 and 40 days, respectively.

Exclusion of the blowing snow process significantly affected peak SWE timing, but BS effects on the climate sensitivity varied according to the particular climate scenario (Figure 3-4b). Warmer and drier conditions favored a larger impact of BS on the peak SWE timing sensitivity, and colder and wetter conditions favored a lower sensitivity. The largest effect of BS was observed under the coldest/driest scenario (Ta_{low}-P_{low}) with 15 days difference between BS and no BS while the lowest effect was observed under Ta_{high}-P_{low} with 15 days difference. The remaining scenarios fall between these two particular scenarios. Furthermore, it's worth noting that in the coldest conditions (T_{low}), the sensitivity of BS condition was greater than that of the no BS condition, whereas in warmer conditions (T_{med} and T_{high}), the sensitivity of the no BS condition exceeded that of BS (Figure 3-4b).

3.3.2.3 Snow cover duration (SCD)

Declining snow cover duration (SCD) was simulated under all scenarios but the coldest/wettest (Ta_{low}-P_{high}), for which SCD increased by 33 days (Figure 3-4c). Similarly to peak SWE timing, increasing precipitation did not compensate for the negative warming impacts on snow cover duration, apart from the coldest/wettest scenario. For instance, despite the higher precipitation in both the moderately wet and warm (Ta_{med}-P_{med}) and highly wet and warm (Ta_{high}-P_{high}) scenarios, the snow cover duration (SCD) exhibited a reduction by 40 and 57 days, respectively. The influence of the blowing snow process on the climate sensitivity of SCD is primarily contingent on temperature. The results showed that under the coldest and driest climate conditions (scenarios) the difference between BS

and noBS was largest by 9 days while the lowest difference (3 days) was observed when climate condition was set to the coldest and wettest conditions. The remaining scenarios fall between these two particular scenarios (Figure 3-4c).

3.3.2.4 Spatial heterogeneity

The spatial heterogeneity of peak SWE, as described by the coefficient of variation (CV), decreased across all scenarios, but changes were small when BS was ignored and larger when BS was activated (Figure 3-4d). The largest decrease in CV was observed under the warmest/driest (Ta_{high}-P_{low}) scenario ($\Delta CV = -0.18$), while the smallest reduction was found in the coldest/wettest (Ta_{low}-P_{high}) scenario ($\Delta CV = -0.05$). The CV decreased by -0.11 to -0.15 under the intermediate scenarios (Figure 3-4d).

Changes in the mean peak SWE spatial distribution in response to climate scenarios are portrayed in Figure 3-5. Despite the fact that the spatial heterogeneity of SWE decreased under all climate scenarios, the distribution pattern remains similar to that seen in the historical period, with deeper snow in ravines, channels and breaks of slopes, and shallower snow observed on flatter ground (Figure 3-5: first row). Deactivating the blowing snow processes led to a much more homogenized snowpack (Figure 3-5 bottom row). The results showed that for equal temperature, increasing precipitation leads to more homogenous snow cover so that changing precipitation from the driest condition to the wettest condition (when the temperature was kept to coldest scenario) CV decreased from 0.28 to 0.2. For equal precipitation, increasing temperature also caused a more homogenous snow cover so that changing temperature from coldest condition to warmest condition (when the temperature was kept to coldest scenario) CV decreased from 0.28 to 0.15.

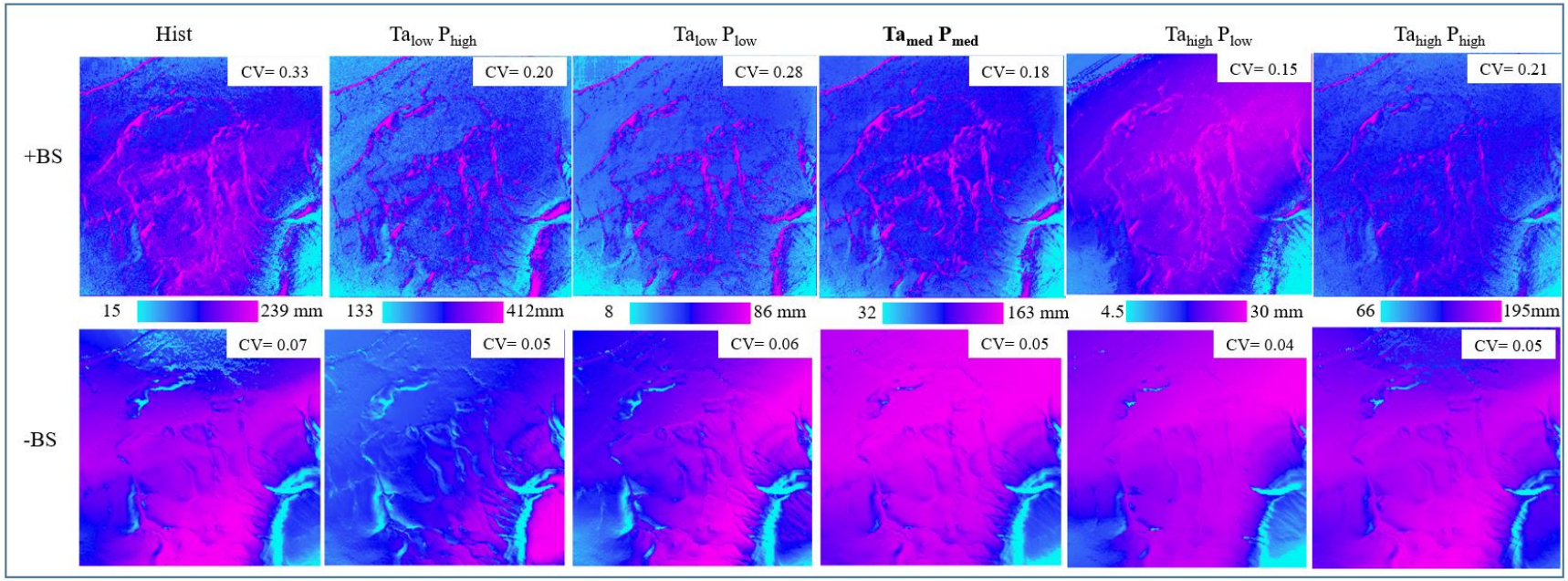

Figure 3-5 Simulated mean peak SWE under RCP 8.5 scenario (low, median, and high percentiles). First panel row shows the peak SWE with BS-enabled and the second row with BS-disabled. A separate color scale is used for each climate scenario to maximize contrasts. The coefficient of variation (CV), an indicator of the mean peak SWE heterogeneity, is shown on each map.

3.3.3 Changes in snow fluxes

The relative contribution of individual snow mass fluxes (snowpack melt, snowpack sublimation, blowing snow sublimation and blowing snow transport) to the snow mass balance under the different climate scenarios is shown in Figure 3-6, and their corresponding changes relative to the reference period are shown in Figure 3-7. During the historical period the dominant snow flux processes were, in decreasing order of importance, melting (63%), blowing snow sublimation (17%), snowpack sublimation (14%), and blowing snow transport (6%). Disabling BS processes significantly increased the relative importance of melting (88%) whereas the importance of snowpack sublimation decreased slightly (12%). Snowmelt remained the dominant mass removal process (>50% and up to nearly 100%), under all climate scenarios, whether BS was considered or not (Figure 3-6).

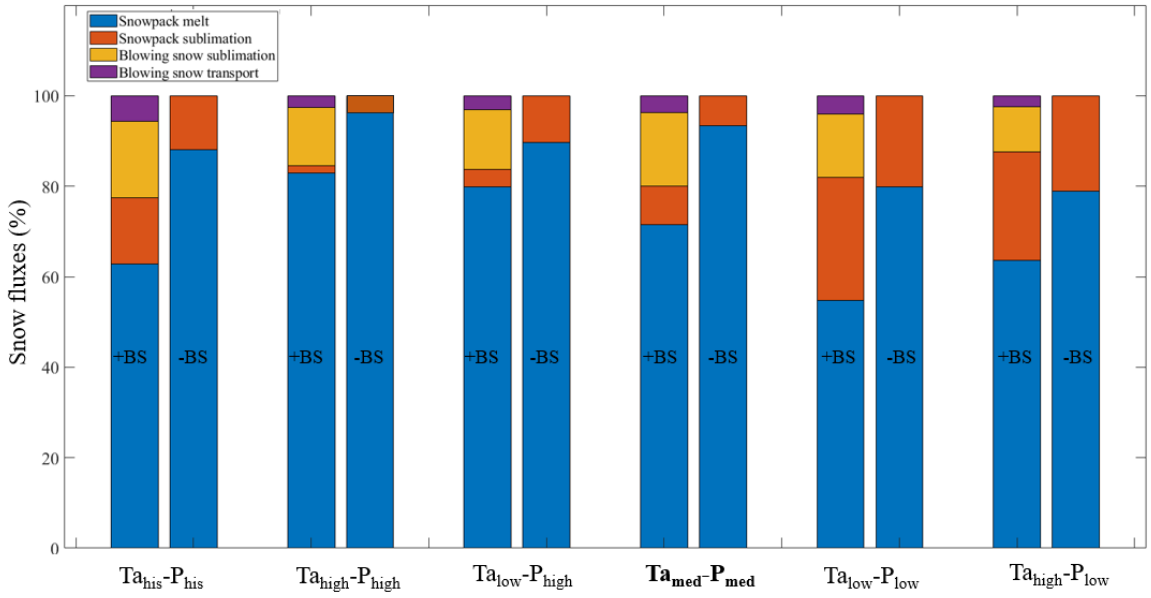

Figure 3-6 Relative contribution of annual total snow fluxes under different climate scenarios. +BS refers to simulations with blowing snow processes and -BS refers to simulations without blowing snow.

Under blowing snow conditions, a notable increase in the snowmelt share of mass loss is observed when the climate is wetter (P_{low} and P_{med}). In contrast, under drier conditions, the share of snowmelt shows a marginal increase (Ta_{high}-P_{low}) or a considerable decrease (Ta_{low}-P_{low}) (Figure 3-7). The share of mass loss from snowpack sublimation shows an opposite trend, decreasing in response to wetter conditions (P_{low} and P_{med}) and increasing under drier (P_{low}) conditions. Blowing snow sublimation losses and the net transport rates are reduced under all climate scenarios, with the largest share reductions for the warmest/driest scenario (Ta_{high}, P_{low}).

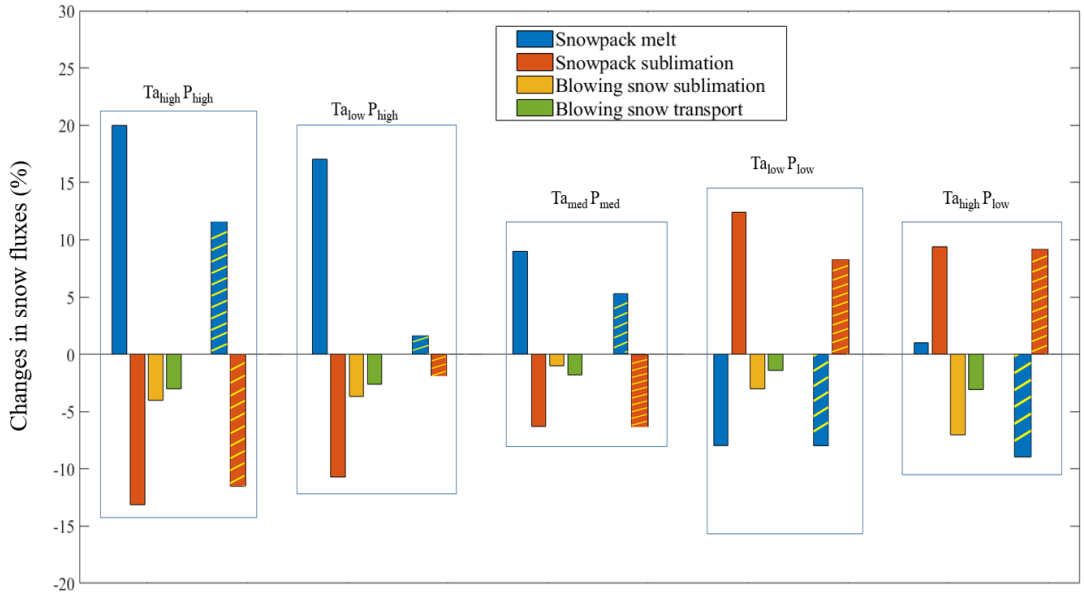

Figure 3-7 Relative changes of snow fluxes under different climate scenarios relevant to reference period (2005-2019) for the gridbox close to the Bylot research camp in Bylot Island, Canada. The crosshatched bars represent simulations with blowing snow-disabled.

Deactivating blowing snow processes significantly attenuated the sensitivity of the melting and snowpack sublimation mass loss shares for the wet scenarios (P_{high}, P_{med}) (Figure 3-7). This is less evident for the dry scenario (P_{low}), and the melt share even decreases under the warmest/driest conditions (Ta_{high}, P_{low}). A sharp reduction of sensitivity is also seen under the coldest/wettest scenario (Ta_{low}, P_{high}), compared to blowing snow-enabled conditions.

3.4 Discussion

3.4.1 Simulated changes in snow cover

The projected scenarios showed that the snow metrics will be significantly modified towards the end of the twenty-first century. The climate responses demonstrated that the timing and magnitude of annual peak SWE is sensitive to warming and changes in precipitation for both BS-enabled and BS-disabled (Figure 3-4a and b). Increasing winter snowfall led to a decrease in annual peak SWE under most plausible scenario (Ta_{med}- P_{med}) by 6% per decade. This is against previous studies by Mudryk *et al.* (2018, 2020), Raisanen (2008) and Shi and Wang (2015) who found an increase between 5 to 10% per decade in annual peak SWE under RCP 8.5 scenarios over the Canadian Arctic regions. Despite an increase in precipitation, the timing of annual peak SWE was shown to be more sensitive to change in temperature than to change in precipitation. Warming temperatures under most plausible scenario (Ta_{med}- P_{med}) will result in shorter snow cover duration (SCD) under high RCP 8.5, but given the long and cold winters that presently characterize the High Arctic, the snow cover would persist towards the end of the 21st century. Consistent with prior regional studies, our findings demonstrate that the snow season in the High Arctic will be shorter compared to present (Brown *et al.*, 2017; Mudryk *et al.*, 2018, 2020). However our study simulated a smaller reduction rate in SCD (5%) compared to the previous studies (10-15%) that are conducted at regional scale across Canadian Arctic regions.

3.4.2 Effect of BS on the climate sensitivity

Under present climate conditions, the model revealed that blowing snow sublimation and snow wind transport were a significant part of snow fluxes leading to a high spatial heterogeneity of snowpack at the Bylot study site. Over the historical period loss of snow mass due to total sublimation (snowpack + blowing snow) accounted for

approximately 31% of cumulative snowfall, with blowing snow sublimation contributing to 17% of cumulative snowfall. This is mostly because the area is exposed to strong winds which favors snow transport and its sublimation. Including blowing allowed to represent snowdrift formation, which greatly increased the coefficient of variation of SWE from 0.07 to 0.32 (Figure 3-5), a value in line with that measured in Bylot, (Chapter 2, CV=0.37) and those reported from other Canadian tundra environments, e.g. 0.31 (Marsh *et al.*, 2020) and 0.40 (Liston, 2004).

The rate of blowing snow sublimation was significantly decreased across all scenarios considered, but the rate of decrease varied by scenario. Warmer scenarios caused a significant reduction in net wind snow transport and blowing snow sublimation that led to a less heterogeneous snowpack. For example, the rate of blowing snow sublimation was projected to decrease between 3 to 10% which led to a decrease of coefficient of variation (CV) between 0.04 and 0.15. Also net transport decreased under all scenario between 2 to 5%. However, the spatial heterogeneity of the snow cover remained always much higher than when BS was ignored, under all scenarios. When BS deactivated, negligible changes in snow cover heterogeneity were observed (Figure 3-5). This is in line with a previous study reporting that the frequency of blowing snow occurrence has decreased significantly in the Canadian Arctic under global warming conditions (Hanesiak and Wang, 2005). Marshall *et al.* (2019) also reported that warming temperatures caused a reduction in snow drifting and led to a more homogenous snowpack in Upper Sheep Creek, Idaho (USA). Other studies by Pomeroy *et al.* (2015) in the Canadian Rockies and Aygün *et al.* (2020) in the Acadie River Catchment in southern Québec have shown that rising temperatures serve as a limiting factor on the erodibility of blowing snow, which is due to the increasing bond strength and cohesion of snow as it warms (Li and Pomeroy, 1997).

The influence of blowing snow processes on the climate sensitivity of snow cover varied between the snow metrics and the climate scenario considered. Generally, the

effect of blowing snow on the climate sensitivity of the snow metrics was greater under colder and drier scenarios, and smaller in warmer and wetter scenarios. This finding is in line with the aforementioned increase in snow resistance to wind transport as the climate warms. While it is observed that the response of max SWE timing to projected climate scenario will be significantly influenced by disabling blowing snow processes (Figure 3-4c) max SWE demonstrated the lowest sensitivity to the disabling BS (Figure3-4a). Among the snow cover metrics, snow cover heterogeneity observed to be the most sensitive snow metric when disabling BS. This is consistent with the responses of snow fluxes to disabling blowing snow processes under different climate scenarios. For example it is seen that largest decrease in blowing snow sublimation happened under warmest and driest conditions (Figure 3-7) which is line with decrease in snow cover heterogeneity under same climate scenario (Figure 3-7). This change in snow fluxes and snow metrics indicate that snowdrift in study area will be strongly affected. These findings are important because snow drifts hold significant ecological implications as they offer crucial sheltered habitats for numerous flora and fauna species throughout the extended frigid winter periods in Arctic (Wohl, 2015; Liston *et al.*, 2016; Poirier *et al.*, 2019).

3.5 Conclusions

Despite the fact that several studies simulated the future changes in snow cover condition under projected climate scenarios, significant uncertainties remain in these simulations from not taking into account the processes that happen at small scale. The GEOtop model, as a grid-based and distributed hydrological model, was used to consider those snow cover processes occurring at fine scales to simulate snow cover conditions under projected climate scenarios for the end of 21st century. Several climate scenarios were considered to investigate the effect of blowing snow on the sensitivity of snow cover to changes in precipitation and temperature across a tundra environment. Our results indicated that considering BS impacted the climate sensitivity

of the snow cover and this impact was contingent upon the evaluated climate scenario. In general, the impact of blowing snow on the climatic sensitivity of snow cover metrics was more pronounced in colder and drier scenarios, but less pronounced in warmer and wetter conditions. The observed patterns in the impact of blowing snow on the climatic sensitivity of snow cover metrics have important implications for various real-life scenarios. In colder and drier conditions, where the influence of blowing snow is more pronounced, we can anticipate heightened sensitivity in snow cover metrics. This increased sensitivity may manifest itself in accelerated changes in snow distribution, thickness, and other relevant parameters, impacting local ecosystems and water resources. Conversely, in warmer and wetter conditions, where the impact of blowing snow is less pronounced, the sensitivity of snow cover metrics may be more stable. This implies that, under these circumstances, changes in blowing snow might have a comparatively smaller influence on the overall dynamics of snow cover. This information is crucial for regions or industries that rely on predictable snow patterns, such as water resource management, agriculture, or infrastructure planning.

Of particular significance is the observation that the influence of the blowing snow process on the sensitivity of SCD to climate alterations is primarily contingent on temperature. This study highlighted that including blowing snow processes for climate change investigation can significantly modify snow spatial variability. Under all tested climate scenarios, warming reduces snow transport, leading to reduced blowing snow sublimation losses and a more homogenized snow cover so that warmer and drier condition favored more homogenized snow cover while under coldest and drier condition less changes in snow cover heterogeneity was observed. These changes can significantly affect the soil moisture availability and greening season in the High Arctic. In warmer and drier scenarios, a more homogenized snow cover can influence the onset and duration of the greening season. A homogenized snow cover promotes more uniform melting, leading to a synchronized release of moisture into the soil. This synchronized moisture availability can extend the greening season by providing a more

favorable environment for plant growth. These insights are crucial for understanding the broader ecological implications of climate change in Polar Regions and can inform adaptive strategies for managing ecosystems in the face of ongoing environmental shifts.

References

Ballantyne, C., Williams, P. J. and Smith, M. W. (1990) The Frozen Earth: Fundamentals of Geocryology, Transactions of the Institute of British Geographers. New York: Cambridge University Press. p 306. doi: 10.2307/622856.

Barnes, S. L. (1964) 'A technique for maximizing details in numerical weather map analysis', Journal of Applied Meteorology and Climatology, pp. 396–409.

Beck, H. E., Zimmermann, N. E., McVicar, T. R., Vergopolan, N., Berg, A. and Wood, E. F. (2018) 'Present and future köppen-geiger climate classification maps at 1-km resolution', Scientific Data, 5, pp. 1–12. doi: 10.1038/sdata.2018.214.

Bigalke, S. and Walsh, J. E. (2022) 'Future Changes of Snow in Alaska and the Arctic under Stabilized Global Warming Scenarios', Atmosphere, 13(4). doi: 10.3390/atmos13040541.

Bintanja, R. and Andry, O. (2017) 'Towards a rain-dominated Arctic', Nature Climate Change, 7(4), pp. 263–267. doi: 10.1038/nclimate3240.

Bokhorst, S. et al. (2016) 'Changing Arctic snow cover: A review of recent developments and assessment of future needs for observations, modelling, and impacts', Ambio, 45(5), pp. 516–537. doi: 10.1007/s13280-016-0770-0.

Brown, R., Schuler, D. V., Bulygina, O., Derksen, C., Luojus, K., Mudryk, L., Wang, L. and Yang, D. (2017) Snow, Water, Ice and Permafrost in the Arctic (SWIPA). Chapter 3: Arctic terrestrial snow cover. Oslo, Norway.

Callaghan, T. et al. (2011) 'The changing face of Arctic snow cover: A synthesis of observed and projected changes', Ambio, 40, pp. 17–31. doi: 10.1007/s13280-011-0212-y.

Callaghan, T. V. et al. (2011) ‘Multiple effects of changes in Arctic snow eover’, Ambio, 40, pp. 32–45. doi: 10.1007/s13280-011-0213-x.

Cannon, A. J., Sobie, S. R. and Murdock, T. Q. (2015) ‘Bias correction of GCM precipitation by quantile mapping: How well do methods preserve changes in quantiles and extremes?’, Journal of Climate, 28(17), pp. 6938–6959. doi: 10.1175/JCLI-D-14-00754.1.

Castaneda-Gonzalez, M., Poulin, A., Romero-Lopez, R., Arsenault, R., Brissette, F. and Turcotte, R. (2019) ‘Sensitivity of seasonal flood simulations to regional climate model spatial resolution’, Climate Dynamics. Springer Berlin Heidelberg, 53(7–8), pp. 4337–4354. doi: 10.1007/s00382-019-04789-y.

CEN (2021) ‘CEN: Climate station data from Bylot Island in Nunavut, Canada, http://www.cen.ulaval.ca/nordicanad/dpage.aspx?doi= 45039SL-EE76C1BDAADC4890.’

Derksen, C. and Mudryk, L. (2023) ‘Assessment of Arctic seasonal snow cover rates of change’, Cryosphere, 17(4), pp. 1431–1443. doi: 10.5194/tc-17-1431-2023.

Déry, S. J., Crow, W. T., Stieglitz, M. and Wood, E. F. (2004) ‘Modeling snow-cover heterogeneity over complex Arctic terrain for regional and global climate models’, Journal of Hydrometeorology, 5(1), pp. 33–48. doi: 10.1175/1525-7541(2004)005<0033:MSHOCA>2.0.CO;2.

Déry, S. J. and Yau, M. K. (2001) ‘Simulation of blowing snow in the canadian arctic using a double-momentmodel’, Boundary-Layer Meteorology, 99, pp. 297–316.

Dharmadasa, V., Kinnard, C. and Baraër, M. (2023) ‘Topographic and vegetation controls of the spatial distribution of snow depth in agro-forested environments by UAV lidar’, Cryosphere, 17(3), pp. 1225–1246. doi: 10.5194/tc-17-1225-2023.

Duclos, I., Lévesque, E., Gratton, D. and Bordeleau, P.-A. (2006) Vegetation mapping of Bylot Island and Sirmilik national park. Iqaluit, Nunavut. 101p.

Ellis, C. J., Rochefort, L., Gauthier, G. and Pienitz, R. (2008) ‘Paleoecological evidence for transitions between contrasting landforms in a polygon-patterned high arctic wetland’, Arctic, Antarctic, and Alpine Research, 40(4), pp. 624–637. doi: 10.1657/1523-0430(07-059)[ELLIS]2.0.CO;2.

Endrizzi, S., Gruber, S., Dall’Amico, M. and Rigon, R. (2014) ‘GEOtop 2.0: Simulating the combined energy and water balance at and below the land

surface accounting for soil freezing, snow cover and terrain effects', Geoscientific Model Development, 7(6), pp. 2831–2857. doi: 10.5194/gmd-7-2831-2014.

Endrizzi, S. and Marsh, P. (2010) 'Observations and modeling of turbulent fluxes during melt at the shrub-tundra transition zone 1: Point scale variations', Hydrology Research, 41(6), pp. 471–491. doi: 10.2166/nh.2010.149.

Engel, M., Notarnicola, C., Endrizzi, S. and Bertoldi, G. (2017) 'Snow model sensitivity analysis to understand spatial and temporal snow dynamics in a high-elevation catchment', Hydrological Processes. Wiley-Blackwell, 31(23), pp. 4151–4168. doi: 10.1002/hyp.11314.

Essery, R., Li, L. and Pomeroy, J. (1999) 'A distributed model of blowing snow over complex terrain', Hydrological Processes, 13, pp. 2423–2438. doi: 10.1002/(SICI)1099-1085(199910)13:14/15<2423::AID-HYP853>3.0.CO;2-U.

Essery, R. and Pomeroy, J. (2004) 'Vegetation and topographic control of wind-blown snow distributions in distributed and aggregated simulations for an Arctic tundra basin', Journal of Hydrometeorology, 5, pp. 735–744. doi: 10.1175/1525-7541(2004)005<0735:VATCOW>2.0.CO;2.

Fortier, D. and Allard, M. (2004) 'Late Holocene syngenetic ice-wedge polygons development, Bylot Island, Canadian Arctic Archipelago', Canadian Journal of Earth Sciences, 41, pp. 997–1012. doi: https://doi.org/10.1139/e04-031.

Gauthier, G., Bêty, J., Cadieux, M.-C., Legagneux, P., Doiron, M., Chevallier, C., Lai, S., Tarroux, A. and Berteaux, D. (2013) 'Long-term monitoring at multiple trophic levels suggests heterogeneity in responses to climate change in the Canadian Arctic tundra.', Philosophical transactions of the Royal Society. The Royal Society, 368(1624), p. 20120482. doi: 10.1098/rstb.2012.0482.

Gubler, S., Endrizzi, S., Gruber, S. and Purves, R. S. (2013) 'Sensitivities and uncertainties of modeled ground temperatures in mountain environments', Geosci. Model Dev, 6, pp. 1319–1336. doi: 10.5194/gmd-6-1319-2013.

Gudmundsson, L., Bremnes, J. B., Haugen, J. E. and Engen-Skaugen, T. (2012) 'Technical Note: Downscaling RCM precipitation to the station scale using statistical transformations – A comparison of methods', Hydrology and Earth System Sciences, 16(9), pp. 3383–3390. doi: 10.5194/hess-16-3383-2012.

Hall, D. K. (1988) ‘Assessment of polar climate change using satellite technology’, Reviews in Geophysics, 26(1), pp. 26–39.

Hanesiak, J. M. and Wang, X. L. (2005) ‘Adverse-weather trends in the Canadian Arctic’, Journal of Climate, 18(16), pp. 3140–3156. doi: 10.1175/JCLI3505.1.

Heginbottom JA (1995) Canada-permafrost. The national Atlas of Canada, fifth edition. Ottawa.

Kochendorfer, J. et al. (2017) ‘Analysis of single-Alter-shielded and unshielded measurements of mixed and solid precipitation from WMO-SPICE’, Hydrology and Earth System Sciences, 21(7), pp. 3525–3542. doi: 10.5194/hess-21-3525-2017.

Largeron, C. et al. (2020) ‘Toward Snow Cover Estimation in Mountainous Areas Using Modern Data Assimilation Methods: A Review’, Frontiers in Earth Science, 8(September). doi: 10.3389/feart.2020.00325.

Lespinas, F., Fortin, V., Roy, G., Rasmussen, P. and Stadnyk, T. (2015) ‘Performance evaluation of the canadian precipitation analysis (CaPA)’, Journal of Hydrometeorology, 16(5), pp. 2045–2064. doi: 10.1175/JHM-D-14-0191.1.

Li, L. and Pomeroy, J. W. (1997) ‘Estimates of threshold wind speeds for snow transport using meteorological data’, Journal of Applied Meteorology, 36(3), pp. 205–213. doi: 10.1175/1520-0450(1997)036<0205:EOTWSF>2.0.CO;2.

Liston, G. E. (2004) ‘Representing subgrid snow cover heterogeneities in regional and global models’, Journal of Climate, 17(6), pp. 1381–1397. doi: 10.1175/1520-0442(2004)017<1381:RSSCHI>2.0.CO;2.

Liston, G. E. and Elder, K. (2006) ‘A meteorological distribution system for high-resolution terrestrial modeling (MicroMet)’, Journal of Hydrometeorology, 7(2), pp. 217–234. doi: 10.1175/JHM486.1.

Liston, G. E., Haehnel, R. B., Sturm, M., Hiemstra, C. A., Berezovskaya, S. and Tabler, R. D. (2007) ‘Instruments and methods simulating complex snow distributions in windy environments using SnowTran-3D’, Journal of Glaciology, 53(181), pp. 241–256. doi: 10.3189/172756507782202865.

Liston, G. E., Perham, C. J., Shideler, R. T. and Cheuvront, A. N. (2016) ‘Modeling snowdrift habitat for polar bear dens’, Ecological Modelling. Elsevier B.V., 320, pp. 114–134. doi: 10.1016/j.ecolmodel.2015.09.010.

López-Moreno, J. I. et al. (2017) ‘Different sensitivities of snowpacks to warming in Mediterranean climate mountain areas’, Environmental Research Letters, 12(7). doi: 10.1088/1748-9326/aa70cb.

Marsh, C. B., Pomeroy, J. W., Spiteri, R. J. and Wheater, H. S. (2020) ‘A Finite Volume Blowing Snow Model for Use With Variable Resolution Meshes’, Water Resources Research, 56(2), pp. 1–28. doi: 10.1029/2019WR025307.

Marshall, A. M., Link, T. E., Abatzoglou, J. T., Flerchinger, G. N., Marks, D. G. and Tedrow, L. (2019) ‘Warming Alters Hydrologic Heterogeneity: Simulated Climate Sensitivity of Hydrology-Based Microrefugia in the Snow-to-Rain Transition Zone’, Water Resources Research, 55(3), pp. 2122–2141. doi: 10.1029/2018WR023063.

Maurer, E. P., Hidalgo, H. G., Das, T., Dettinger, M. D. and Cayan, D. R. (2010) ‘The utility of daily large-scale climate data in the assessment of climate change impacts on daily streamflow in California’, Hydrology and Earth System Sciences, 14(6), pp. 1125–1138. doi: 10.5194/hess-14-1125-2010.

McCrystall, M. R., Stroeve, J., Serreze, M., Forbes, B. C. and Screen, J. A. (2021) ‘New climate models reveal faster and larger increases in Arctic precipitation than previously projected’, Nature Communications. Springer US, 12(1), pp. 1–12. doi: 10.1038/s41467-021-27031-y.

Mohammadzadeh Khani, H., Kinnard, C. and Lévesque, E. (2022) ‘Historical Trends and Projections of Snow Cover over the High Arctic: A Review’, Water. MDPI AG, 14(4), p. 587. doi: 10.3390/W14040587.

Mohammadzadeh Khani, H., Kinnard, C. and Lévesque, E. (2023) ‘Fine scale distributed snow cover modeling in a High Arctic tundra landscape using the physically based GEOtop model’, Cryosphere.

Mohammadzadeh Khani, H., Kinnard, C., Lévesque, E. and Gascoin, S. (2023) ‘Fine scale environment control on ground surface temperature and active-layer thickness in a High Arctic tundra landscape’, Permafrost and Periglacial Processes, pp. 1–14. doi: 10.1002/ppp.2203.

Mudryk, L., Chereque, A. E., Derksen, C., Luojus, K. and Decharme, B. (2021) Terrestrial Snow Cover.

Mudryk, L. R., Derksen, C., Howell, S., Laliberté, F., Thackeray, C., Sospedra-Alfonso, R., Vionnet, V., Kushner, P. J. and Brown, R. (2018) ‘Canadian snow and sea ice: historical trends and projections’, The Cryosphere, 12, pp. 1157–1176. doi: 10.5194/tc-12-1157-2018.

Mudryk, L., Santolaria-Otín, M., Krinner, G., Ménégoz, M., Derksen, C., Brutel-Vuilmet, C., Brady, M. and Essery, R. (2020) 'Historical Northern Hemisphere snow cover trends and projected changes in the CMIP6 multi-model ensemble', Cryosphere, 14(7), pp. 2495–2514. doi: 10.5194/tc-14-2495-2020.

Navarro-Racines, C., Tarapues, J., Thornton, P., Jarvis, A. and Ramirez-Villegas, J. (2020) 'High-resolution and bias-corrected CMIP5 projections for climate change impact assessments', Scientific Data, 7(1), pp. 1–14. doi: 10.1038/s41597-019-0343-8.

Niittynen, P., Heikkinen, R. K. and Luoto, M. (2018) 'Snow cover is a neglected driver of Arctic biodiversity loss', Nature Climate Change. Springer US, 8(11), pp. 997–1001. doi: 10.1038/s41558-018-0311-x.

Perreault, N., Lévesque, E., Fortier, D. and Lamarque, L. J. (2016) 'Thermo-erosion gullies boost the transition from wet to mesic tundra vegetation', Biogeosciences, 13(4), pp. 1237–1253. doi: 10.5194/bg-13-1237-2016.

Peters-Lidard, C. D., Clark, M., Samaniego, L., Verhoest, N. E. C., Van Emmerik, T., Uijlenhoet, R., Achieng, K., Franz, T. E. and Woods, R. (2017) 'Scaling, similarity, and the fourth paradigm for hydrology', Hydrology and Earth System Sciences, 21(7), pp. 3701–3713. doi: 10.5194/hess-21-3701-2017.

Poirier, M., Gauthier, G. and Domine, F. (2019) 'What guides lemmings movements through the snowpack?', Journal of Mammalogy, 100(5), pp. 1416–1426. doi: 10.1093/jmammal/gyz129.

Pomeroy, J. W. and Brun, E. (2001) Snow ecology: Physical properties of snow. Edited by H. G. Jones, J. W. Pomeroy, D. A. Walker, and R. W. Hoham. Cambridge University Press. 378 p.

Pomeroy, J. W., Gray, D. M. and Landine, P. G. (1993) 'The Prairie Blowing Snow Model: characteristics, validation, operation', Journal of Hydrology, 144(1–4), pp. 165–192. doi: 10.1016/0022-1694(93)90171-5.

Pomeroy, J. W. and Jones, H. G. (1996) 'Wind-blown snow: Sublimation, transport and changes to Polar snow', in Processes of chemical exchange between the atmosphere and polar Snow. Berlin, Germany, pp. 453–490. doi: 10.1007/978-3-642-61171-1_19.

Pomeroy, J. W. and Li, L. (2000) 'Prairie and arctic areal snow cover mass balance using a blowing snow model', Journal of Geophysical Research Atmospheres, 105(D21), pp. 26619–26634. doi: 10.1029/2000JD900149.

Pomeroy, J. W., Marsh, P. and Gray, D. M. (1997) 'Application of a distributed blowing snow model to the arctic', Hydrological Processes, 11(11), pp. 1451–1464. doi: 10.1002/(sici)1099-1085(199709)11:11<1451::aid-hyp449>3.0.co;2-q.

Pouliot, R., Rochefort, L. and Gauthier, G. (2009) 'Moss carpets constrain the fertilizing effects of herbivores on graminoid plants in arctic polygon fens', Botany, 87(12), pp. 1209–1222. doi: 10.1139/B09-069.

Raisanen, J. (2008) 'Warmer climate : less or more snow ?', Climate Dynamics, 30, pp. 307–319. doi: 10.1007/s00382-007-0289-y.

Rantanen, M., Karpechko, A. Y., Lipponen, A., Nordling, K., Hyvärinen, O., Ruosteenoja, K., Vihma, T. and Laaksonen, A. (2022) 'The Arctic has warmed nearly four times faster than the globe since 1979', Communications Earth and Environment. Springer US, 3(1), pp. 1–10. doi: 10.1038/s43247-022-00498-3.

Schwalm, C. R., Glendon, S. and Duffy, P. B. (2020) 'RCP8.5 tracks cumulative CO2 emissions', Proceedings of the National Academy of Sciences of the United States of America, 117(33), pp. 19656–19657. doi: 10.1073/PNAS.2007117117.

Serreze, M. C. and Barry, R. G. (2011) 'Processes and impacts of Arctic amplification: A research synthesis', Global and Planetary Change. Elsevier, 77(1–2), pp. 85–96. doi: 10.1016/J.GLOPLACHA.2011.03.004.

Shi, H. X. and Wang, C. H. (2015) 'Projected 21st century changes in snow water equivalent over Northern Hemisphere landmasses from the CMIP5 model ensemble', The Cryosphere, 9, pp. 1943–1953. doi: 10.5194/tc-9-1943-2015.

Stuecker, M. F. et al. (2018) 'Polar amplification dominated by local forcing and feedbacks', Nature Climate Change. Springer US, 8(12), pp. 1076–1081. doi: 10.1038/s41558-018-0339-y.

Sturm, M., McFadden, J. P., Liston, G. E., Stuart Chapin, F., Racine, C. H. and Holmgren, J. (2001) 'Snow-shrub interactions in Arctic Tundra: A hypothesis with climatic implications', Journal of Climate, 14(3), pp. 336–344. doi: 10.1175/1520-0442(2001)014<0336:SSIIAT>2.0.CO;2.

Tam, B. Y., Szeto, K., Bonsal, B., Flato, G., Cannon, A. J. and Rong, R. (2019) 'CMIP5 drought projections in Canada based on the Standardized Precipitation Evapotranspiration Index', Canadian Water Resources Journal. Taylor & Francis, 44(1), pp. 90–107. doi: 10.1080/07011784.2018.1537812.

Thackeray, C. W., Fletcher, C. G., Mudryk, L. R. and Derksen, C. (2016) 'Quantifying the uncertainty in historical and future simulations of Northern Hemisphere spring snow cover', Journal of Climate, 29, pp. 8647–8663. doi: 10.1175/JCLI-D-16-0341.s1.

Wang, X., Wang, T., Guo, H., Liu, D., Zhao, Y., Zhang, T., Liu, Q. and Piao, S. (2018) 'Disentangling the mechanisms behind winter snow impact on vegetation activity in northern ecosystems', Global Change Biology, 24(4), pp. 1651–1662. doi: 10.1111/gcb.13930.

Wani, J. M., Thayyen, R. J., Ojha, C. S. P. and Gruber, S. (2021) 'The surface energy balance in a cold and arid permafrost environment, Ladakh, Himalayas, India', Cryosphere, 15(5), pp. 2273–2293. doi: 10.5194/tc-15-2273-2021.

Wohl, E. E. (2015) Transientlandscapes: insights on a changing planet. University Press of Colorado.

Woo, M. (2012) Permafrost Hydrology. Berlin Heidelberg: Springer New York. 574 p. doi: 10.1007/978-3-642-23462-0.

Xu, X., Liu, X., Li, X., Shi, Q., Chen, Y. and Ai, B. (2022) 'Global Snow Depth Retrieval from Passive Microwave Brightness Temperature with Machine Learning Approach', IEEE Transactions on Geoscience and Remote Sensing. IEEE, 60, pp. 1–17. doi: 10.1109/TGRS.2021.3127202.

Zanotti, F., Endrizzi, S., Bertoldi, G. and Rigon, R. (2004) 'The GEOtop snow model', in 61st Eastern snow conference, pp. 87–100. Available at: http://citeseerx.ist.psu.edu/viewdoc/download?doi=10.1.1.571.599&rep=rep1&type=pdf (Accessed: 26 September 2018).

CONCLUSIONS

Synthesis and concluding remarks

This thesis provides a summary of our efforts and research contribution to Arctic region hydrology. The thesis research utilized key parameters (such snow depth, soil moisture, vegetation etc.) to identify seasonal influences on the permafrost active layer and its thermal regime. Late winter snowpack thickness was found to be the prime control on the spatial variability in winter soil temperatures due to the highly heterogeneous snow cover induced by blowing snow, and this thermal effect carried over into summer. So, a physically-based model (GEOtop) was implemented to simulate the spatial heterogeneity of snow cover over a small area at the hillslope scale. Furthermore, our research assessed the effect of blowing snow processes on the sensitivity of the snow cover conditions to projected changes in precipitation and temperature across a High Arctic tundra environment of Northern Canada. The methodology used in this thesis has the following important components: 1) the consideration of major environmental controls that govern the microscale spatial variability of the active layer; 2) the simulation of the key snow processes found in the open terrain of High Arctic environment, such as wind-blowing snow using a fully distributed and physically based hydrological model; and 3) the exploration of the impact of blowing snow processes on the sensitivity of snow cover to projected changes in precipitation and temperature.

The key findings in relation to the particular goals outlined in the thesis introduction are provided below.

Objective 1: Measure and investigate the spatial heterogeneity of surface temperature and its relationship with snow depth, the type and height of vegetation, soil type, soil moisture, and topography.

By implementing comprehensive surveys across various land cover types, our methodology has facilitated the assessment of the significance of pivotal variables governing active layer thickness (ALT) in the High Arctic tundra ecosystem, as well as elucidating their interconnectedness in modifying ALT. Results revealed that landscape settings have a significant influence in modifying the seasonal active layer thermal regime and thaw depth patterns between and within these landscapes. Particularly in the summer, the microscale (within-landform) variation in GST and thaw depth was fairly high and occasionally even exceeded the variation at the hillslope scale. These results highlight the importance of considering surface feedback effects in future projections of active layer thermal conditions within heterogeneous tundra landscapes (Nitzbon *et al.*, 2021).Our approach of conducting detailed surveys across multiple land cover types has allowed us to determine the relative importance of the critical factors controlling ALT in tundra environment, and has also revealed how they interact to modify ALT. Due to the highly heterogeneous snow cover caused by blowing snow, late-winter snowpack thickness was discovered to be the primary environmental control of winter soil temperatures, and this thermal influence persisted into summer. When the snow cover is sparse and heterogeneous, temperature differences are most noticeable. These results underscore the importance of accurately simulating the snow cover in future climate projections in order to properly capture the impact of snow depth and snow cover duration on permafrost temperature and thawing. Given the formidable spatial heterogeneity of the snow cover in Arctic tundra landscapes, this is still a challenging task for large scale models. On the other hand, while microtopography was the predominant driver of the spatial variability in summer GST, followed by altitude and moss thickness the spatial variability in thaw depth was influenced predominantly by variations in moss thickness. Future increases in

vegetation productivity could counteract warming-induced active layer deepening in summer (Fisher *et al.*, 2016; Grünberg *et al.*, 2020), but this simple extrapolation hides the significant microtopographic heterogeneity of High Arctic tundra environments and associated plant communities. It is imperative to gain insights into the mechanistic relationships between vegetation, edaphic factors, and their interactions concerning ALT. This understanding is crucial for anticipating future rates of permafrost degradation and the associated carbon cycle implications in response to evolving climate conditions, such as alterations in fire regimes or precipitation patterns (Hansen *et al.*, 2014; Fisher *et al.*, 2016).

Objective 2: Use a physically-based and spatially-distributed snow and hydrological model to simulate historical snow cover conditions and perform a sensitivity analysis at the study site.

To accomplish this objective a physically based hydrological model, GEOtop was used to simulate key snow cover processes across a High Arctic tundra environment over the 2005-2019 period. The major snowpack characteristics related to snow meltout timing and snow accumulation amount guided the selection of these variables. Key parameters influencing snow depth fluctuation during the accumulation period and melt phase were identified using a sensitivity analysis.

In conclusion, the use of the physically based hydrological model, GEOtop, has proven effective in simulating key snow cover processes. Although computationally demanding, the wind blowing routine provided by the GEOtop model has shown satisfying results in a complex topography of tundra environment and shows that a model of this kind can give a realistic picture of the snow distribution based on the climate during the accumulation season. Simulated late-winter accumulations of snow and the melting process by GEOtop for open tundra compare reasonably well with measurements, provided snowpack sublimation processes are included; a simulation

neglecting blowing snow sublimation gives much greater accumulations than observed. The observed distribution of snow depths is well reproduced, and the spatial variations in the temporal evolution of snow cover metrics in the area are captured. Sensitivity analysis has allowed for the identification of key parameters influencing snow depth fluctuation, and only a few parameterization changes were needed to significantly improve model performance. The results revealed that the importance of model parameterization is highly dependent on the period (snow accumulation and ablation). Overall, the use of GEOtop has offered valuable insights into the understanding of snow cover characteristics and processes in tundra Arctic regions, with potential future applications in climate modeling and water resource management.

Objective3: Explore the effect of blowing snow processes on the sensitivity of snow cover properties to projected changes in precipitation for the case study area.

This study was an initial attempt to evaluate how future snow conditions in the Canadian High Arctic tundra environment would be affected by blowing snow under various climate change scenarios. Prescribed baseline climate changes in Chapter III have demonstrated that while the regional climate conditions (temperature and precipitation) are primary drivers of the snow cover condition responses to climate change (Derksen *et al.*, 2018), blowing snow processes can alter the response of snow cover conditions to a common external climate change forcing. Incorporating blowing snow processes had a notable impact on the climate sensitivity of snow cover and the degree of this impact varies depending on the specific scenario under examination. The influence of blowing snow diminished in warmer scenarios, whereas only slight changes were observed in colder climate scenarios (Marshall *et al.*, 2019). In conclusion, this research dictates the need for taking into account snow cover redistribution due to wind when projecting future changes in snow cover condition.

Overall, our findings emphasized the importance of a detailed understanding of the complex interactions between environmental variables in controlling the permafrost state and snow cover conditions. The intricate nature of permafrost and snow cover interactions and their dynamics are highly contingent on local environmental conditions. To enhance our understanding, it becomes crucial to integrate local data and models that capture the specific nuances of tundra environments. This could include factors such as topography, vegetation types, and microclimatic variations, which significantly influence the permafrost state. The complexity highlighted in our findings necessitates the refinement of predictive models at a local scale. By incorporating site-specific data, these models can offer more accurate predictions of permafrost and soil carbon dynamics under changing climate scenarios. This tailored approach is essential for developing targeted mitigation and adaptation strategies that account for the unique characteristics of different tundra environments.

Understanding the active layer's thermal and moisture regime is critical for assessing the vulnerability of permafrost to climate change. Our findings provide valuable insights into these processes, serving as a foundation for identifying areas at higher risk of permafrost degradation. This knowledge is indispensable for land-use planning, infrastructure development, and ecological conservation in tundra regions. Also, by deciphering the complex interactions between environmental variables, our research contributes to a more nuanced assessment of the impact of climate change on permafrost and soil carbon dynamics. This has practical implications for policymakers, land managers, and researchers involved in climate change mitigation and adaptation efforts, allowing them to make informed decisions based on a deeper understanding of the local intricacies influencing permafrost conditions.

In conclusion, by acknowledging the need for local data and models and emphasizing the practical implications of our findings, we aim to bridge the gap between scientific insights and actionable outcomes in the context of permafrost and tundra environments. These findings have important implications for understanding the active layer thermal and moisture regime in tundra environments and for predicting the impact of climate change on permafrost and soil carbon dynamics.

Limitation and future work development

The current thesis, investigated the sensitivity of snow cover and permafrost active layer to the spatial heterogeneity of landscape and climate change across a High Arctic tundra environment. The analysis revealed that ALT and ground surface temperature (GST) were highly heterogeneous and varied significantly over short distances due to different landforms and cryoturbation processes. Due of the short ground surface temperature and thaw depth measurement periods, the utility of the measured temperature of the current study in this environment is limited. Assessment of the temporal and spatial transferability of our empirical findings will be possible with continued monitoring of GST in the area. Certain elements of the snowpack's influence on the thermal regime of permafrost were omitted from the investigation, notably the impact of snow density. This variable warrants additional data collection in the field and inclusion in subsequent studies to enhance the comprehensiveness of the research.

How inaccuracies in forcing data and model physics spread as the simulation develops is a significant source of uncertainties in snow modeling (Raleigh *et al.*, 2015). The subjective decisions made in snow cover modeling within this thesis may influence the level of uncertainty presented in the resulting output. Parameter uncertainty can be a result of the inability to estimate or measure these effective parameters that integrate and conceptualize processes (Gelfan et al., 2017). Some of the model parameters in the hydrological model in the current thesis were imported from studies in catchments with

similar biophysical and hydrological characteristics due to the lack of data which can lead to uncertainties for the hydrological models. The main uncertainty of parameters rises from wind-induced gauge undercatch in the open terrain of the High Arctic (Yang, 1999). Also, the separation of precipitation into rainfall or snowfall is one of the most sensitive parameterization in simulating cold regions hydrological processes. However, in this study, this parameter was set from a study performed at the regional scale, and needs for further examination and sensitivity analyses. On the other hand, due to the lack of observed data, some of meteorological data were either retrieved from another station within a limited distance (Pond inlet station), interpolated data or were taken from data source that provided the data at a large scale (such as CaPA precipitation data and cloud factor data from ERA5 data sources).

GEOtop 3.0 may enhance our capacity to predict how climate change will affect snow cover in cold areas through its physically based estimate of snow transport and blowing snow routine. As a physically-based model, it is regarded to have the potential to improve the catchment hydrological process simulation and prediction capability. However applying the distributed blowing snow model of GEOtop to a large area is computationally demanding. Also, future applications should investigate additional improvements to current algorithms used for representing specific hydrological processes, even though this study had a significant focus on the physical-based algorithms' representation of the hydrological processes found in the Canadian High Arctic. Relevant to this study, the model is not well developed to consider snow depth hoar in the simulation (Engel et al., 2017), especially when it is mentioned that the Arctic snowpack consists of a basal depth hoar layer overlaid by a wind slab (Ballantyne *et al.*, 1990; Benson and Sturm, 1993; Dominé *et al.*, 2002).

Although the wind effect on future changes in snow cover condition was taken into account in this study, the climate sensitivity framework only considers mean monthly changes in air temperature and precipitation, not future variations in precipitation

intensity, frequency, duration, number, or length of wet and dry spells. Also, the climate changes scenarios used in this study just focus on the worst case scenario (RCP 8.5) so future research should consider other possible scenarios. Since studies have shown the significant changes in shifting vegetation intensity and type in Arctic, a potential next step is to simulate the future changes in snow cover conditions by taking into account these changes.

REFERENCES

Agosta, C., Favier, V., Krinner, G., Gallée, H., Fettweis, X. and Genthon, C. (2013) 'High-resolution modelling of the Antarctic surface mass balance, application for the twentieth, twenty first and twenty second centuries', Climate Dynamics, 41(11–12), pp. 3247–3260. doi: 10.1007/s00382-013-1903-9.

AMAP (2017) Snow, water, ice and permafrost in the Arctic (SWIPA). Changing permafrost and its impacts. Oslo, Norway. Arctic Monitoring and Assessment Programme (AMAP). 856 p.

Atchley, A. L., Coon, E. T., Painter, S. L., Harp, D. R. and Wilson, C. J. (2016) 'Influences and interactions of inundation, peat, and snow on active layer thickness', Geophysical Research Letters. Wiley-Blackwell, 43(10), pp. 5116–5123. doi: 10.1002/2016GL068550.

Aygün, O., Kinnard, C., Campeau, S. and Krogh, S. A. (2020) 'Shifting hydrological processes in a Canadian agroforested catchment due to a warmer and wetter climate', Water (Switzerland), 12(3). doi: 10.3390/w12030739.

Ballantyne, C., Williams, P. J. and Smith, M. W. (1990) The Frozen Earth: Fundamentals of Geocryology, Transactions of the Institute of British Geographers. New York: Cambridge University Press. p 306. doi: 10.2307/622856.

Belshe, E. F., Schuur, E. A. G., Bolker, B. M. and Bracho, R. (2012) 'Incorporating spatial heterogeneity created by permafrost thaw into a landscape carbon estimate', Journal of Geophysical Research: Biogeosciences, 117(1), pp. 1–14. doi: https://doi.org/10.1029/2011JG001836.

Benson, C. S. and Sturm, M. (1993) 'Structure and wind transport of seasonal snow on the Arctic slope of Alaska', Annals of Glaciology, 18, pp. 261–267. doi: 10.3189/s0260305500011629.

Biskaborn, B. et al. (2019) 'Permafrost is warming at a global scale', Nature Communications, 10(2019), pp. 1–11. doi: https://doi.org/10.1038/s41467-018-08240-4.

Bliss, L. C., Courtin, G. M., Pattie, D. L., Riewe, R. R., Whitfield, D. W. A. and Widden, P. (1973) 'Arctic tundra ecosystems', Annual Review of Ecology and Systematics, 4, pp. 359–399. doi: 10.1146/annurev.es.04.110173.002043.

Bliss, L C, Courtin, G. M., Pattie, D. L., Riewe, R. R., Whitfield, D. W. A. and Widden, P. (1973) 'Arctic Tundra Ecosystems', Annual Review of Ecology and Systematics, 4(1), pp. 359–399. doi: 10.1146/annurev.es.04.110173.002043.

Brown, R. D. and Robinson, D. A. (2011) 'Northern Hemisphere spring snow cover variability and change over 1922-2010 including an assessment of uncertainty', The Cryosphere, 5, pp. 219–229. doi: 10.5194/tc-5-219-2011.

Brown, R., Schuler, D. V., Bulygina, O., Derksen, C., Luojus, K., Mudryk, L., Wang, L. and Yang, D. (2017) Snow, Water, Ice and Permafrost in the Arctic (SWIPA). Chapter 3: Arctic terrestrial snow cover. Oslo, Norway.

Bui, M. T., Lu, J. and Nie, L. (2020) 'A review of hydrological models applied in the permafrost-dominated Arctic region', Geosciences (Switzerland). MDPI AG, 10(10), pp. 1–27. doi: 10.3390/GEOSCIENCES10100401.

Callaghan, T. et al. (2011) 'The changing face of Arctic snow cover: A synthesis of observed and projected changes', Ambio, 40, pp. 17–31. doi: 10.1007/s13280-011-0212-y.

Callaghan, T. V. et al. (2011) 'Multiple effects of changes in Arctic snow eover', Ambio, 40, pp. 32–45. doi: 10.1007/s13280-011-0213-x.

Cassano, J. J., Uotila, P., Lynch, A. H. and Cassano, E. N. (2007) 'Predicted changes in synoptic forcing of net precipitation in large Arctic river basins during the 21st century', Journal of Geophysical Research: Biogeosciences, 112(4), pp. 1–20. doi: 10.1029/2006JG000332.

Chapin, F. S. et al. (2005) 'Role of Land-Surface Changes in Arctic Summer Warming', 657(2005), pp. 657–660. doi: 10.1126/science.1117368.

Cohen, J. and Rind, D. (1990) 'The effect of snow covr on the climate', Journal of Climate, 4, pp. 689–706.

Derksen, C., Burgess, D., Duguay, C., Howell, S., Mudryk, L., Smith, S., Thackeray, C. and Kirchmeier-Young, M. (2018) Changes in snow, ice, and permafrost across Canada, Chapter 5: Canada's Changing Climate Report. Ottawa, Canada. pp 194-260.

Devia, G. K., Ganasri, B. P. and Dwarakish, G. S. (2015) 'A Review on Hydrological Models', Aquatic Procedia, 4(Icwrcoe), pp. 1001–1007. doi: 10.1016/j.aqpro.2015.02.126.

Dominé, F., Cabanes, A. and Legagneux, L. (2002) 'Structure, microphysics, and surface area of the Arctic snowpack near Alert during the ALERT 2000 campaign', Atmospheric Environment, 36(15–16), pp. 2753–2765. doi: 10.1016/S1352-2310(02)00108-5.

Endrizzi, S., Gruber, S., Dall'Amico, M. and Rigon, R. (2014) 'GEOtop 2.0: Simulating the combined energy and water balance at and below the land surface accounting for soil freezing, snow cover and terrain effects', Geoscientific Model Development, 7(6), pp. 2831–2857. doi: 10.5194/gmd-7-2831-2014.

Engel, M., Notarnicola, C., Endrizzi, S. and Bertoldi, G. (2017) 'Snow model sensitivity analysis to understand spatial and temporal snow dynamics in a high-elevation catchment', Hydrological Processes. Wiley-Blackwell, 31(23), pp. 4151–4168. doi: 10.1002/hyp.11314.

Farquharson, L. M., Romanovsky, V. E., Cable, W. L., Walker, D. A., Kokelj, S. V. and Nicolsky, D. (2019) 'Climate Change Drives Widespread and Rapid Thermokarst Development in Very Cold Permafrost in the Canadian High Arctic', Geophysical Research Letters, 46(12), pp. 6681–6689. doi: 10.1029/2019GL082187.

Fisher, J. P. ., Estop-Aragones, C., Thierry, A., Charman, D., Wolfe, S. A., Hartley, I. P. and Murton, J. B. (2016) 'The influence of vegetation and soil characteristics on active-layer thickness of permafrost soils in boreal forest', Global Change Biology, 22, pp. 3127–3140. doi: https://doi.org/10.1111/gcb.13248.

Francis, J. A., White, D. M., Cassano, J. J., Gutowski, W. J., Hinzman, L. D., Holland, M. M., Steele, M. A. and Vörösmarty, C. J. (2009) 'An arctic hydrologic system in transition: Feedbacks and impacts on terrestrial, marine, and human life', Journal of Geophysical Research: Biogeosciences, 114(4), pp. 1–30. doi: 10.1029/2008JG000902.

Gauthier, G., Bêty, J., Cadieux, M.-C., Legagneux, P., Doiron, M., Chevallier, C., Lai, S., Tarroux, A. and Berteaux, D. (2013) 'Long-term monitoring at multiple trophic levels suggests heterogeneity in responses to climate change in the Canadian Arctic tundra.', Philosophical transactions of the Royal Society. The Royal Society, 368(1624), p. 20120482. doi: 10.1098/rstb.2012.0482.

Gelfan, A., Gustafsson, D., Motovilov, Y., Arheimer, B., Kalugin, A., Krylenko, I. and Lavrenov, A. (2017) 'Climate change impact on the water regime of two great Arctic rivers: modeling and uncertainty issues', Climatic Change. Climatic Change, 141(3), pp. 499–515. doi: 10.1007/s10584-016-1710-5.

Godin, E., Fortier, D. and Lévesque, E. (2016) 'Nonlinear thermal and moisture response of ice-wedge polygons to permafrost disturbance increases heterogeneity of high Arctic wetland', Biogeosciences, 13, pp. 1439–1452. doi: https://doi.org/10.5194/bg-13-1439-2016.

Grünberg, I., Wilcox, E. J., Zwieback, S., Marsh, P. and Boike, J. (2020) 'Linking tundra vegetation, snow, soil temperature, and permafrost', Biogeosciences, 17(16), pp. 4261–4279. doi: 10.5194/bg-17-4261-2020.

Gubler, S., Endrizzi, S., Gruber, S. and Purves, R. S. (2013) 'Sensitivities and uncertainties of modeled ground temperatures in mountain environments', Geosci. Model Dev, 6, pp. 1319–1336. doi: 10.5194/gmd-6-1319-2013.

Hansen, B. B., Isaksen, K., Benestad, R. E., Kohler, J., Pedersen, Å., Loe, L. E., Coulson, S. J., Larsen, J. O. and Varpe, Ø. (2014) 'Warmer and wetter winters: Characteristics and implications of an extreme weather event in the High Arctic', Environmental Research Letters. IOP Publishing, 9(11). doi: 10.1088/1748-9326/9/11/114021.

J Goetz, N. S., Mack, M. C., Gurney, K. R., Sulla-Menashe, D., Woodcock, C. E. and Friedl, M. A. (2018) 'Environmental Research Letters Canadian boreal forest greening and browning trends: an analysis of biogeographic patterns and the relative roles of disturbance versus climate drivers Canadian boreal forest greening and browning trends: an analysis of biog', Environ. Res. Lett, 13.

Jing-Yi, Z. (2018) 'Snow cover influences the thermal regime of active layer in Urumqi River Source , Tianshan Mountains , China', Journal of mountain Science, 15, pp. 2622–2636. doi: https://doi.org/10.1007/s11629-018-4856-y.

Van Der Kolk, H.-J., Heijmans, M. M. P. D., Van Huissteden, J., Pullens, J. W. M. and Berendse, F. (2016) 'Potential Arctic tundra vegetation shifts in response to changing temperature, precipitation and permafrost thaw', Biogeosciences, 13, pp. 6229–6245. doi: 10.5194/bg-13-6229-2016.

Krogh, S. A. and Pomeroy, J. W. (2018) 'Recent changes to the hydrological cycle of an Arctic basin at the tundra-taiga transition', Hydrology and Earth System Sciences, 22(7), pp. 3993–4014. doi: 10.5194/hess-22-3993-2018.

Krogh, S. A., Pomeroy, J. W. and Marsh, P. (2017) 'Diagnosis of the hydrology of a small Arctic basin at the tundra-taiga transition using a physically based hydrological model', Journal of Hydrology. Elsevier, 550, pp. 685–703. doi: 10.1016/J.JHYDROL.2017.05.042.

Lara, M. J., Nitze, I., Grosse, G., Martin, P. and David McGuire, A. (2018) 'Reduced arctic tundra productivity linked with landform and climate change interactions', Nature: Scientific Reports, 8(1), pp. 1–10. doi: https://doi.org/10.1038/s41598-018-20692-8.

Lawrence, D. M. and Slater, A. G. (2010) 'The contribution of snow condition trends to future ground climate', Climate Dynamics, 34(7), pp. 969–981. doi: 10.1007/s00382-009-0537-4.

Lizarralde, . D, Gaherty, J. B., Collins, J. A., Hirth, G. and Kim, S. D. (2004) 'Role of Land-Surface Changes in Arctic Summer Warming', Chem. Geol, 432, p. 1. doi: 10.1126/science.1116349.

Loranty, M. M. et al. (2018) 'Reviews and syntheses: Changing ecosystem influences on soil thermal regimes in northern high-latitude permafrost regions', Biogeosciences, 15(17), pp. 5287–5313. doi: https://doi.org/10.5194/bg-15-5287-2018.

Marshall, A. M., Link, T. E., Abatzoglou, J. T., Flerchinger, G. N., Marks, D. G. and Tedrow, L. (2019) 'Warming Alters Hydrologic Heterogeneity: Simulated Climate Sensitivity of Hydrology-Based Microrefugia in the Snow-to-Rain Transition Zone', Water Resources Research, 55(3), pp. 2122–2141. doi: 10.1029/2018WR023063.

Meehl, G. A. et al. (2007) Climate change 2007: the physical science basis contribution of Working Group I to the fourth assessment report of the intergovernmental panel on climate change. Cambridge.

Michlmayr, G., Lehning, M., Koboltschnig, G., Holzmann, H., Zappa, M. and And, R. M. (2008) 'Application of the Alpine 3D model for glacier mass balance and glacier runoff studies at Goldbergkees, Austria', Okt 2005 Abrufbar uber httpwww tldp orgLDPabsabsguide pdf Zugriff 1112 2005, 2274(November 2008), pp. 2267–2274. doi: 10.1002/hyp.

Mitch Campbell, Grant Gilchrist, Mark Mallory, Jennie Rausch, Tyler Ross, P. S. (2012) CANADA ARCTIC TUNDRA.

Mohammadzadeh Khani, H., Kinnard, C. and Lévesque, E. (2022) 'Historical Trends and Projections of Snow Cover over the High Arctic: A Review', Water. MDPI AG, 14(4), p. 587. doi: 10.3390/W14040587.

Morgner, E., Elberling, B., Strebel, D. and Cooper, E. J. (2010) 'The importance of winter in annual ecosystem respiration in the High Arctic: effects of snow depth in two vegetation types', Polar Research, 29(1), pp. 58–74. doi: 10.1111/j.1751-8369.2010.00151.x.

Nitzbon, J., Langer, M., Martin, L. C. P., Westermann, S., Schneider Von Deimling, T. and Boike, J. (2021) 'Effects of multi-scale heterogeneity on the simulated evolution of ice-rich permafrost lowlands under a warming climate', Cryosphere, 15(3), pp. 1399–1422. doi: 10.5194/tc-15-1399-2021.

Pavelsky, T. M. and Smith, L. C. (2006) 'Intercomparison of four global precipitation data sets and their correlation with increased Eurasian river discharge to the Arctic Ocean', Journal of Geophysical Research Atmospheres, 111(21), pp. 1–20. doi: 10.1029/2006JD007230.

Phoenix, G. K. and Bjerke, J. W. (2016) 'Arctic browning: extreme events and trends reversing arctic greening', Global change biology, 22(9), pp. 2960–2962. doi: 10.1111/gcb.13261.

Pomeroy, J. W. et al. (2022) 'The cold regions hydrological modelling platform for hydrological diagnosis and prediction based on process understanding', Journal of Hydrology, 615(May). doi: 10.1016/j.jhydrol.2022.128711.

Raleigh, M. S., Lundquist, J. D. and Clark, M. P. (2015) 'Exploring the impact of forcing error characteristics on physically based snow simulations within a global sensitivity analysis framework', Hydrology and Earth System Sciences, 19(7), pp. 3153–3179. doi: 10.5194/hess-19-3153-2015.

Rantanen, M., Karpechko, A. Y., Lipponen, A., Nordling, K., Hyvärinen, O., Ruosteenoja, K., Vihma, T. and Laaksonen, A. (2022) 'The Arctic has warmed nearly four times faster than the globe since 1979', Communications Earth and Environment. Springer US, 3(1), pp. 1–10. doi: 10.1038/s43247-022-00498-3.

Saito, K., Zhang, T., Yang, D., Marchenko, S., Barry, R. G., Romanovsky, V. and Hinzman, L. (2013) 'Influence of the physical terrestrial Arctic in the eco-climate system', Ecological Applications, 23(8), pp. 1778–1797. doi: https://doi.org/10.1890/11-1062.1.

Sazonova, T. S., Romanovsky, V. E. and Walsh, J. E. (2004) 'Permafrost dynamics in the 20th and 21st centuries along the East Siberian transect', Journal of Geophysical Research, 109, pp. 1–20. doi: 10.1029/2003JD003680.

Shi, H. X. and Wang, C. H. (2015) 'Projected 21st century changes in snow water equivalent over Northern Hemisphere landmasses from the CMIP5 model ensemble', The Cryosphere, 9, pp. 1943–1953. doi: 10.5194/tc-9-1943-2015.

Slater, A. G. and Lawrence, D. M. (2013) 'Diagnosing present and future permafrost from climate models', Journal of Climate, 26(15), pp. 5608–5623. doi: 10.1175/JCLI-D-12-00341.1.

Smith, S. L., Burgess, M. M., Riseborough, D. and Nixon, F. M. (2005) 'Recent trends from Canadian permafrost thermal monitoring network sites', Permafrost and Periglacial Processes, 16(1), pp. 19–30. doi: 10.1002/ppp.511.

Sorooshian, S., Kuo-Lin Hsu, Coppola, E., Tomassetti, B., Verdecchia, M. and Visconti, G. (2020) Hydrological modelling and the water cycle: Coupling the atmospheric and hydrological models. Springer. Available at: http://journal.um-surabaya.ac.id/index.php/JKM/article/view/2203.

Stuecker, M. F. et al. (2018) 'Polar amplification dominated by local forcing and feedbacks', Nature Climate Change. Springer US, 8(12), pp. 1076–1081. doi: 10.1038/s41558-018-0339-y.

Thackeray, C. W., Fletcher, C. G., Mudryk, L. R. and Derksen, C. (2016) 'Quantifying the uncertainty in historical and future simulations of Northern Hemisphere spring snow cover', Journal of Climate, 29, pp. 8647–8663. doi: 10.1175/JCLI-D-16-0341.s1.

Williams, J. P. and Smith, M. W. (1989) The Frozen Earth-Fundamentals of Geocryology, … of the American Astronomical Society. doi: 10.1017/CBO9780511564437.

Woo, M.-K., Kane, D. L., Carey, S. K. and Yang, D. (2008) 'Progress in permafrost hydrology in the new millennium', Permafrost and Periglacial Processes. Wiley-Blackwell, 19(2), pp. 237–254. doi: 10.1002/ppp.613.

Woo, M. (2012) Permafrost Hydrology. Berlin Heidelberg: Springer New York. 574 p. doi: 10.1007/978-3-642-23462-0.

Woo, M. K. and Young, K. L. (2014) 'Disappearing semi-permanent snow in the High Arctic and its consequences', Journal of Glaciology, 60(219), pp. 192–200. doi: 10.3189/2014JoG13J150.

Yang, D. (1999) 'An Improved Precipitation Climatology For The Arctic Ocean', Geophysical Research Letters, 26(11), pp. 1625–1628.

Yang, D. et al. (1999) 'Quantification of precipitation measurement discontinuity induced by wind shields on national gauges', Water Resources Research, 35(2), pp. 491–508. doi: 10.1029/1998WR900042.

Yi, Y., Kimball, J. S., Chen, R. H., Moghaddam, M., Reichle, R. H. and Mishra, U. (2018) 'Characterizing permafrost active layer dynamics and sensitivity to landscape spatial heterogeneity in Alaska', The Cryosphere, 12, pp. 145–161. doi: https://doi.org/10.5194/tc-12-145-2018.

Yokohata, T., Saito, K., Takata, K., Nitta, T., Satoh, Y., Hajima, T., Sueyoshi, T. and Iwahana, G. (2020) 'Model improvement and future projection of permafrost processes in a global land surface model', Progress in Earth and Planetary Science. Progress in Earth and Planetary Science, 7(1). doi: 10.1186/s40645-020-00380-w.

Zanotti, F., Endrizzi, S., Bertoldi, G. and Rigon, R. (2004) 'The GEOtop snow model', in 61st Eastern snow conference, pp. 87–100. Available at: http://citeseerx.ist.psu.edu/viewdoc/download?doi=10.1.1.571.599&rep=rep1&type=pdf (Accessed: 26 September 2018).

Zhang, T. (2005) 'Influence of seasonal snow cover on the ground thermal regime: an overview', Reviews in Geophysics, 43, pp. 1–23. doi: https://doi.org/10.1029/2004RG000157.

Zhang, T., Barry, R. G., Knowles, K., Heginbottom, J. A. and Brown, J. (2008) 'Statistics and characteristics of permafrost and ground-ice distribution in the Northern Hemisphere', Polar Geography. Taylor & Francis Group , 31(1–2), pp. 47–68. doi: 10.1080/10889370802175895.

Zhou, J., Pomeroy, J. W., Zhang, W., Cheng, G., Wang, G. and Chen, C. (2014) 'Simulating cold regions hydrological processes using a modular model in the west of China', Journal of Hydrology. Elsevier B.V., 509, pp. 13–24. doi: 10.1016/j.jhydrol.2013.11.013.

Zorigt, M., Kwadijk, J., Van Beek, E. and Kenner, S. (2016) 'Estimating thawing depths and mean annual ground temperatures in the Khuvsgul region of Mongolia', Environmental Earth Sciences. Springer Berlin Heidelberg, 75(10), p. 897. doi: 10.1007/s12665-016-5687-1.